Coordination Chemistry Reviews 337 (2017) 145–177

Contents lists available at ScienceDirect

Coordination Chemistry Reviews

journal homepage: www.elsevier.com/locate/ccr

Review

STM probing the supramolecular coordination chemistry on solid surface: Structure, dynamic, and reactivity

Yan-fang Geng [a,1], Ping Li [a,1], Ji-zhen Li [b], Xue-mei Zhang [a,b,*], Qing-dao Zeng [a,*], Chen Wang [a,*]

[a] CAS Key Laboratory of Standardization and Measurement for Nanotechnology, CAS Center for Excellence in Nanoscience, National Center for Nanoscience and Technology (NCNST), No. 11 Beiyitiao, Zhongguancun, Beijing 100190, PR China
[b] School of Economics and Management, Tsinghua University, Beijing 100084, PR China

ARTICLE INFO

Article history:
Received 2 December 2016
Accepted 30 January 2017
Available online 16 February 2017

Keywords:
Coordination chemistry
Supramolecular structures
Dynamic
Activity
Scanning tunneling microscopy

ABSTRACT

Supramolecular coordination chemistry is currently a very popular topic in metallorganic chemistry and has a very large impact on a broad field of applications. More importantly, the invention of STM has opened new doorways to study these concepts on surfaces. This review summarizes the recent progress on surface-confined metallosupramolecular engineering based on the supramolecular coordination chemistry, with the aid of STM. At the beginning, a discussion of metalloids, alkali metals, and alkaline earth metal-based metallosupramolecular engineering is conducted. Next, transition metal-based coordination chemistry on surfaces is discussed. Then, polygonal, double- and triple-decker structures based on rare-earth-metal coordination chemistry are presented. Based on these supramolecular structures, the dynamics of coordination as well as the formed supramolecules are discussed. In the end, the coordination chemistry, including stability of coordination bonds, organic molecules, and gas molecule adsorption is described. Throughout this review, the coordination structures, dynamics and reactivity have been emphasized, which are important current and future research themes.

Contents

Abbreviations: 1D, one-dimensional; 2D, two-dimensional; 3D, three-dimensional; BDBA, 4,4′-di-(1,4-buta-1,3-diynyl)benzoic acid; BP, 4,4′-bipyridine; *t*-Bu_2Ph, 3,5-di-*tert*-butylphenyl; *cis*-BTP-TPE, *cis*-bis-terpyridine tetraphenyl ethylene; $(C_{12}OPc)_2$Er, bis[octakis(dodecyloxy) phthalocyaninato] erbium(III) complexes; Co-TPP, Co-tetraphenylporphyrin; CPP, mono-cyanophenyl-functionalised porphyrin; CsA, cyclosporine A; CTP, chiral trigonal prism; DABCO, 1,4-diazabicyclo[2.2.2]octane; DCA, 9,10-dicyanoanthracene; DCVST-Me_2, Dicyanovinyl-quinquethiophene; DFT, density function theory; DHBQ, 2,5-dihydroxybenzoquinone; DMC, dimetacyanoazobenzene; DPE, 1,2-di(4-pyridyl)ethylene; DPP, 1,3-di(4-pyridyl)propane; Fe-TPP, Fe^{II}-tetraphenylporphyrin; F4TCNQ, 2,3,5,6-tetrafluoro-7,7,8,8-tetracyanoquino-dimethane; HBB, hexabromobenzene; HOPG, highly oriented pyrolytic graphite; Mel, melamine; MOCN, metal-organic coordination network; MOCP, metal-organic coordination polymer; PDI, 1,4-phenylene diisocyanide; SDA, stillbenedicarboxylic acid; StOF-$COOH_3$, star-shaped oligofluorene; STM, scanning tunneling microscopy; STS, scanning tunneling spectroscopy; TBP, trigonal bipyramid; $TbPc_2$, bis(phthalocyaninato) terbium(III); TCNQ, 7,7,8,8-tetracyanoquinodimethane; TCNE, tetracyanoethylene; TCDB, 1,3,5-tris(10-carboxydecyloxy)benzene; TiOPc, titanyl phthalocyanine; TMA, 1,3,5-benzoic tricarboxylic acid; TPA, 1,4-benzenedicarboxylic acid; TPP, tetraphenyl porphyrin; TPyB, 1,3,5-trispyridylbenzene; TPyP, tetra(4-pyridine) porphyrin; *sym*-TTT, symmetric triphenylene derivative with three carboxyl groups; TTF, Tetrathiafulvalene; UHV, ultrahigh vacuum; ZnOEP, zinc (II) octaethylporphyrin; Zn-Pc, zinc (II) phthalocyanine; Zn-TBPP, zinc tetrakis(3,5-di-*t*-butylphenyl)porphyrin; Zn-TMP, zinc *meso*-tetramesitylporphyrin; Zn-TDPs, zinc-5,10,15,20-*meso*-tetradodecylporphyrins; Zn-TPyP, zinc-5,10,15, 20-tetra(4-pyridyl)porphyrin.

* Corresponding authors at: CAS Key Laboratory of Standardization and Measurement for Nanotechnology, CAS Center for Excellence in Nanoscience, National Center for Nanoscience and Technology (NCNST), No. 11 Beiyitiao, Zhongguancun, Beijing 100190, PR China.
E-mail addresses: zhangxuemei_1985@163.com (X.-m. Zhang), zengqd@nanoctr.cn (Q.-d. Zeng), wangch@nanoctr.cn (C. Wang).
[1] These authors equally contributed to this work.

http://dx.doi.org/10.1016/j.ccr.2017.01.014
0010-8545/

1. Introduction

Molecular self-assembly, or the so-called "bottom-up" method, has been well recognized as one of the most promising approaches to realize the ultimate goal of selectively creating functional nanomaterials, which is also considered one of the greatest challenges in nanoscience and technology. Using molecular self-assembly, there has been tremendous progress in the precise arrangement of individual molecules and the engineering of highly ordered molecular architectures [1–12]. In general, supramolecular architectures are formed by weak non-covalent forces between molecules, such as hydrogen bonds, π-π stacking, electrostatic interactions, metal-ligand coordination, van der Waals interactions, and so forth [13–22].

Although supramolecular chemistry has successfully manipulated hydrogen bonding to control the self-assembly of building blocks, the organized aggregates exhibit low thermal and mechanical stability. Thus, there is still great interest in exploring more rigid supramolecular architectures. Since Werner first introduced metal-ligand interactions in 1893 [23], coordination interactions have been recognized as an excellent strategy for fabricating supramolecular arrangements due to the advantage of decisive molecular recognition. In addition, the reason metal-ligand coordination interaction is the optimal method for fabricating stable and periodic nanostructures is that the highly efficient formation of metal coordination bonds usually offers considerable synthetic advantages, such as fewer steps, fast and simple construction of the final products, and inherently self-correcting, defect-free assembly [24–33].

Using various solid surfaces, the coordination-driven assembly method has progressed in recent years for the direct preparation of novel nanostructures with increasing structural complexity, ranging from 1D chains or polymers, to 2D coordination networks or frames, and to 3D structures [34–36]. Numerous studies have demonstrated the development of several organic ligands consisting with functional groups, such as carboxylate, hydroxyl, pyridine, carbonitrile and guanine. Additionally, metalloids (Si), alkali metals (typically, Na and K) and alkaline earth metals (Mg), transition metals (i.e. Mn, Fe, Co, Ni, Cu, Zn, Pd) as well as rare-earth metals (i.e. Y, Ce, Pr, Eu, Tb, Dy, Er, Lu) have served as acceptor units that can logically self-assemble with various rigid or flexible donors (ligands) into predictable architectures because of their preferred coordination geometries.

In parallel, current interest in constructing functional molecular materials is increasingly appealing for molecular- and atomic-resolution analytical tools. For this purpose, several surface techniques have been developed [37–43]. In particular, STM with its intrinsic submolecular resolution has become an outstanding tool in surface science since its inception in the early 1980s [44,45]. STM allows for direct observation of surface topography of supramolecular aggregates, especially for those assemblies that could not be characterized by traditional analysis tools [46–58]. Furthermore, incidental STS can be introduced to probe the electronic structure of physisorbed monolayers at the single molecule level [59–64]. Beyond the mere determination of the perfect ordering of physical adsorbed monolayers, STM has great potential for a wide range of applications, *i.e.* monitoring molecular dynamics, substrate-induced restructuring, and chemical reactions on surfaces or interfaces [65–87].

In order to obtain stable molecular adsorption on solid surfaces, one effective method is to sublime molecules under UHV. In this case, metallic substrates, such as Cu (100), Ag (111), Au (111), etc. are used extensively, possibly due to their attractive interactions to the adsorbates. The UHV environment is ideal for epitaxial growth of molecular films and subsequent studies, and unprecedented high resolution can be obtained under this condition. However, this method is not suitable for the self-assembly of high molecular weight molecules. Therefore, STM experiments on a solid interface are typically performed under ambient conditions. In this case, HOPG has been the most popular substrate because of the highly ordered arrays of liquid crystalline molecules on the HOPG surface. In addition, HOPG is highly stable in air and is commercially available at an affordable price. It should be noted that not all supramolecular systems can directly assemble packed

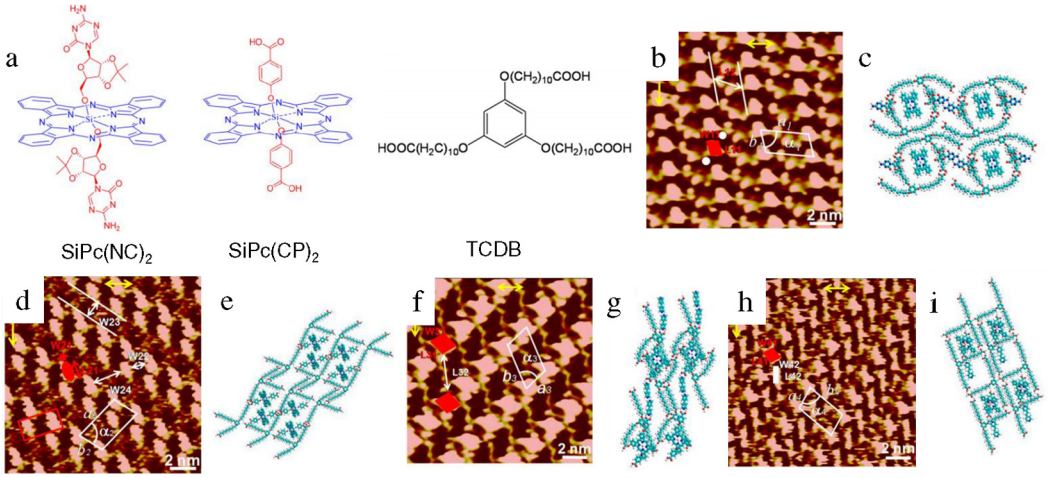

Fig. 1. Chemical structures of silicon (IV) phthalocyanine derivatives $SiPc(NC)_2$, $SiPc(CP)_2$ and template TCDB. High-resolution STM images of $SiPc(NC)_2$/TCDB (b), $SiPc(CP)_2$/TCDB (d), BP/$SiPc(CP)_2$/TCDB coadsorbed monolayer (f), and DPE/$SiPc(CP)_2$/TCDB self-assembly (h) on the HOPG surface. The proposed top-view molecular models (c, e, g, i) corresponding to STM images (b, d, f, h), respectively. (Reprinted with permission from Ref. [88]).

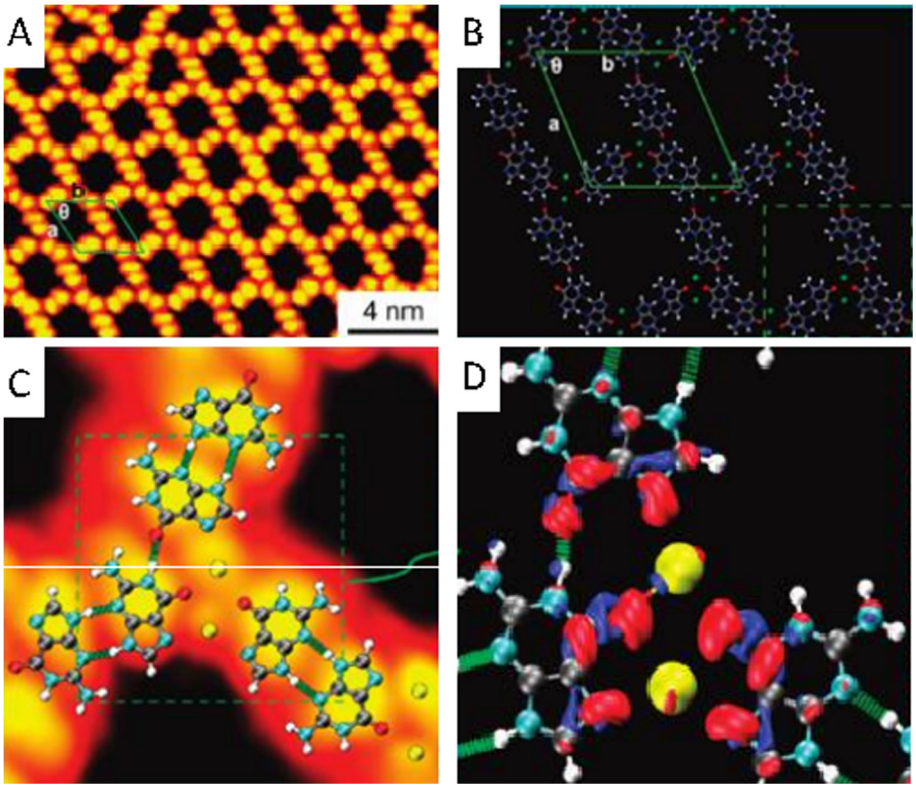

Fig. 2. (A) High-resolution STM image of the ordered guanine-K network. (B) DFT model of the guanine-K network with K atoms indicated as green spots. (C) The elementary building block including three guanine dimers and two K dimers is superimposed on the high-resolution STM image. (D) The cutoff of charge density difference between the three guanine dimers and two K atoms. (Reprinted with permission from Ref. [91]).

arrays on crystal graphite suitable for STM observation. In order to resolve this problem, one promising strategy is to use a molecular template or network that can immobilize unstable architectures, especially for coordinated complexes and in particular those with high dimensions. Therefore, it is a requirement to design molecular structures that are attached to appropriate substituents in order to assemble predictable and highly-ordered molecular structures.

In this review, STM investigation of supramolecular coordination chemistry at the single molecule level is discussed, including static structural characterization, dynamic process monitoring, and reactivity probing. Metalloids, alkali metal and alkaline earth metal-based assemblies are discussed first, followed by transition metal-based supramolecular coordination phenomena and surface-assisted assembly behavior of rare-earth metals on solid surfaces. The mentioned coordination ensembles mainly include those obtained by (1) self-organization of metal-organic complexes on substrate, (2) on-surface coordination reaction after deposition of organic ligands and metal atoms and (3) metal substrate coordinated complexes. Finally, the coordination dynamics, including the coordination procedure; molecular dynamics; as well as the activity of coordination supramolecules, such as adsorbed organic molecules and gases related to metallophthalocyanines or

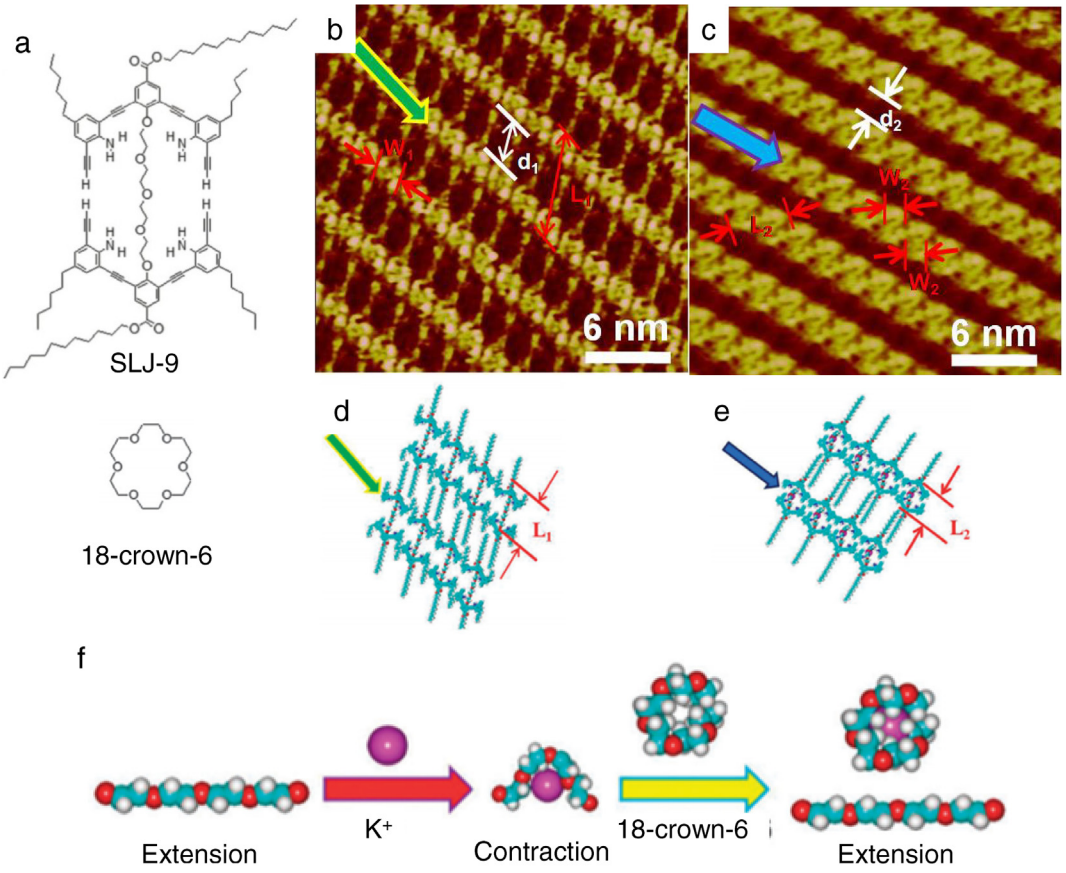

Fig. 3. (a) Chemical structures of tetraethylene glycol derivative SLJ-9 and 18-crown-6. (b, c) High-resolution STM images of the self-assembled structures of compound SLJ-9 before and after addition of K_2CO_3 on HOPG, respectively. (d, e) Molecular models of the STM images in (b) and (c), respectively. (f) An illustration model for the transformation of specimen from extension to contraction and back to extension as well as the chemical structures of specimen and 18-crown-6. (Reprinted with permission from Ref. [92]).

porphyrins, are given special attention. Through this review, a comprehensive discussion of supramolecular coordination and surface crystal engineering will be provided.

2. Metalloids, alkali metals and alkaline earth metals coordinated assemblies

2.1. Metalloid coordinated assemblies

There are few metalloid-related coordination assemblies. Recently, edge-on self-assemblies of silicon (Si) phthalocyanine derivatives $SiPc(NC)_2$ and $SiPc(CP)_2$ on the HOPG surface with the help of TCDB template was observed (Fig. 1) [88]. By using two kinds of pyridine compounds (BP and DPE) to tune the supramolecular structure, new axial self-assemblies in edge-on controlling were observed. However, the self-assembly behavior of $SiPc(NC)_2$ in the presence of pyridine ligands on the surface cannot be observed. Therefore, the type of axial moieties is important to tune the assembled structure of Si-phthalocyanine derivatives. The intermolecular hydrogen bonding along the axial direction in combination with the role of the TCDB template stabilized those coordination supramolecule assemblies. This study provided a pathway to obtain functional structures of metal-phthalocyanines on surfaces.

2.2. Alkali metal coordinated assemblies

Alkali metals, in particular Na and K elements play a significant role in cellular environment [18,21,89]. Guanine as a versatile building block can self-assemble into various architectures, such as dimers, ribbons, and macrocycles, depending on its environment. The guanine-based structures have been applied to the synthesis of supramolecular hydrogels and organic electronic materials. Guanine quartets have great potential in biological processes and the design of anticancer drugs. For example, they are important for controlling tumor immortalization. Upon adding and removal of $[K^+(pic)^-]$ and [2.2.2] cryptand into the guanine-based nanostructures, guanine can assemble/reassemble into highly-ordered quartets and ribbons [90]. The self-assembly of the octadecyl guanine derivative self-assembled into a ribbon-like structure on HOPG, which can be transformed into a guanine-quartet upon the addition of $K^+(pic)^-$. The serial addition of [2.2.2] cryptand restores the original guanine-ribbon features, indicating that the process of formation and cleavage of the K^+-guanine complex is fully reversible. The inter conversion between two different highly-ordered supramolecular motifs was successfully triggered by alkali metal ions. Under UHV conditions, two-dimensional coordination network of a guanine-K formed on an inert Au (111) surface [91]. As displayed in Fig. 2, a novel porous network formed by sequential co-deposition of guanine molecules and K atoms. This porous network is dramatically different from the previously reported guanine-quartet network [90]. Moreover, the high-resolution STM images revealed that this guanine-K network is chiral, in which some guanine dimers face upward and others face downward. Those coordinated systems would provide new insight into the fundamental physiochemical of biologically relevant systems.

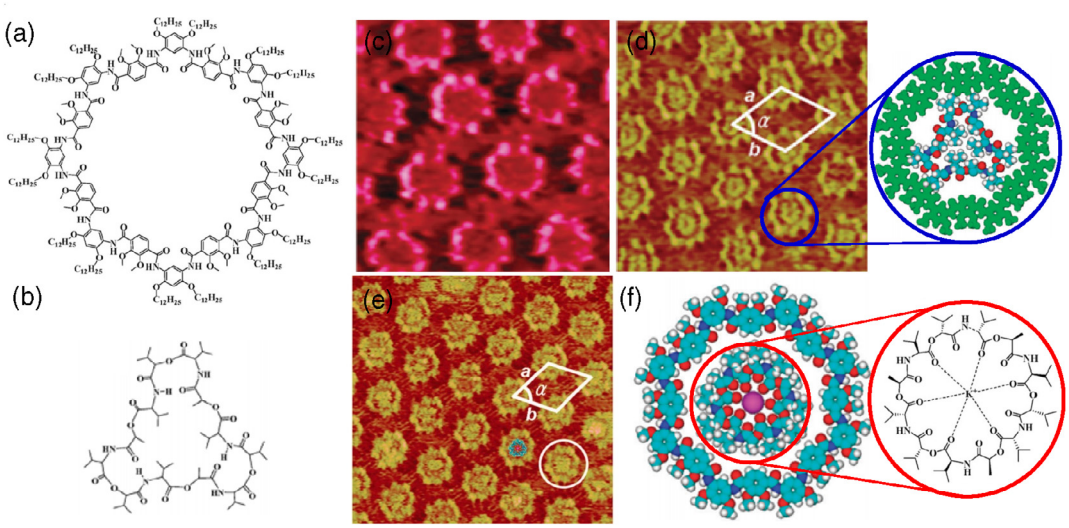

Fig. 4. Chemical structures of cyclo[16]aramide (a) and valinomycin (b). STM images of cyclo[16]aramide (c), cyclo[16]aramide/valinomycin (d) and cyclo[16]aramide/valinomycin-K^+ complex (e). (f) Proposed structural model for one unit of cyclo[16]aramide and the valinomycin-K^+ complex. (Reprinted with permission from Ref. [95]).

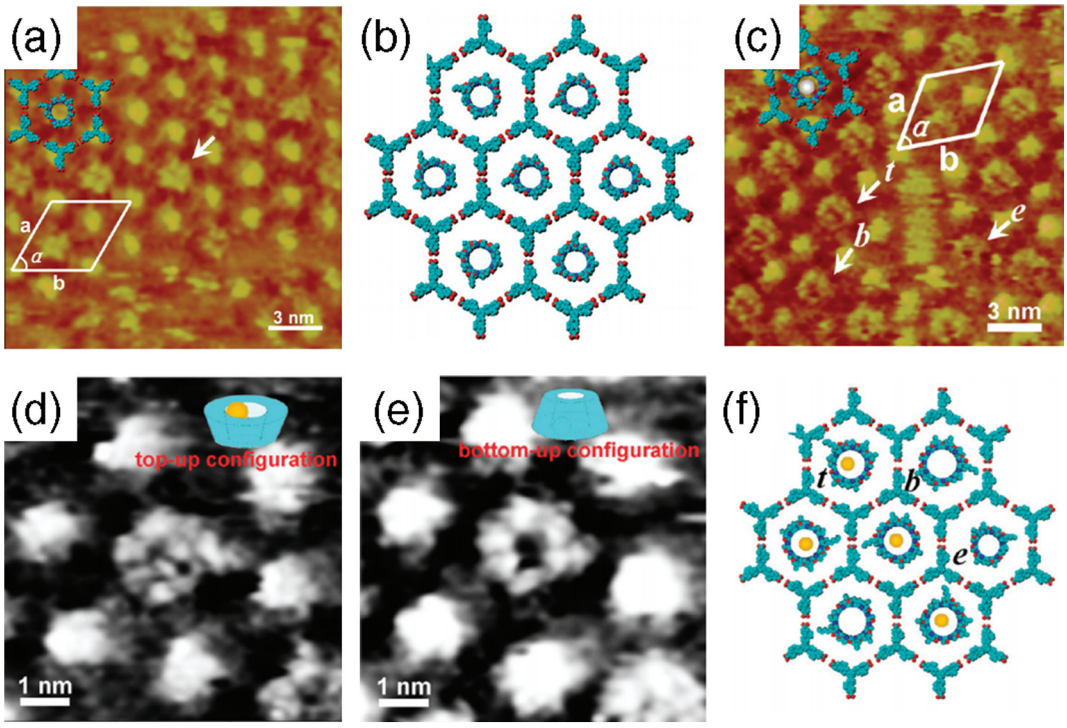

Fig. 5. (a) High resolution STM image of StOF-$COOH_3$/CsA. (b) Molecular model corresponding to (a). (c) High resolution STM image of StOF-$COOH_3$/CsA-Mg^{2+} complex. (d, e) High-resolution STM images of CsA-Mg^{2+} complexes observed from top or bottom and the hypothesized cartoon model (upper right) illustrating the corresponding top-up and bottom-up configurations. (f) Proposed structural model of the assembly structure. (Reprinted with permission from Ref. [96]).

Coordination can also drive reversible extension → contraction → extension process of an ether bridged tetraethylene glycolderivative (SLJ-9) on HOPG surface [92]. The sub-molecular resolved STM images (Fig. 3) revealed that this derivative generally adopted a fully extended state consisting of three bright pillars and two bright beads. There appeared to be a significant structural change in the assembled structure after the introduction of K_2CO_3, where the measured distance between two half rings changed from $L_1 = 3.3 \pm 0.1$ nm to $L_2 = 2.7 \pm 0.1$ nm. This indicated the formation of the coordinated complex with a contracted state had occurred. The original extended structure can be recovered by the addition of 18-crown-6 solution, which can be attributed to the strong metal-coordination interaction between the cyclic 18-crown-6 and alkali metals. This kind of coordination-controlled reversible assembly, in response to chemical stimuli, would be of great interest to materials and bionics sciences.

Cyclic peptide is an important biological system with various applications, such as ion channels, models of bioactive peptides and enzymes, etc. [93,94]. Even though one type of cyclic peptide, valinomycin alone cannot readily adsorb on a graphite surface, valinomycin can be immobilized in cyclo[16]aramide networks at the liquid/solid interface [95]. In the cyclo[16]aramide/

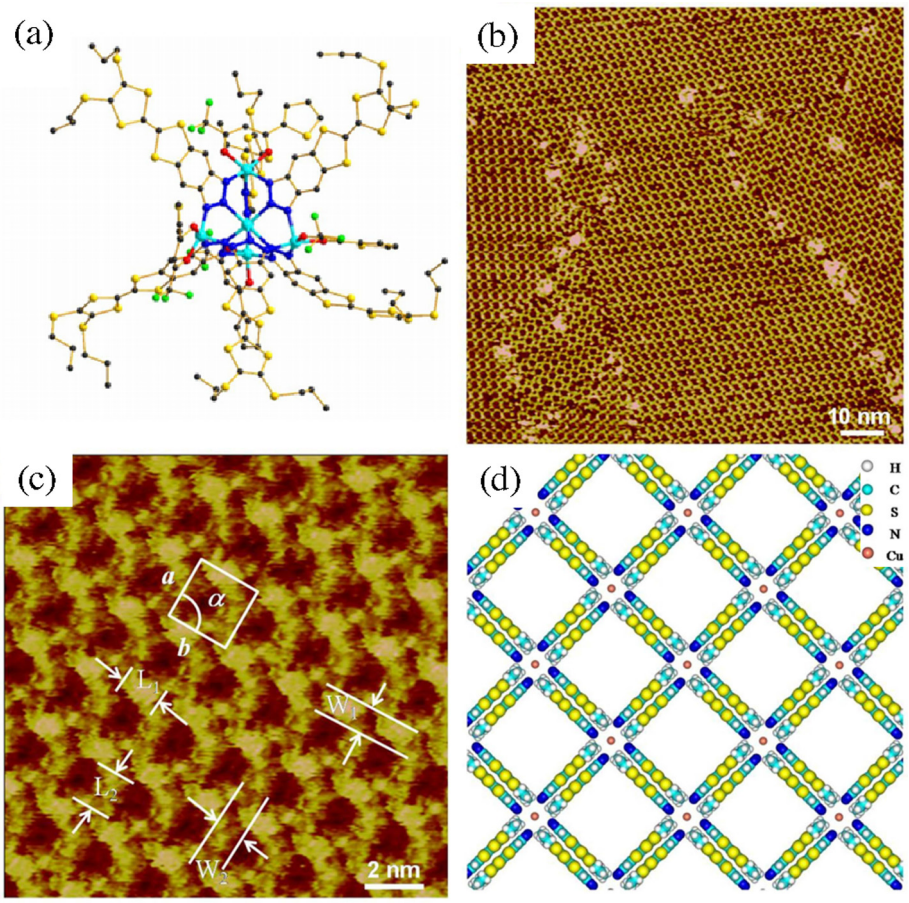

Fig. 6. (a) Crystal structure of Cu(II) complex. (b) Large scale and (c) High resolution STM images of Cu(II) complex on HOPG surface. (d) A suggested molecular model. (Reprinted with permission from Ref. [119]).

valinomycin binary supramolecular structure, each cavity of the cyclo[16]aramide networks entrapped one valinomycin molecule (Fig. 4). The diameter of the network cavity is about 2.8 nm, which is much larger than that of valinomycin (2.0 nm). After the introduction of KCl solution, the typical triangular geometry of valinomycin changed to a nearly filled circle with a diameter of 1.7 nm, as identified by STM observations. It was proposed that the metal-ligand coordination interaction between K^+ and valinomycin led to the shrinking diameter of individual valinomycin molecules. In other words, the complexation interaction led to different adsorption characteristics.

2.3. Alkaline earth metal coordination supramolecules

Another cyclic peptide, CsA is usually utilized as an immunosuppressant [96]. From the high-resolution STM image, individual CsA molecule displays polygon-like characteristic with a diameter of approximate 1.7 nm in the StOF-$COOH_3$ molecular networks at the phenyloctane/HOPG interface (Fig. 5). After $MgSO_4$ solution was added to the CsA/StOF-$COOH_3$ network, an apparent change in geometry of CsA, from irregular polygon to circular with a 2.0 nm diameter white spot, was observed. These spots within the peptide rings are always located at one side with higher contrast on the ring, which could correspond to the longer side chain. The round-shaped-ring structure might be attributed to the unfilled CsA molecules. High-resolution STM results revealed that CsA-Mg^{2+} complexes had two different adsorption characteristics including top-up configurations and bottom-up configurations. These two observed adsorption configurations might be induced by different binding energies. Meanwhile, the dimension distributions of top-up and bottom-up configurations are nearly identical. Note that CsA cannot bind with other metal ions such as Na^+ and K^+, which demonstrated a special ion recognition characteristic of CsA to Mg^{2+}.

3. Transition metal-based coordination architectures

From both a fundamental and applied perspective, the organization of metal-containing complexes on solid surfaces is important for the construction of surface molecular nanostructures. This section mainly discusses STM studies of coordination-assembled supramolecular architectures based on the coordination interactions between transition metal ions and several common organic ligands. The arrangement of adsorbed molecules not only depends on the intermolecular interactions but also the molecule-surface interactions.

3.1. Self-Organization of coordinated complexes

3.1.1. Low-dimensional ensembles

Due to magnetic, electrostatic and photophysical properties, metal-containing molecules, in particular metal-containing macrocycles with a particular shape and size, have been considered promising supramolecules for applications in nanotechnology. A series of Pd-pyridine-based 2D rectangular and square metallacycles on HOPG or Au (111) substrates were reported [97–99]. The effects of size, symmetry, and dimensionality of supramolecular adsorbates were studied by selecting a substrate and molecular

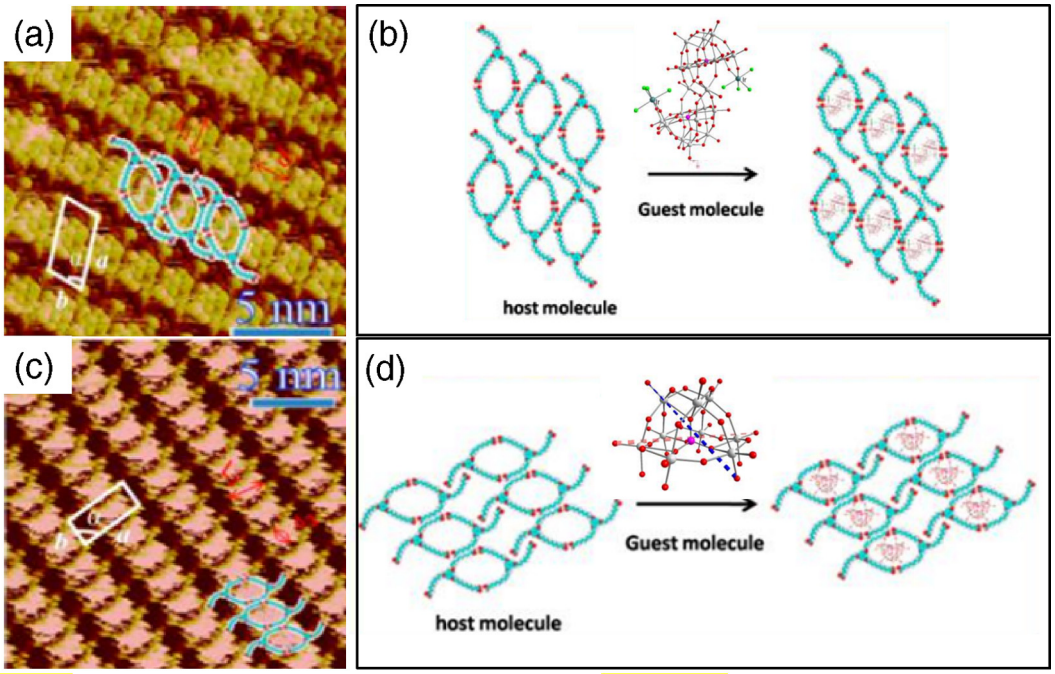

Fig. 7. (a) High-resolution STM image of cluster (**1**)/TCDB on the HOPG surface. (b) Proposed molecular model showing the STM image of the cluster (**1**)/TCDB. (c) High-resolution STM image of precursor **(2)**/TCDB on the HOPG surface. (d) Proposed molecular model showing the STM image of the precursor **(2)**/TCDB complex. (Reprinted with permission from Ref. [120]).

template. As a result, various adsorbate-adsorbate and substrate-adsorbate interactions largely determined the architecture of each assembly and affect their performance in a materials setting. Since the adsorption of the metallosupramolecules on HOPG is not stable, the shape-persistent macrocycles and hydrogen-based networks were used to immobilize these coordination metallocycles [100]. The STM results exhibited well-ordered adlayers of metallosupramolecules located above the underlying macrocycles. The H-bonded network formed by TCDB molecules can also be used to immobilize metallocycles [34]. The conformation of metallocycles in the TCDB networks is similar to that on Au (111) because the adaptability of TCDB networks.

Metal-phthalocyanines have received considerable attention due to their inherent planarity, electro-optical, and magnetic properties as well as the ability to bind with N-based ligands [101–104]. The supramolecular structures of Zn-Pc and Cu-Pc as well as their derivatives on the surface have attracted much attention [105–109]. Two individual ZnPc molecules can be immobilized in the TCDB network on the HOPG surface. The TCDB nanoporous network can also be used as the host network to accommodate CuPc molecules and finally form binary supramolecular architectures. A stable ternary supramolecular structure controlled by π-π stacking interactions and hydrogen bonding was observed [109]. FePc molecules can form Kagome networks on highly-ordered graphene monolayer (MG), which stacked on a Ru substrate [110]. The STM measurements showed that the epitaxial MG acted as an effective template for the self-assembly of magnetic FePc into a unique nanoarchitecture.

Additionally, metal porphyrin and phthalocyanine assemblies are some of the most promising building blocks for two-dimensional molecular patterning and the development of new functional properties [95,111–115]. A series of self-assembled imidazolylporphyrinatozin macrocycles from dimer to decamer consisting of different porphyrin units assembled large hollow rings [116]. These coordination-complexes can be further reinforced by covalent linking based on the ring-closing metathesis reaction using Grubbs's catalyst. After deposition onto the Au (111) surface, a real 2D structures of the coordination-assembled porphyrin decamer and pentamer macrorings were observed under UHV conditions [117]. The bright spot correspond to the dimer unit including two ferrocene moieties and two central porphyrins. The absence of clear internal structure suggests that the porphyrin planes are not sitting on the metal surface. In addition, the high-resolution STM image did not show unclear circular image for the decamer ring without covalent linking, indicating that the coordination alone is not sufficient to maintain the supramolecular structure of decamer on the metal surface. Therefore, the covalent of the coordination pairs played an important role on reinforcing the supramolecular structure on metal surface. Note that the multiple coordination sites of these macrocycles would make them versatile hosts for a wide variety of guest molecules.

Except for 2D coordination molecules, coordination complexes can also form extended 2D supramolecular architectures. The precise control of the molecular self-assembly is important for functional nanostructures. Zn-porphyrin derivative formed a multilevel and ordered chiral hexagonal porous architecture, including α-chirality and β-chirality on the Ag (111) surface [118]. A copper coordinated supramolecular complex (Cu^{II} complex, Fig. 6) was formed by coordinating one Cu^{2+} bound with six TTF-triazole ligands that were substituted with benzyl [119]. The ligand (L) was composed of TTF moieties and triazole, which are linked through the C–C single bond. On the HOPG surface, the Cu^{II} complex can spontaneously form a large-area periodic rectangular pattern. The length and width of the recorded bright rectangles were estimated to be 1.5 nm and 0.5 nm, respectively. Each rectangle was assigned to parallel L molecules. The dark crossing region might be occupied by Cu^{II} as shown in the high-resolution STM image Fig. 6(c). The adjacent L molecules with opposite direction formed the 2D array through π-π interactions. Therefore, the adsorption geometry of the metalcomplex relies on the complex structure as well as intermolecular interactions.

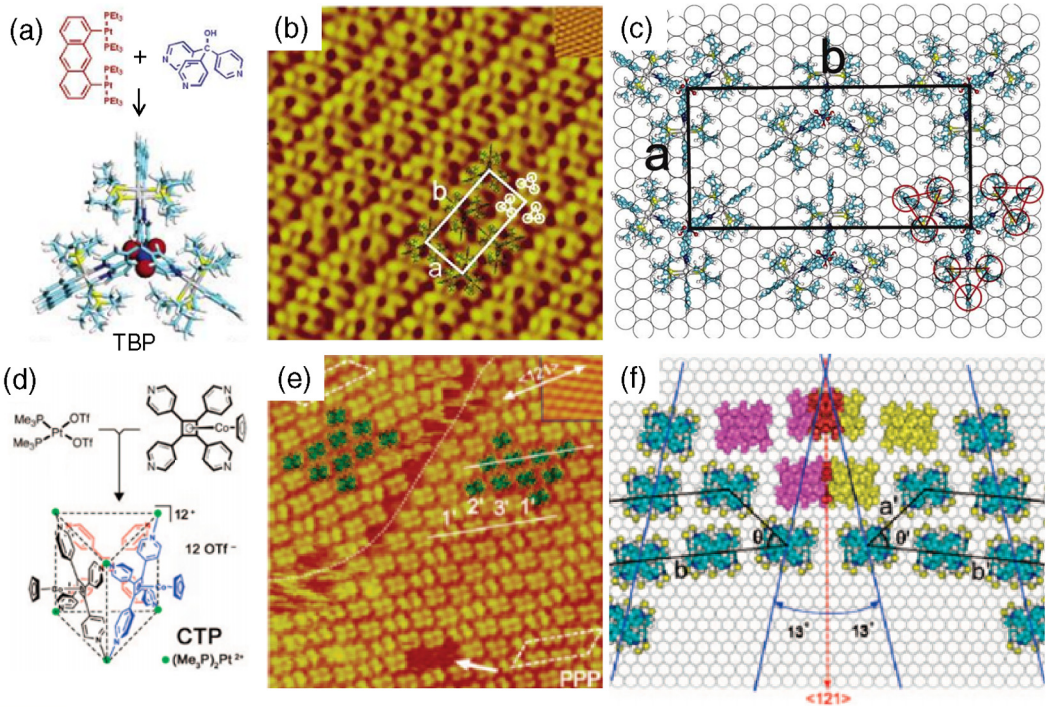

Fig. 8. (a) Chemical structure of TBP. (b) High-resolution STM image of the adlayer of TBP and showing the underlying Au (111)-(1 × 1) lattice in the upper right corner. (c) Proposed structural model for the adlayer. (d) Chemical structure of CTP. (e) High-resolution STM images of the adlayer of CTP on Au (111) and (f) proposed structural model and unit cell of the CTP adlayer. (Reprinted with permission from Ref. [98,122]).

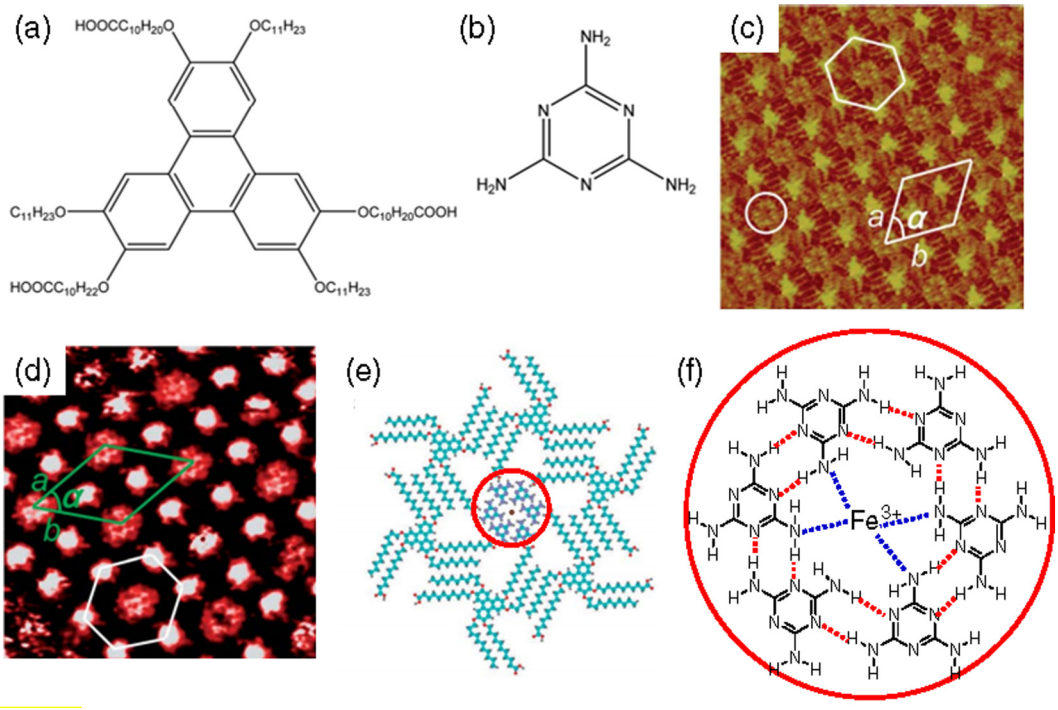

Fig. 9. (a) and (b) Chemical structures of *sym*-TTT and melamine, respectively.(c) High-resolution STM image of *sym*-TTT/melamine network. (d) High-resolution STM image showing *sym*-TTT/melamine/Fe(III) ion structure. The circle indicates the *sym*-TTT/melamine structure, still an empty cavity. (e) Proposed molecular model for the *sym*-TTT/melamine/Fe(III) ion structure. (f) The schematic diagram of $[Fe(melamine)_4]^{3+}$ model. The red dashed lines indicate N/H–N H-bonds and the blue dashed lines represent the metal–ligand coordination between Fe(III) ion and four amino-groups of four melamine molecules, respectively. (Reprinted with permission from Ref. [127]).

3.1.2. Three-dimensional nanocages

On the HOPG surface, the sole 3D nanocage structure cannot be stably immobilized [120]. The supramolecular TCDB network was used as a host network to accommodate the Ir^{III}-based polytungstate cluster $K_{12}Na_2H_2[Ir_2Cl_8P_2W_{20}O_{72}]\cdot 37H_2O$ (**1**) and precursor $Na_8[HPW_9O_{34}]$ (**2**), leading to the formation of the TCDB/(**1**) and

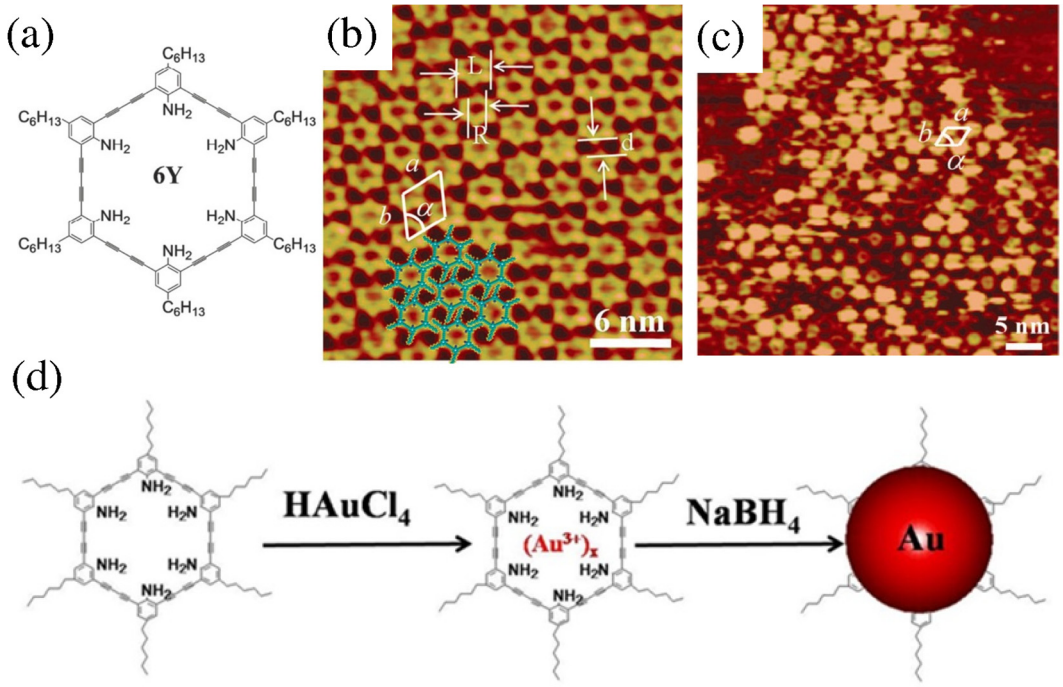

Fig. 10. (a) Chemical structure of 6Y. (b) High-resolution STM image of 6Y on HOPG surface with unit cell and tentative molecular model. (c) STM image of AuNPs on HOPG surface upon addition of $HAuCl_4$ and $NaBH_4$ after washing with ethanol–water mixed solution. (d) Schematic illumination of the formation of AuNPs. (Reprinted with permission from Ref. [128]).

TCDB/(**2**) structures. STM images (Fig. 7) show that the Ir^{III}-based polytungstate cluster (**1**) entrapped in the TCDB cavity appeared as an S-shaped feature with a measured length of 2.1 ± 0.1 nm and width of 1.9 ± 0.1 nm. While the $Na_8[HPW_9O_{34}]$ ensemble appeared as bright semicircle spots on HOPG with a length of 1.6 ± 0.1 nm and width of 1.2 ± 0.1 nm. These two clusters adsorbed onto the surface with distinctive crystalline structures in the presence of host networks.

There is another STM study of a 3D metallocage constructed by D_{3h}-symmetric TBP on Au (111) surfaces [98,121]. The 3-fold symmetric metallocage exhibits a propeller shape when viewed from above, but when viewed from the side, appears as a rectangle. The high-resolution STM image (Fig. 8) revealed that such 3D nanocages can form regular molecular rows of assemblies with well-ordered adlayers on gold surfaces. Each ordered row contains sets of nine bright spots, which correspond to TBP cages. In addition, well-ordered chiral domains formed after depositing a racemic mixture of chiral CTP on both the bare and nonchiral Au (111) surfaces [122]. This is a facile method to fabricate 2D chiral structures by using 3D self-assembled metallacages. Moreover, the fabricated chiral surface has great potential for applications in chiral sensing and stereo-selective syntheses.

3.2. On-Surface coordination reaction

Due to the selectivity, directionality and high bonding strength of metal-organic bonding, various metal-ligand coordination interactions have been utilized to construct metallo-supramolecular polymers in solution for nanoscience and nanotechnology applications [123–125]. Different from direct self-organization of metal-organic coordination molecules on the surface, the synthesis of coordination complexes on the surface is controlled by choosing suitable ligands and metal ions. The coordination supramolecules can be obtained by depositing ligand solution onto the modified surface with prior metal clusters or by depositing metal onto a preformed ligand monolayers and even mutilayers, or by depositing a mixed solution onto the surface [126]. This section summarizes the synthesis of supramolecular structures with transition metal and organic ligands including amido (—NH_2, —C═N—), carbonitrile (—C≡N) and carboxylate (—C═O) as well as the thermodynamic process for self-assembly.

3.2.1. Metal-amido coordinated complexes

A symmetric triphenylene derivative with three carboxyl groups (*sym*-TTT) and Mel can form 2D porous multi-component network though hydrogen bonding [127]. In the *sym*-TTT/Mel system (Fig. 9), every close-packed network formed by six *sym*-TTT molecules capture six melamine molecules connected by a kind of double hydrogen bond (N···H—N), leading to the formation of a hexagonal structure. Accordingly, all carboxylic acid groups participate in the formation of the H-bonding, while amino groups inside the melamine cluster create functionalized nanopores. Thus, only the melamine can coordinate with iron ions upon addition of the $Fe(ClO_4)_3{\cdot}6H_2O$ solution. Notably, the Fe-coordination structure is in fact distorted hexagonal rather than a sixfold symmetric structure, which further indicates that the formed structure has only four-ligands, rather than six.

Except for the metal-ligand coordinated complexes, the on-surface assembly can also be used as a template to fabricate nanoparticles via metal-ligand interactions. Gold nanoparticles were prepared by directly depositing $HAuCl_4$ solution and deoxidizer $NaBH_4$ on the ligand network as a template at solid/liquid interface [128]. The statistical measurements from STM image showed the size of the fabricated gold nanoparticles (AuNPs) have a narrow distribution of 2.2 ± 0.1 nm. It was suggested that the Au^{3+} was first bound to the amine-substituted macrocycle, 6Y, via metal-ligand interactions (Fig. 10). The relatively faint spots on the HOPG surface may result from $AuCl_4^-$ clusters interacting with amine groups inside the macrocycle. After chemical reduction by the addition of $NaBH_4$ solution, bright, large sphere-shaped spots appeared. Therefore, gold nuclei grew into larger nanoparticles after Au^{3+} ions were reduced to Au atoms. The direct growing

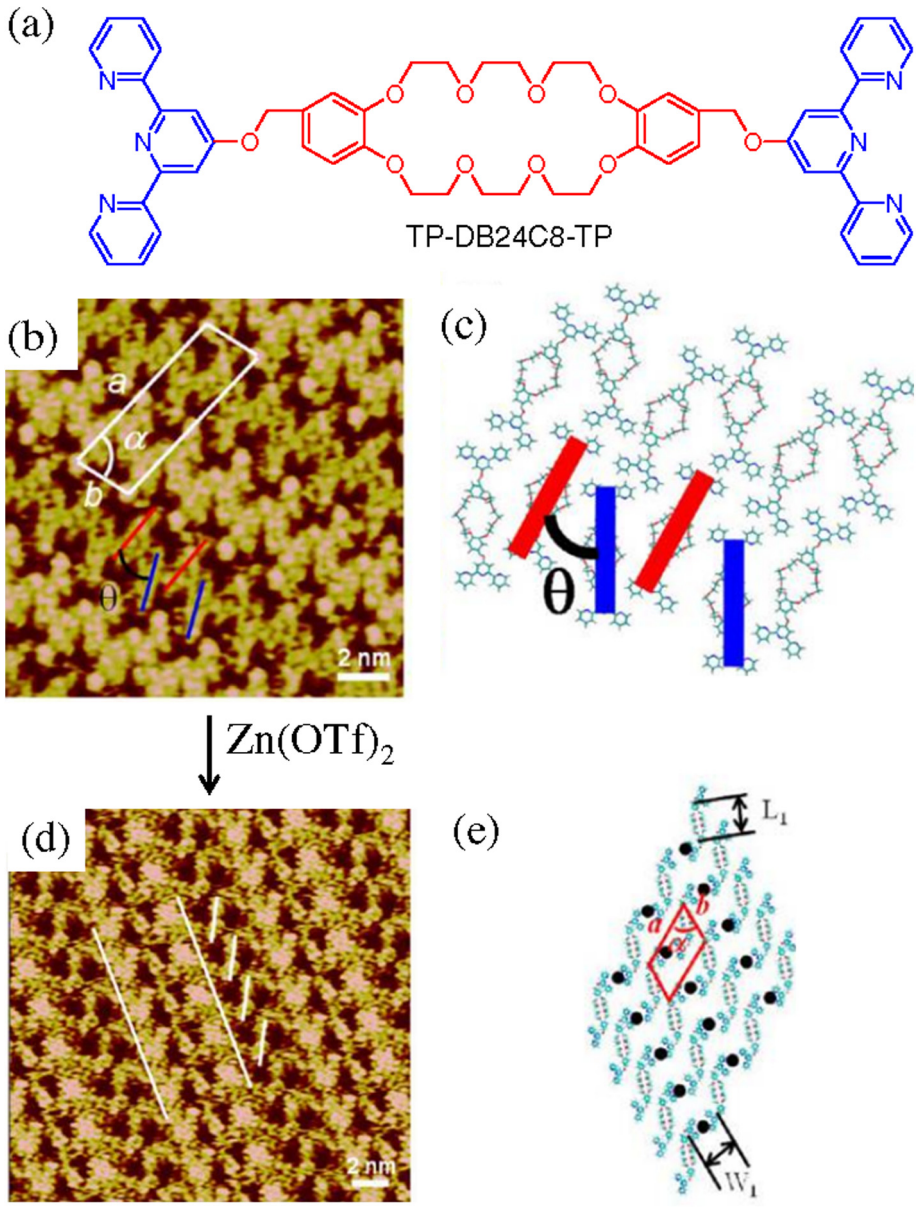

Fig. 11. (a) High-resolution STM image of the self-assembled structures of monomer TP-DB24C8-TP at the 1-phenyloctane/HOPG interface. (b) A suggested molecular model corresponding to the observed structure in (a). (c) High-resolution STM image of the self-assembled structures after metal coordination treatment of the TP-DB24C8-TP-covered HOPG surface. (e) A suggested molecular model corresponding to the observed structure in (c). (Reprinted with permission from Ref. [137]).

of gold nuclei on HOPG should be ascribed to the coordination interaction between the surface atoms of AuNPs and the surface template. Additionally, the rigid macrocyclic backbone structure of 6Y suppressed the further growth of AuNPs during the reduction step. Although there is no evidence for the formation of metal-ligand complexes, the obtained gold nanoparticles proved metal-ligand interactions did occur.

Pyridine derivatives are important ligands in supramolecular coordination chemistry, as the N atom can coordinate easily with various transition metals through strong metal-organic coordination interactions. Based on these metal-pyridine coordination interactions, stable 1D nanochains and 2D MOCNs were constructed under UHV system [129–131]. After thermal treatment of glutamic acid-modified nickel nanoclusters, 1D metal-organic coordination networks formed on Au (111) [132]. The STM results showed that Ni clusters with initial diameters <3 nm were completely corroded, and 1D molecular chain features were observed by the adsorption of (*S*)-glutamic acid at 350 K. There are two distinct pyroglutamate chains stabilized by ionic interactions and intermolecular hydrogen bonding interactions, respectively. Afterwards, 1D chains containing approximate 20 units formed on Au surface partially covered with smaller Ni cluster (diameter of ~1 nm) [133]. The chirality of the pyroglutamate affected the growth directions of chains. Similarly on Au (111) surfaces, a simple one-step approach can also be used for the preparation of stable 1D MOCP in ambient air conditions [134]. The MOCPs were synthesized by dropping a heated solution of DHBQ ligands and copper ions onto a preheated Au (111) surface. However, no ordered structures could be observed after the subsequent depositing of the ligand and metal ion solution onto the surface, which might be due to the absence of ligand monolayers.

Many metal-organic complexes can be formed by *in situ* addition of metal salt solutions on pre-assembled structures. There is an *in situ* STM study of metal-organic coordination-driven

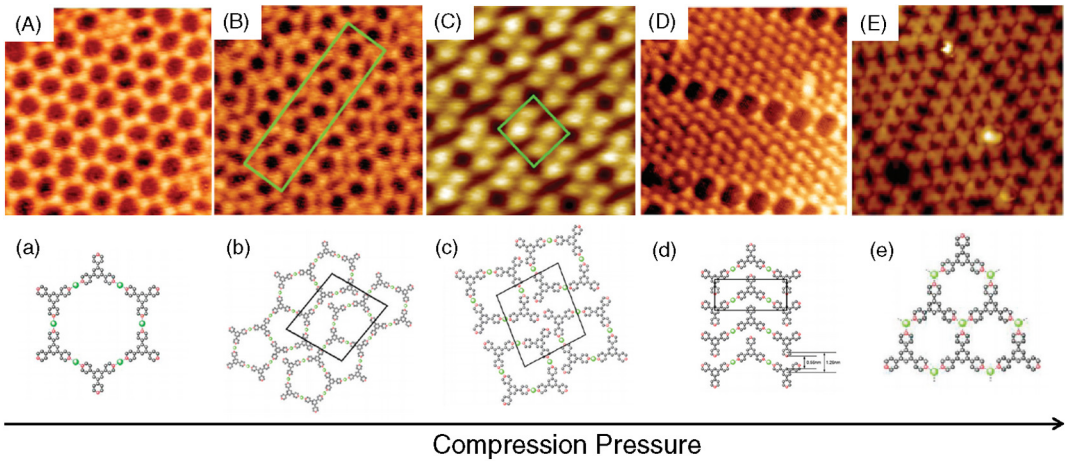

Fig. 12. (A) High-resolution image of the TPyB-Cu honeycomb networks. (B) High-resolution image of the pentagon network. (C) High-resolution image of the rhombic cyclic network. (D) High-resolution image of the zigzag phase. (E) High-resolution image of the phase formed at a molecular density of 0.47 TPyB/nm^2. (a)–(e) Structural models corresponding to the STM images A, B, C, D, and E, respectively (Cu in green and N in red). (Reprinted with permission from Ref. [104]).

supramolecular self-assembly at the solid/liquid interface [135]. As a preliminary step, two-dimensional orderings of symmetric and asymmetric alkylated BP derivatives were formed at the 1-heptanol/HOPG interface, which was recorded by STM. Then, the functionalized bipyridine derivatives were used as coordination scaffolds, followed by the addition of meal salts, such as Pd$(OAc)_2$, $PdCl_2$, $Cu(OAc)_2$, and $CuCl_2$, and leading to the formation of metal-organic patterns. The intermolecular distance that depended on the functionalized units within bipyridine monolayers was critically important to determining whether the coordination had occurred. When the urea group attached to BP, the intermolecular distance was too small, meaning coordination did not occur. However, complexes can be observed upon *ex situ* or *in situ* addition of a metal complex to alkylated bipyridine derivatives. Overall, coordination between metal ions and 2D ordering of bipyridine can lead to identical 2D orderings. For a series of bipyridine derivatives with different lengths of alkyl chains, there is a coordination-driven odd-even effect [136]. The STM results indicated that the bipyridine molecules assembled into 2D odd-even alternating structures. However these kinds of assemblies can be transformed into lamellar structures upon coordination with Pd^{2+} from $Pd(CH_3CN)_2Cl_2$. Furthermore, the odd-even effect was quenched because of molecular width variation, which indicates that tuning molecular width could be an effective strategy in controlling the assembled structure.

By using metal-ligand interaction, metal-organic complexes can also be constructed directly on surface. For example, a linear orthogonal supramolecular polymer was formed by an on-surface coordination reaction between a low-molecular-weight monomer TP-DB24C8-TP and $Zn(OTf)_2$ [137]. The TP-DB24C8-TP was synthesized by linking dibenzo-24-crown-8 with two terpyridine units. TP-DB24C8-TP can assemble into large-scale regular patterns on the HOPG surface (Fig. 11) via weak intermolecular interactions, including π-π interactions, hydrogen bonding between tripyridine groups, and van der Waals forces. After a suspension of $Zn(OTf)_2$ in acetonitrile/chloroform was deposited onto the assembled pattern, the surface morphology significantly changed due to the formation of a supramolecular complex (TP-DB24C8-TP/Zn^{2+}) through metal-ligand interactions. Each Zn^{2+} ion bound to two pyridine groups of two adjacent monomers, resulting in an extended 2D structure on HOPG surface.

However, the size of the polymeric chains is difficult to control due to the variable external parameters. Therefore, it is necessary to further understand the polymerization mechanism. The self-assembled 1D polymeric chains of multifunctional monomers, through metal-organic coordination interaction, are thermodynamically equilibrated structures due to the reversibility of the coordination bond [138]. By using the STM technique, a chain growth mechanism attributed to the polymerization of multi-strand polymers was firstly discovered on the Au (111) surface, however the polymerization in solution obeyed the step-growth mechanism. In particular, the balance between the surface diffusion barrier and the binding energy played an important role on the growth of multi-strands. After varying growth temperature and adding specific molecular modulators, both the length and width of the polymers were controlled. The formed monodisperse double-strand and triple-strand ladders depend on the molecular structures of monomer compounds. These results revealed the self-assembly process and uncovered the mechanism of metallo-supramolecular polymerization at the molecular level.

The formed coordination networks can be tuned by external stimulus such as pressure, temperature, illumination and so on. Moreover, the formation of coordination structures can be induced by changes in molecular density. Using TPyB as a molecular ligand, the structural transformation of TPyB-Cu coordination networks was driven by in-plane compression [104]. Firstly, a honeycomb network is observed (Fig. 12). With increasing molecular density, it transforms to a pentagonal network or rhombic structures at a molecular density of 0.34 TPyB/nm^2, then to a zigzag structure at a molecular density of 0.40 TPyB/nm^2, and finally to a triangular network at a molecular density of 0.47 TPyB/nm^2. This kind of structural change may result from the transformation of the coordination binding mode, which undergoes a change from 2-fold Cu-pyridyl binding in the honeycomb, pentagonal, rhombic and zigzag structures to 3-fold Cu-pyridyl coordination in the triangular structure. This study demonstrates that the coordination configuration of Cu-pyridyl can be altered by the modification of compression, offering a promising route in 2D supramolecular self-assembly.

These distinctive coordination structures discussed above mainly resulted from the modification of compression, which may provide an alternative technique for surface-confined supramolecular self-assembly. On the other hand, bi-metallic systems exhibiting new properties or functions, due to their two metal sites, have attracted considerable attention. A 2D bimetallic coordination system was formed by co-depositing Cu atoms with Zn-TPyP molecules onto Au (111) surfaces [139]. Zn-TPyP molecules coordinated with Cu atoms through twofold pyridyl-Cu coordination bonds have led to extended two-dimensional networks. Besides the rhombic lattice there are two types of coordination structures, including disordered networks and rosette structures,

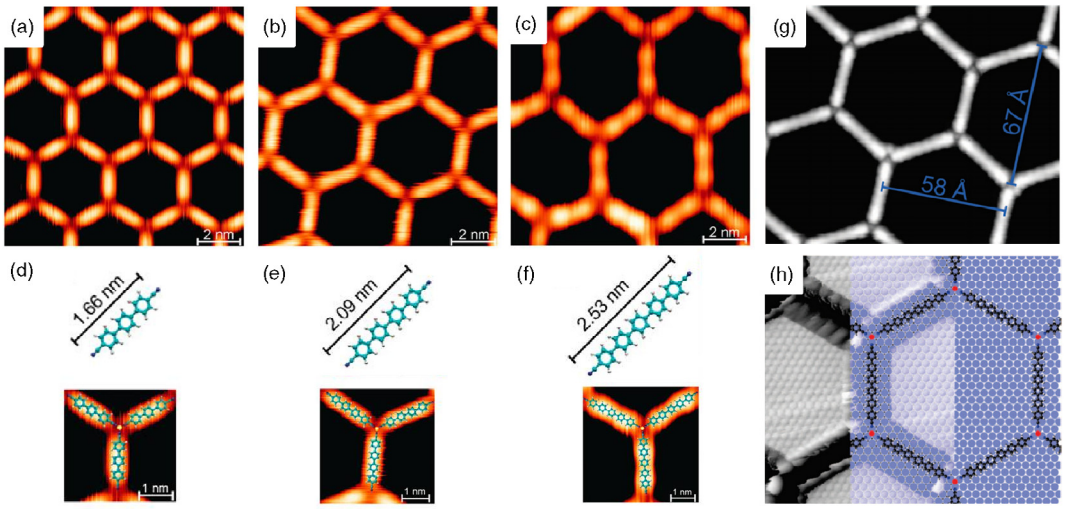

Fig. 13. STM images of Co-directed assembly of NC-pH_3-CN (a), NC-pH_4-CN (b), and NC-pH_5-CN (c) on Ag (111) surface, respectively. Molecular structures of NC-pH_3-CN (d), NC-pH_4-CN (e), and NC-pH_5-CN (f) including their length and models of the threefold Co-carbonitrile coordination motif resolved in images of (a), (b), and (c), respectively. Super-lattice of NC-pH_6-CN featuring a 67 Å pore diameter on Ag (111) surface (g) with a corresponding ball model (h). (Reprinted with permission from Refs. [144,145]).

produced after the co-deposited sample was annealed at 150 °C, as a result of labile coordination. Note that annealing at a higher temperature of 200 °C, close-packed arrays with larger rhombic lattices can only occur through hydrogen-bonding between Zn-TPyP molecules. In this case, the Cu coordination might be suppressed. When the concentration of Cu atom was increased, a reversible transition could be achieved. Such reversible conversions might exemplify a unique strategy to dynamically control the supramolecular structures on surfaces. This structure offers possibilities for exploring bi-functionality of the Zn and Cu sites.

In another system, TPyP molecules coordinated neutral Cu(0) with N atoms from peripheral pyridyl groups and porphyrin macrocycles at 300 K [140]. After elevating the temperature to 450 K, the coordinated Cu(0)-porphyrin macrocycle underwent an intramolecular oxidation to Cu(II). The Cu(0)-TPyP complex was transformed to Cu(II) TPyP oxide. As a result, the coordination between one Cu(0) and two pyridyl groups of neighboring TPyP molecules resulted in the formation of metal-organic coordination network by linear pyridyl−Cu−pyridyl bridges. When the temperature was increased to 570 K, the pyridyl-Cu-pyridyl bridges degraded, and the stable Cu(II)-TPyP complexes formed a close-packed structure similar to a Zn(II)-TPyP assembly, which is stabilized by weak intermolecular interactions. It should be noted that free Cu(0) atoms diffused into the Au (111) substrate. Above 520 K, this network and any Cu atoms in linking positions diffuse into the substrate. The coordination bonds can be disrupted and new coordination bonds formed between Co atoms and N atoms of porphyrin. A metal-free porphyrin molecule, DPPyP, bearing two pyridyl for coordinating sites can form a close-packed self-assembled structure with a rhombic unit cell on Ag (111) surface at room temperature [141]. Upon deposition of Co atoms onto the pre-formed monolayer, Co atoms coordinate with N atoms of pyridyl groups, resulting in a hexagonal porous network. After annealing the sample at 450 K, the porous network was transformed into another close-packed structure. In fact, the coordination of Co with peripheral pyridyl groups was transformed to coordination with the DPPyP macrocycles.

3.2.2. Metal-Carbonitrile coordinated complexes

Carbonitrile compounds can coordinate strongly with transition metal centers [142]. The linear dicarbonitrile-based polyphenyl species NC–Ph_n–CN (n = 3, 4, 5) can self-assemble into a series of 2D coordination honeycomb networks with Co atoms on a crystal Ag (111) surface [143,144]. These four simple molecules all have the same carbonitrile endgroups, while the lengths of these monomers increase with *n* from 1.66 nm to 2.53 nm. (Fig. 13) By controlling the reaction of central cobalt atoms with pre-adsorbed molecules, a group of open multi-level nanomeshes can be realized, such as close-packed chevrons, open rhombic networks, and nanoporous chiral kagomé lattices. By using this approach, a controlled open nanomesh with pore diameter up to 6.7 nm was successfully fabricated by Co-directed assembly of NC–pH_6–CN on Ag (111) [145]. These honeycomb nanomeshes were extended over μm^2 areas and were thermally robust. With increasing number of phenyl units in the molecular backbone, the cell size of the enclosed hexagons expanded stepwise from 10 nm^2 to 15 nm^2, then from 20 nm^2 to 24 nm^2 (when $n = 3, 4, 5, 6$ respectively). In all cases, the supramolecular structures based on dicarbonitrile coordination with Co centers on Ag (111) substrate are of a highly structural quality. The formation of a large pore with perfect regularity would open opportunities for organizing such materials at the nano scale and exploring 2D systems with confined molecular rotation.

Conducting a detained minute structural analysis of the surface supported Co-linked NC-pH_3-CN molecules on Ag (111), different surface patterns formed depending on the constraints applied to the system [146]. For example, when Co atoms are added to the NC-pH_3-CN phase at room temperature, they coordinate with NC-pH_3-CN ligands in a 3-fold motif. As a consequence, the extended regular honeycomb nanomeshes, with two rotational domains, formed due to the appreciable mobility and absence of spatial constraints at the surface. In the process of cooling the sample down to about 10 K, free molecules not linked by Co atoms assemble about the honeycomb domains to minimize the number of impeding carbonitrile groups. An additional Co-directed, six-star configuration that can fully disorder the networks was identified when additional constraints (Co deficiency, kinetic or spatial limitation) were imposed. These STM results demonstrate long-range ordered, periodic networks should be associated with substrate epitaxial fitting, lateral interactions, as well as the conformational flexibility of ligands. With diazo N-based moieties and carbonitrile as possible ligands, *trans*-DMC was chosen as a building block for constructing coordination structures on Au (111) [147]. Low-temperature STM highly resolved the string-shaped

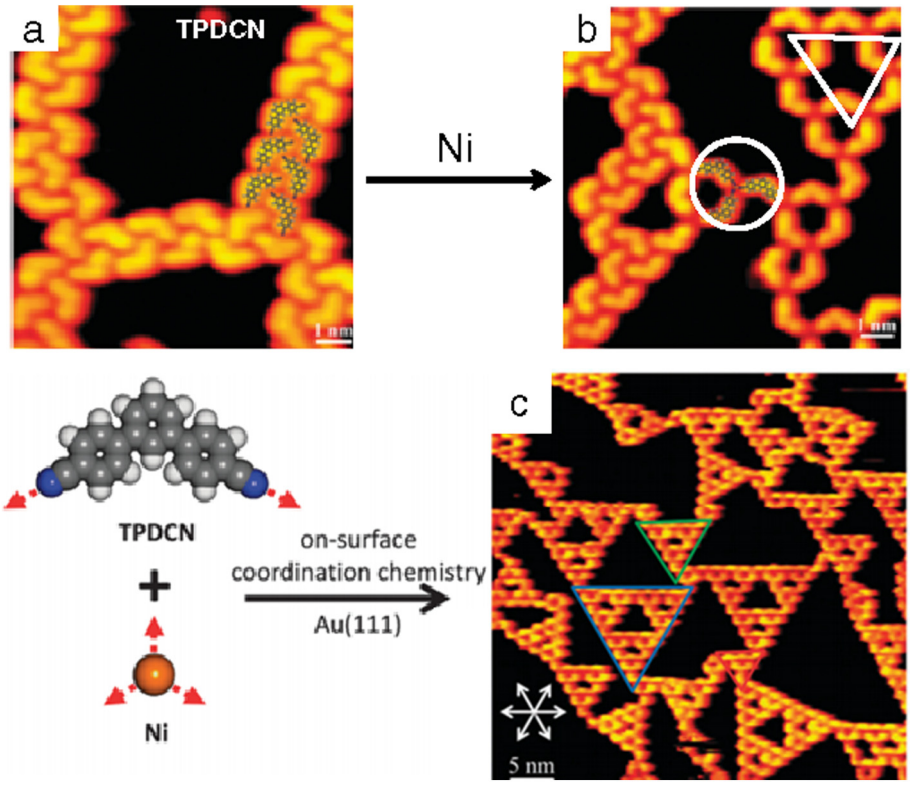

Fig. 14. (a) STM images of the self-assembled chain structures formed by the TPDCN molecules on Au (111), (b) STM images show the appearance of the coordination structures after depositing a small amount of Ni atoms on the TPDCN covered surface. (c) STM images showing the formation of the metal–organic Sierpiński triangles after codeposition of TPDCN molecules and Ni atoms on Au (111). (Reprinted with permission from Ref. [149]).

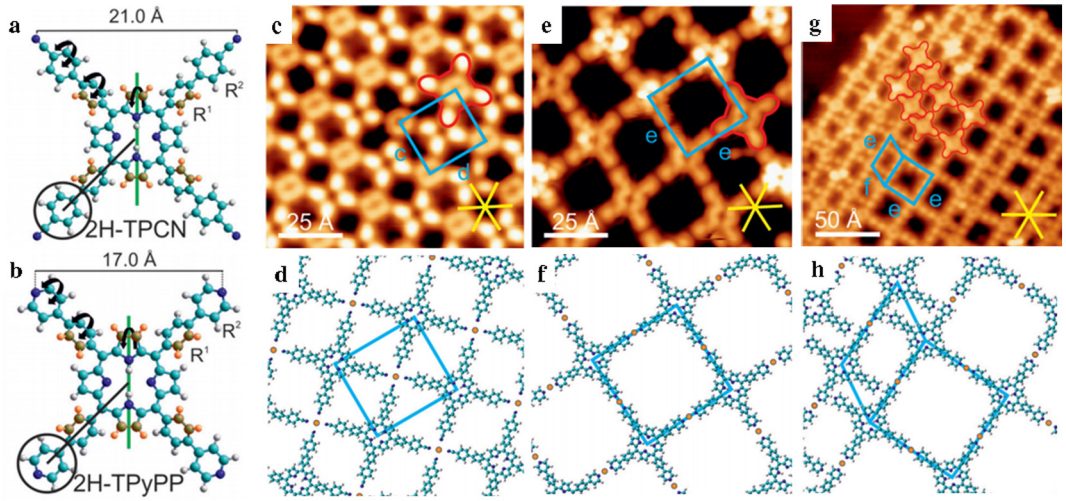

Fig. 15. (a, b) Structural models of the porphyrin derivatives TPCN and TPyPP, respectively. (c, e) Formation of metal-organic networks upon deposition of Cu atoms for TPCN and TPyPP, respectively. (d, f) Model sketches of the networks corresponding to (c) and (e). (g, h) STM image and model of TPyPP/Cu depending on the (local) Cu density. (Reprinted with permission from Ref. [150]).

Co-coordinated metal-organic motif, which exhibited a disordered structure due to the assembly of molecules with degrees of freedom. Here, different characteristics of the coordination bond of a transition–metal atom to N atoms with different chemical surroundings can be selectively probed.

TCNQ as a strong electron-accepting molecule has been used to form various surface coordination nanostructures by controlling the fabrication parameters. On Cu (100) surface, a 2D monolayer formed by mixing Mn atoms and TCNQ molecules [148]. STM images showed that the Mn-TCNQ compound exhibited a long-range ordered square network including 4-fold coordinated Mn centers. The close-packed TCNQ molecular phase converts to the Mn-TCNQ network phase with a quantitative yield as Mn coverage on the surface increases. Two domains of the network, with different orientation, show distinct organizational chirality with an angle difference of 16°. Strong bonding of TCNQ with both the

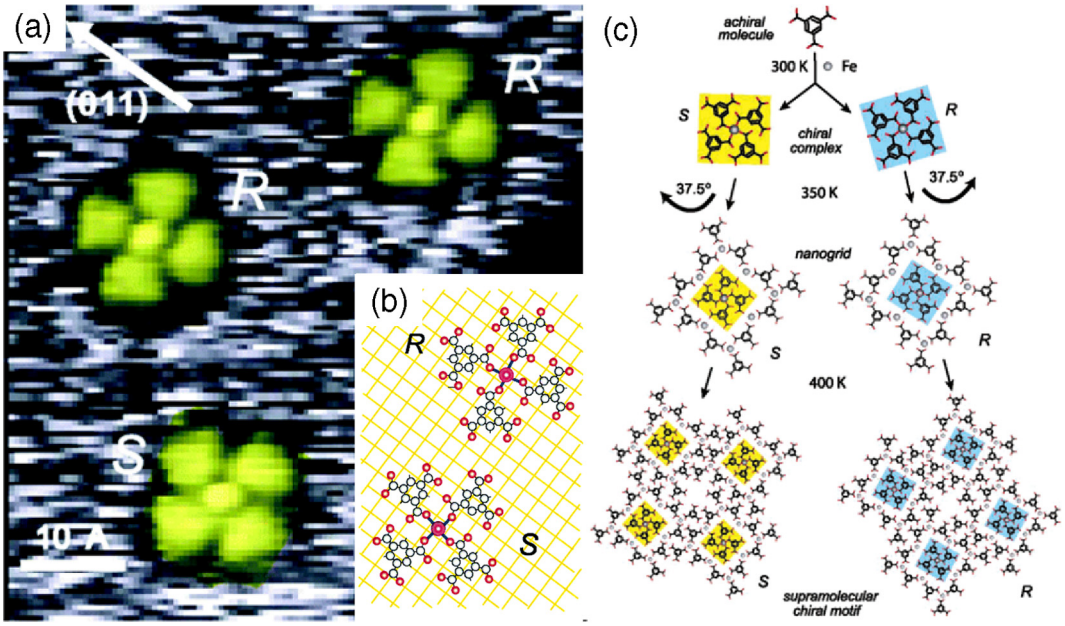

Fig. 16. (a) High-resolution image showing the two $Fe(TMA)_4$ stereoisomers, labeled *R* and *S*, representing mirror-symmetric species with respect to the [011] substrate direction. (b) A corresponding model. (c) Hierarchical assembly of simple achiral TMA with Fe. (Reprinted with permission from Refs. [151,152]).

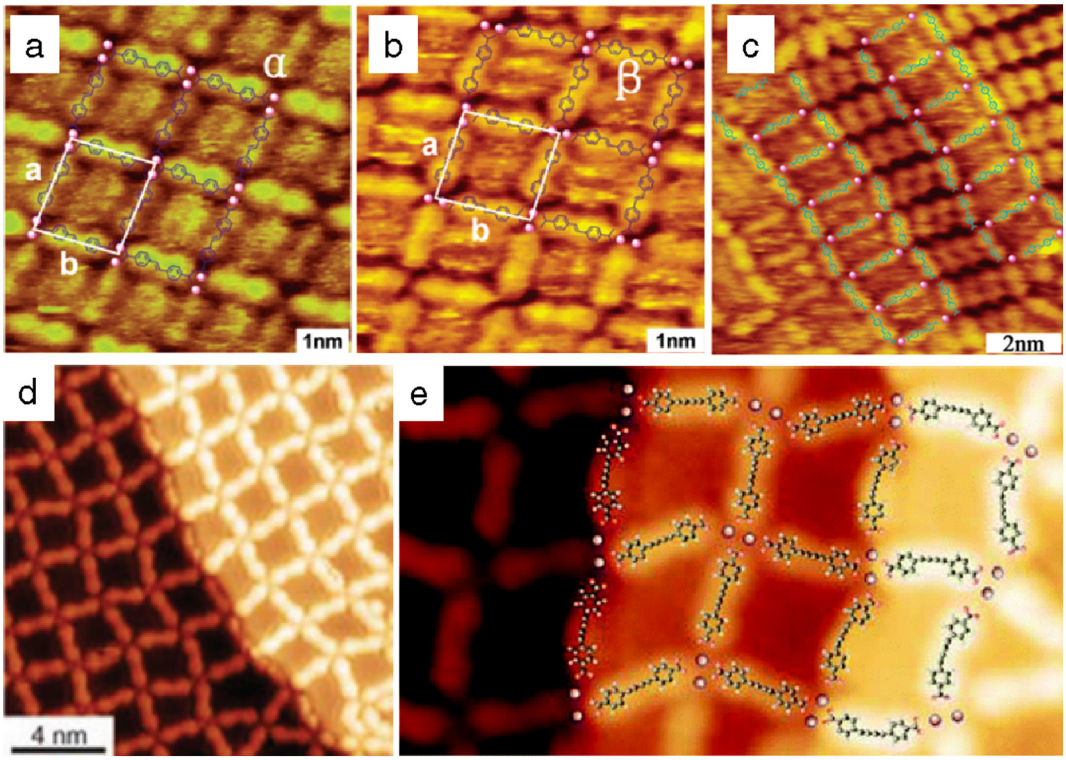

Fig. 17. High-resolution STM images with molecular models of α (a) and β (b) phase. (c) Specific configuration for the ladder structure with two Mn atoms coordinating with three SDA molecules. (d) High-resolution STM topographs of BDBA-Fe MOCNs crossing a Au (111) step. (e) The submolecular resolution exhibits the configurational degree of freedom of the edge molecules. (Reprinted with permission from Refs. [154,155]).

Mn adsorbate and the surface Cu atoms occurred, as indicated by the formation of a complex charge-transfer scenario and revealed by electronic-state analysis.

Recently, metal-organic Sierpiński triangles were successfully constructed by on-surface coordination on Au (111) [149]. The influence of a deposition method on metal-organic nanostructures was observed. As shown in Fig. 14, the TPDCN molecules formed chain-like structures through intermolecular hydrogen bonding between —CN groups and phenyl groups when deposited onto the Au (111) surface at room temperature. When a small amount of Ni were deposited on the pre-covered TPDCN surface, a portion of chain-like structures evolved into Sierpiński triangles, as marked by the white triangle in Fig. 14. Upon closer inspection of the coordination motif, Ni coordinated with three CN groups belonging to

three TPDCN molecules and formed a threefold structure marked with a white circle. Astonishingly, after depositing a mixture of Ni atoms and TPDCN on the Au (111) surface, more ordered Sierpiński triangles with different generations were constructed. In particular, the first generation and second generation structures were observed, as highlighted by green and blue triangles in Fig. 14. Note that this metal-organic structure showed high thermal stability and could withstand thermal treatment up to 45 K.

As discussed above, the excellent combination of organic (or metal-organic ligands) and metal atoms has yielded various structures with functional properties. Specifically, molecular functional groups and metal atoms play an important role in the engineering of metal-organic architectures. Very recently, how functional groups attached on metal-organic molecules and the effects of metal density on the coordination of nanostructures were disclosed through low-temperature STM experiments [150]. Two porphyrin derivatives such as TPCN and TPyPP functionalized with cyano and pyridyl substituents were selected. After consecutive depositions of ligand and Cu atoms onto the Ag (111) surface, two distinct networks formed due to spatial constraints around the coordination centers. TPCN formed fourfold-coordinated networks with small pores, whereas TPyPP formed metal-organic networks with large pores and twofold coordination nodes (Fig. 15). Importantly, TPCN directly formed reticulated coordination architecture, and in contrast, TPyPP hierarchically coordinated with Cu atoms upon increasing density of Cu atoms. A chain-like porous array appeared when a small amount of Cu atoms were deposited onto the TPyPP submonolayer. When the dosage of Cu exceed a 1:1 Cu:TPyPP ratio, the intermolecular interactions were transformed into N—Cu—N coordination bonds and a fully reticulated network formed. This study introduced prospects for controlling metal-organic architectures by design molecular and monoatomic building block.

3.2.3. Metal-carboxylate coordinated complexes

TMA has been considered a polyfunctional carboxylic acid due to its threefold symmetry. After co-depositing Fe and TMA onto a Cu surface at low temperature, a unique arrangement formed [151]. When Fe and TMA are deposited in a ratio of 1:4, flower-shaped structures formed with central Fe atoms surrounded by four TMA molecules (Fig. 16). The peripheral TMA molecules did not point toward the central Fe atom, and the oxygen atoms involved in the bonding are closer to the Fe atom. As a consequence, the species marked *R* and *S* are mirror-symmetric complexes in two dimensions. Further increasing the ratio of Fe atoms resulted in extended Fe-TMA nanostructures [152]. The hierarchical assembly of Fe-TMA architectures was observed at single-molecule level. Recently, a chiral domain assembled from another acid, TPA, and Fe atom on a Cu (110) surface was obtained [153]. Using STM, the evolution of hierarchical assembly of the supramolecular structures was recorded. It was suggested that the competition between the coordination bonding and hydrogen bonding was the main factor driving the generation of such chiral architectures.

Like TMA and TPA molecules, linear SDA can also be used as a linker in coordinating with transition metals. STM study indicate that Mn-SDA-coordinated complex can form metal-ligand networks on Au (111) surface (Fig. 17) [154]. In two types of network phases, the node Mn atoms adapted parallel or perpendicular geometry relative to the adjacent units. Due to the substrate reconstructions, the periodic alteration of configurations resulted in a herringbone structure of the substrate; while a novel ladder-type structure appeared for a surface oversaturated with SDA, revealing that the Mn atoms had different locations under different binding conditions. More recently, highly adaptable 2D-MOCNs formed by coordinating the rod-like ligand BDBA with iron atoms on both Au (111) and Ag (100) surfaces [155]. When a Fe:BDBA ratio of 1:1 was employed, triangular and pentagonal BDBA-Fe networks with iron dimers at the nodes formed on the surfaces demonstrated by the UHV-STM investigations. Due to the flexible conformation of the butadiyne backbone, BDBA exhibits a high degree of orientation, which resulted in the independence of the formed MOCNs on the substrate. Note that four carboxylate groups from BDBA molecules coordinated with Fe adatoms in two modes at each network node. On both Au (111) and Ag (100) surfaces, the MOCNs are robust against thermal treatment greater than 490 K despite their flexibility.

Additionally, 1D metal-organic coordination chains can be formed by thermal treatment of glutamic acid-modified Ni clusters on Au (111) [132]. At 300 K, the adsorption of glutamic acid completely destroyed the Ni clusters. The formation of the 1D molecular feature was observed after annealing the glutamic acid-coated surface at 350 K. This further supports the idea that metal-organic coordination structures are mainly determined by the properties of ligands as well as the electronic structures of metal ions. Moreover, the coordination algorithm can be altered by the solid substrate, resulting in different coordination geometry. The influence of the valence states of metal ions on coordination geometry has been recently demonstrated by depositing different metal nitrates onto pre-formed hydrogen-bonded TMA [156]. The full orbital metal nitrates $AgNO_3$ and $ZnNO_3$ were directly embedded into the TMA networks, while the vacant orbital metal nitrates $Cu(NO_3)_2$, $Mn(NO_3)_2$, and $Fe(NO_3)_3$ formed new structures with different coordination bonds depending on the electron structures of incorporated metal ions.

3.3. Surface-participated coordination complexes

The location of functional molecules on a specific substrate is a crucial aspect of molecular devices [157]. Metal-coordinated structures adsorbed on various metal surfaces have attracted much attention because the geometry of the formed structures can be easily controlled by selecting appropriate organic ligands and metal substrates. As an important tool for visualization and characterization of coordinated supramolecular structures, the ability of STM to manipulate metal-coordinated structures has boosted research in surface-confined supramolecular coordination chemistry. To date, most of the reported coordination structures are formed and stabilized on Cu, Au or Ag surfaces. In this section, specific molecular coordination structures based on various organic ligands and Cu, Au or Ag adatoms have been reviewed.

3.3.1. Coordination of Cu surface

A study on *in situ* coordination between a porphyrin molecule H2PPIX and Cu substrate atoms was performed under UHV conditions [158]. On both Cu (110) and Cu (100) surfaces, the deposited H2PPIX molecules can form metalloporphyrin CuPPIX at room temperature. There are several factors influencing the metalation process, such direct molecule-metal contact enabled by the planar structure of the molecule; high density of metal atoms on the crystal surface; deprotonation rate of the molecule at room temperature, and so on.

On the Cu (100) surface, one kind of surface-confined 1D molecular chains formed by depositing the linear 1,4-bis(4-pyridyl) benzene and rigid 4,4′-bis(4-pyridyl)biphenyl molecules [159]. The chains were formed by the coordination of terminal pyridyl groups with Cu adatoms diffused from the substrate edges. The interaction is not only selective but also reversible; therefore, this type of self-assembly is very effective. STM images showed that the chain growth was partially affected by several dynamic aspects, such as commensurability, repulsion between molecular chains, and the metal-organic coordination bond on solid substrates. In the [110] direction, the 1D coordination chains exhibited clear

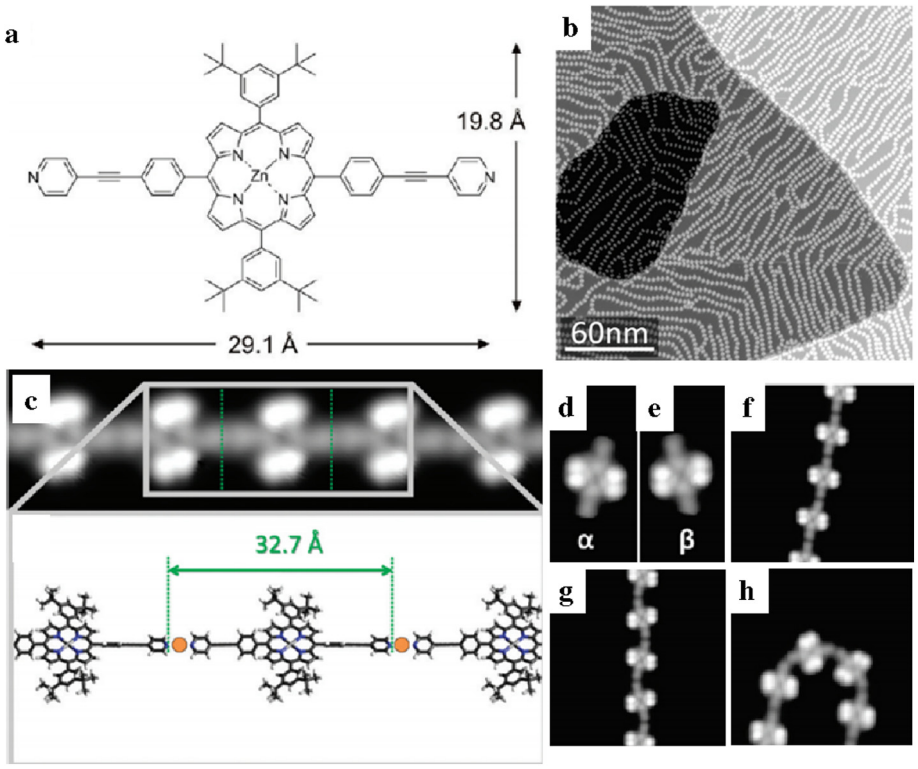

Fig. 18. (a) Chemical structure of porphyrin derivative. (b) STM images of Cu (111) surface after the evaporation of 0.4 ML (1 ML is defined as one surface fully covered by molecules) of porphyrin at a substrate temperature of about 350 K. (c) High-resolution STM image of a straight coordination chain segment of porphyrin derivative on Cu (111) with schematic plot of the pyridyl-Cu-pyridyl linear chaining arrangement. (d, e) STM images of the two conformational isomers α and β of porphyrin derivative on Cu (111). (f, g, h) Straight chain constituted only by α enantiomers, zig-zag chains constituted by alternating enantiomers and example of a U-turn, respectively. (Reprinted with permission from Ref. [161]).

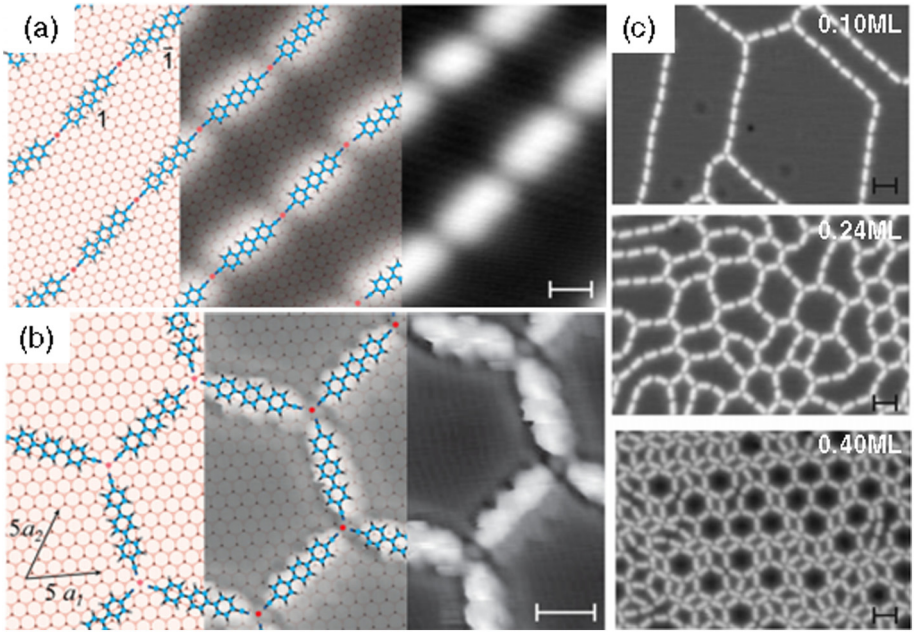

Fig. 19. (a) Close-up view accompanied by a model of the metal-organic chains. (b) Detail of the regular honeycomb network and model. (c) Coverage dependence of STM images of different amount of NC-pH_3-CN deposited at RT on Cu (111). (Reprinted with permission from Ref. [165]).

reversibility of the N—Cu—N, which facilitated successful self-assembly as reversibility allows for both growth and error correction during assembly. The 1D bonding geometries, as well as the unusual 2-fold coordination, resulted from steric and electronic interactions with the Cu (100) substrate, which differed from the 3D coordination chemistry. Moreover, growth kinetics and structure stability are strongly affected by the epitaxial relationship between the molecular structure and substrate lattice.

The porphyrin species substituted with terminal pyridyl groups were widely used as motifs to construct various low-dimensional metallosupramolecular architectures. This is because the porphyrin derivatives can be easily modified by changing the central metal or selecting suitable axial ligation. The formed structures can act as functionalized platforms for further constructing highly functional nanostructures after coordinating with other active ligands. The ordering of TPyP molecules on a Cu (111) surface over a large temperature range of 300–500 K was presented [160]. At 300 K, the molecules formed a saddle-shaped macrocycle with terminal pyridyl groups pointing toward the Cu surface. Upon annealing, twofold metal-ligand coordination formed between the mesopyridyl and copper adatoms. At temperatures exceeding 450 K, high-resolution STM showed a variable structure. 1D Cu-coordinated polymers metal-directed assembled on both Cu (111) and Ag (111) surfaces by employing a synthesized porphyrin module [161]. Based on a tetrapyrrolic core, the porphyrin derivative was substituted with two phen-1,4-diyl-ethynyl-pyridyl and two *t*-Bu_2Ph substituents at the four *meso*-positions (Fig. 18a). The STM measurements showed that this porphyrin module assembled into sinuous metal-organic polymers through a pyridyl-Cu-pyridyl coupling motif due to the conformational flexibility and functionality of porphyrin as well as substrate interactions. The obtained polymers displayed two enantiomeric conformations on the surface, which led to a striking flexibility in the morphology. Notably, the STM results revealed that there are two enantiomers because of surface confinement, which allowed the module to have 2D chiral conformational isomers with site-specific surface anchoring. The direction and curvature of the chains are determined by the sequence and mutual arrangement of the species. The sequence and arrangement of the straight and zigzag segments, including turns and U-turns, make the structure of the chains anchor at the site-specific surface. Such coordination chains exhibit a high degree of flexibility in the range of 180–240 K, and when temperature was increased to 240 K, chains partially dissolved into the fluid phase and were fully dissolved at 320 K [162].

In a later study, the supramolecular assembly of a ligand, *cis*-BTP-TPE, on a Cu (111) surface was observed by using low-temperature STM [163]. This pyridine derivative can form three supramolecular structures: triangular metallacycles, propeller clusters, and linear chains at different molecular deposition rates. Only when the multifunctional *cis*-BTP-TPE ligands were deposited at a molecular deposition rate of ~0.013 ML min^{-1} (1 ML is defined as one surface fully covered by molecules) onto the Cu (111) substrate at room temperature were the terminal terpyridine groups coordinated effectively by Cu because the Cu adatom density was sufficiently high. As a result, the triangle-shaped metallacycles were formed by the BTP-TPE *cis*-isomers. In another study, a related set of bis-cyanophenyl-substituted zinc porphyrins self-assembled on Cu (111) surfaces upon annealing at temperatures >150 °C [164]. Two porphyrins coordinated with Cu atoms from the surface through CN–Cu–CN coordination bonds. STM results showed that the cyanobiphenyl substituents attached to the porphyrin backbone tend to bend towards each other. These results indicate that, compared with intermolecular bonding, adsorbate–substrate interactions can enable a broader variety of assembled structures. Except for a series of Co-NC-Ph_n-CN coordination honeycomb networks, the NC–pH_3–CN molecules formed two kinds of structures, which consisted of chain-and-honeycomb networks linked to the Cu adatoms supplied by metal substrate [165]. Moreover, the network changed with increases to the molecular coverage on the surface. The molecules arranged themselves along two directions (Fig. 19), depending on the coordination number and the bond length between the CN and the Cu atoms.

A series of systematic investigations demonstrated the construction of the metal–carboxylate based coordination cluster, the polymeric chains, and the reticulated frames. Note that the catalytic activity of Cu (100) substrate can deprotonate the carboxyl groups, leading to chemisorbed TMA molecules on Cu (100) through carboxylate formation [166]. Cu–TMA complexes on a Cu (100) surface were obviously identified [167,168]. There are two types of complexes: cloverleaf-shaped $Cu(TMA)_4$ and $Cu_2(TMA)_6$ along the closely packed 1D strings, which were attributable to the deprotonated carboxylic moieties by the Cu adatoms from the metal substrate. The resulting Cu–TMA cloverleaves appeared only when temperatures were above 280 K [169]. Below this threshold, only portions of the TMA molecules were deprotonated and formed Kagomé structures through hydrogen bonding.

3.3.2. Coordination of Au surface

Gold as a fascinating metal has long been considered as one of the noblest metals [170]. Even though inert Au surface results in high reaction barriers to the reactants, the surface can form strong coordinated bonds with various adsorbates [171]. For example, isophthalic acid can formed long-range adlayers on Au (111) depending on the temperature [172]. After adsorbing low coverage of PDI on Au (111) at 300 K, long chains consisting of alternating Au atoms and PDI molecules formed [173]. HBB arranged with either hexagonally closely packed or tetragonal structure on Au (111) surface, which depends on temperature [174]. Higher substrate temperature facilitates the formation of coordination bond between Au adatoms and HBB molecules because of the enhanced adatom diffusion. Generally, the electronic properties of the coordinated networks depend on both the type of metal center and its coordination number. The amount of electrons donated from the 2-fold coordinated Au adatoms to F4TCNQ is lower than that donated from the 4-fold coordinated Mn atoms to TCNQ [175]. The asymmetric coordination of Au atom to only one side end group of symmetrical A-D-A molecule DCVST-Me_2 can lead to asymmetric localization of the lowest unoccupied molecular orbital (LUMO) [176]. In addition, depending on the applied potential, uracil and 2,2′-bipyridine molecules can form highly-ordered adlayers by substrate-adsorbate coordination [177,178].

The self-assembly kinetics of TPyP molecules coordinated by Cu atoms was studied on Au (111) substrate [179]. Fourfold symmetrical TPyP molecules were simplified to square dots during the simulation. STM images showed that these square dots diffused on the surface and nucleated to rectangular-shaped islands without molecular rotation. To better uncover the underlying coordination mechanism on the surface, a STM investigation of metal-coordinated network self-assembled from the pyridyl-functionalized porphyrin derivative TPyP on clean single-crystal Au (111) surface was performed [180]. A typical STM image was recorded on a sample at 250 °C post-annealing (Fig. 20). It can be identified that each TPyP displayed a square shape connected with four neighboring TPyP molecules. Adatoms of metal surface can coordinate with the surface organic ligands. Therefore, the neighboring N atoms coordinated with an Au atom showing a twofold linear configuration. The extended Au-coordinated Kagome periodic network might result from the lifting of the herringbone reconstruction on Au surface, the geometric matching between the Kagome network, and the Au lattice, as well as the faintish molecule–substrate interactions. Porphyrin derivative ZnTPyCN formed a nanoribbon-like structure with two different conformational isomers after depositing onto the Au (111) surface at room temperature [181]. The underlying Au (111) play a significant role on the ZnTPyCN adsorbed conformation, resulting in the axes of the unit cell running parallel to the Au. After annealing, ZnTPyCN submonolayer (at 160 °C and 210 °C) and 1D flexible polymer with variable lengths were formed on Au substrate (Fig. 20). The

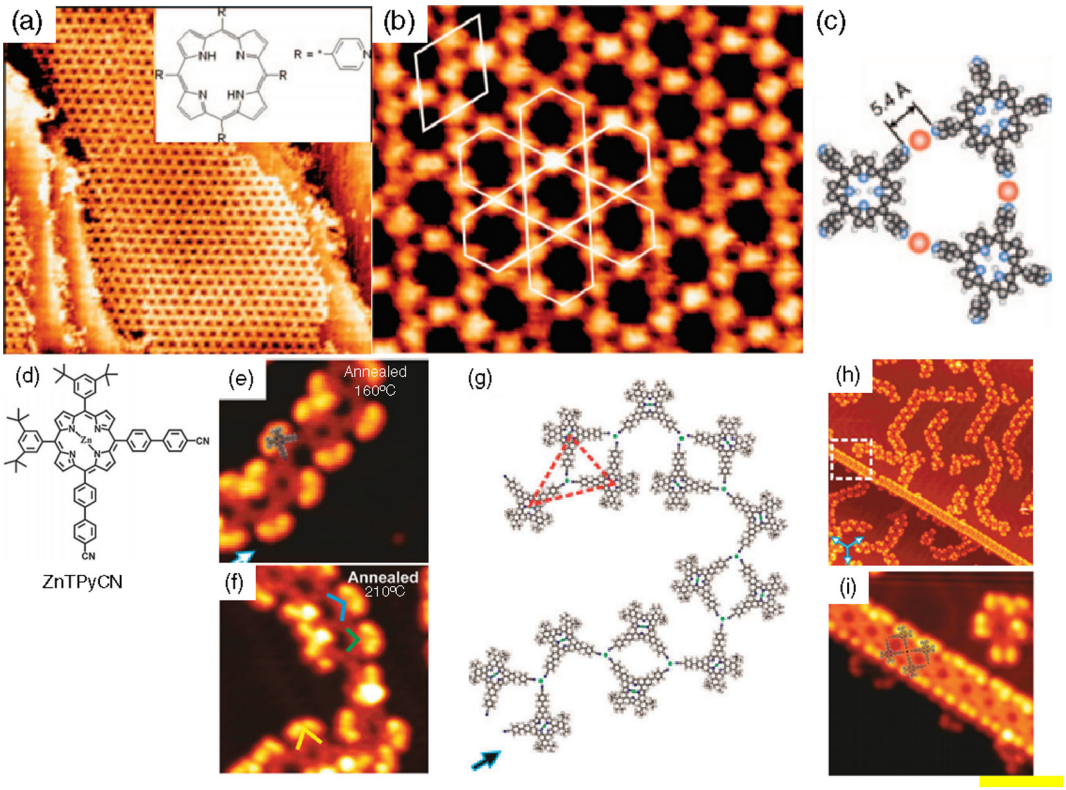

Fig. 20. (a) STM topography of network structures of TPyP self-assembled on Au (111) surface (Inset: Chemical structure of TPyP). (b) High-resolution STM image of Au-TPyP network structures assembled on Au (111). The rhombic-shape frame defines the network unit cell. The network frame highlights the Kagomé lattice. (c) Structural models based on STM data of three-branch joint. Orange-color spheres between TPyP molecules represent Au ad-atoms. (d) Chemical structure of ZnTPyCN. (e, f) Close-up STM images showing the formation of 1D coordination polymers of ZnTPyCN on Au (111) induced by annealing at 160 °C and 210 °C, respectively. (g) The proposed model for the 1D coordination polymer of ZnTPyCN on Au (111). (h, i) Overview and close-up STM images showing the molecular arrangement of ZnTPyCN at the step edges of the Au (111) surface after annealing at 210 °C. (Reprinted with permission from Refs. [180,181]).

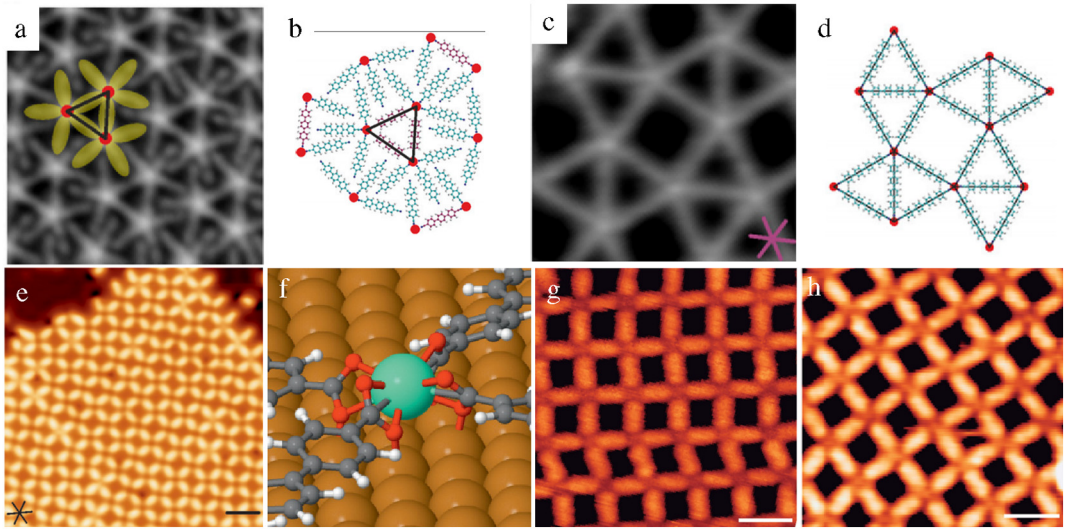

Fig. 21. (a) Hierarchic metallosupramolecular network from Ce-directed assembly of NC-pH_3-CN linkers on Ag (111), for a 4:1 (linker/Ce) stoichiometric ratio. (b) Atomistic model of the network (a). (c). High-resolution image of a snub square tiling motif constituted of NC-pH_4-CN linkers and Ce centers. (d) Structure model of image (c) showing the fivefold coordination of the Ce centers. (e) High-resolution image. (f) Zoom-in perspective view emphasizing the eightfold Gd-O coordination motif. (g, h) High-resolution STM images at 306 K and 360 K, respectively. (Reprinted with permission from Refs. [186,189]).

supplied energy by annealing to the system enables the –CN angle to distort to coordinate with Au adatoms created on Au (111) surface. An unusual threefold coordination bond formed between one Au atom and the N atoms of three terminal CN groups. In addition, fourfold Au–CN coordination occurred at the Au (111) step edges, by which a straight 1D polymer formed.

Except for the fact that the substituents of the porphyrin derivatives can react with surface adatoms, the central pore of the porphyrin can also trap metal adatoms on the surface. The TPP molecules displayed different appearances in the same scanning area depending on the bias voltage applied [182]. All the molecules appeared bright at −1.5 and −1.0 V, whereas at

−0.5 V, the molecules exhibited a completely different appearance. In combination with the DFT study, it was concluded that the adatoms on the Au (111) surface play a vital role in the appearance of the TPP molecules and that a coordination bond formed between the adsorbed underneath TPP molecules and the Au adatoms. Moreover, an STM manipulation experiment was conducted on a single molecule, which further confirmed the disruption and the formation of the coordination bond between the TPP molecules and the Au adatoms.

3.3.3. Coordination of Ag surface

Metal-free Pc and porphyrin molecules can form various coordinated complexes on single-crystal surfaces such as Cu and Au. Note that most cases are on closely packed (111) surfaces. The coordination reaction of H_2Pc on an Ag (110) surface was firstly observed [183]. At room temperature, only a small percentage of the deposited H_2Pc molecules can coordinate with the Ag atoms from the Ag (110) surface. After thermal annealing, the central hydrogen atoms of H_2Pc tend to dissociate, and the Ag atom diffuses to dehydrogenated molecules followed by coordination with four N atoms. The absence of AgPc on the Ag (111) surface indicates the orientation of the substrate is crucial for the coordination reaction. Upon deposition of TCNE on Ag (111) surface both at 150 K and 300 K temperatures, two different networks involving Ag-N coordination were formed [184]. The coordinated Ag adatoms arised partially from the step edges, suggesting that high density of the diffusing free surface metal adatoms is important to be incorporated into the coordinated networks. Unfortunately, no extended networks have been obtained. Ag adatoms can stabilize negatively charged CuPc molecules via Ag-CuPc coordination interactions at different Ag-CuPc densities [185]. At saturation adatom density, a closed-packed layer without voids formed, while at lower adatom density, an irregular arrangement of subunits formed. Note that submonolayer coverage of CuPc molecules on Ag (100) at 200 K is unable to formed islands owing to two reasons: high molecular mobility and weak repulsive intermolecular interactions.

4. Rare-earth metal-based coordination assembles

Owing to the high coordination number of the rare-earth metals, ligands can be finely tuned. For this advantage, diverse supramolecular structures have been fabricated by selecting the appropriate ligands and rare-earth metals. Lanthanides are versatile metals with functional properties, which have been exploited for a wide variety of applications. Considerable efforts have been devoted to coordination architecture, which has given rise to interesting topologies on substrate surfaces.

4.1. Low-dimensional architectures

It is significant to devote effort to engineering specific 2D tessellations at the molecular level. Ce- or Gd coordinated with linear polyphenyl molecular linkers with terminal carbonitrile on the Ag (111) surface [186–188]. The spontaneously formed fivefold Ce-ligand coordination motifs are planar and flexible, displaying trigonal and square polygons (Fig. 21). After tuning the concentration, as well as the stoichiometric ratio of rare-earth metal centers to the ligands, a hierarchic assembly with a surface-confined metal–organic coordination network was fabricated. This study introduced the possibility of lanthanide rare-metal elements with prospects for photovoltaics, photonics, and magnetism. Another pentameric mononuclear supramolecule is comprised of a Gd rare-metal center surrounded by five *para*-quarterphenyl-dicarbonitrile NC-pH_4-CN linkers.

Except for the fivefold coordination between Ce (or Gd) atoms and carbonitrile functional linkers, lanthanide-based nanostructures on the surface still need further advances to exploit the application potential of such structure in bulk or interfacial nanoarchitectures. In addition, these previously discussed surface-confined carboxylic acid species mainly undergo coordination with the alkali and the d-block transition metals. Another study focused on the coordination arrays between Gd metallic atoms and linear ditopic linker TDA with carboxyl groups on a pristine Cu surface (Fig. 21) [189]. Upon deposition of Gd atoms onto Cu (111) surface covered with TDA molecules, a reticular assembly structure was formed. Unprecedentedly, eightfold lateral coordination bonds Gd-O formed between the Gd and four TDA molecules after the deprotonation of the carboxylic acid groups at 425 K. This distinct kind of coordinative coupling showing an ionic character can be attributed to the large diameter of the Gd center and the high coordination numbers. Although the coordination nodes show a certain degree of flexibility, the assembled coordination structures are thermally robust. A selective metalation yielded a gridlike Gd-Co bimetallic nanoarchitecture considering the low activation barrier of the metalation of 2H-TPCN (the molecular structure is shown in Fig. 15a) with small transition metal atoms [190].

4.2. Double- and triple-decker sandwich assemblies

4.2.1. Double-decker assemblies

Rare-earth metal ions can be introduced between two macrocyclic tetrapyrrole compounds, such as porphyrin and phthalocyanine macrocycles, to form double-decker or triple-decker sandwich complexes *via* axial coordination interactions [191]. Among these structures, the macrocyclic ligands rotated with respect to each other, by 45° around their normal axes, to form the metal–ion coordinate with the eight nitrogen atoms. The double-decker complexes have rich properties, including electrochromicity, semiconductivity, and nonlinear optical. These functional properties have drawn much attention to these complexes, especially in the field of display devices, bipolar transistors, and chemical sensors. Additionally, the triple-decker complexes, which have a motif of ligand–metal–ligand–metal–ligand, can be used to extend the 3D functional nanostructures. This section will focus on the assembled static structures of double- and triple-decker sandwich-type complexes on various surfaces.

Several double-decker compounds, such as the bisphthalocyanine or porphyrin complexes of Y, Ce, Pr, Eu, Tb, Dy, Er, and Lu, can form adlayers at the liquid–solid interface on HOPG and metal surfaces. In 1991, the single-molecule images of a double-decker complex [$Lu(Pc)_2$] on a graphite surface was first captured by means of STM [192]. Then, this metallosupramolecule formed lamellar structures on HOPG [30]. Because of the limited resolution at that time, however it was difficult to obtain the fine structures and to assign the observed features to the molecular structures. With the development of STM techniques in the past few years, the 3D submolecular structures—as well as the single electronic structures—can be achieved.

A series of double-decker complexes of lutetium containing a naphthalocyanine (Nc) unit as one of the ligands, [Lu(OEP)(Nc)], [Lu(TBPP)(Nc)], and [Eu(r-TPPc)(Nc)] form ordered arrays with a common lattice constant of 1.7 nm (Fig. 22)[193]. This structure matches the optimized arrangement of naphthalocyanine, indicating that the Nc unit adsorbs on the surface, presenting the other ligand off the surface towards the solution. Three double-decker complexes of cerium(IV) with porphyrin or phthalocyanine ligands ([Ce(Pc)(C_{22}OPP)], [Ce(C_{22}OPP)$_2$], and [Ce(BPEPP)(C_{22}OPP)] were synthesized [194]. By using STM investigation at the 1-phenyloctane/HOPG interface, the self-assembled structures of these three complexes on surface were observed (Fig. 22). On

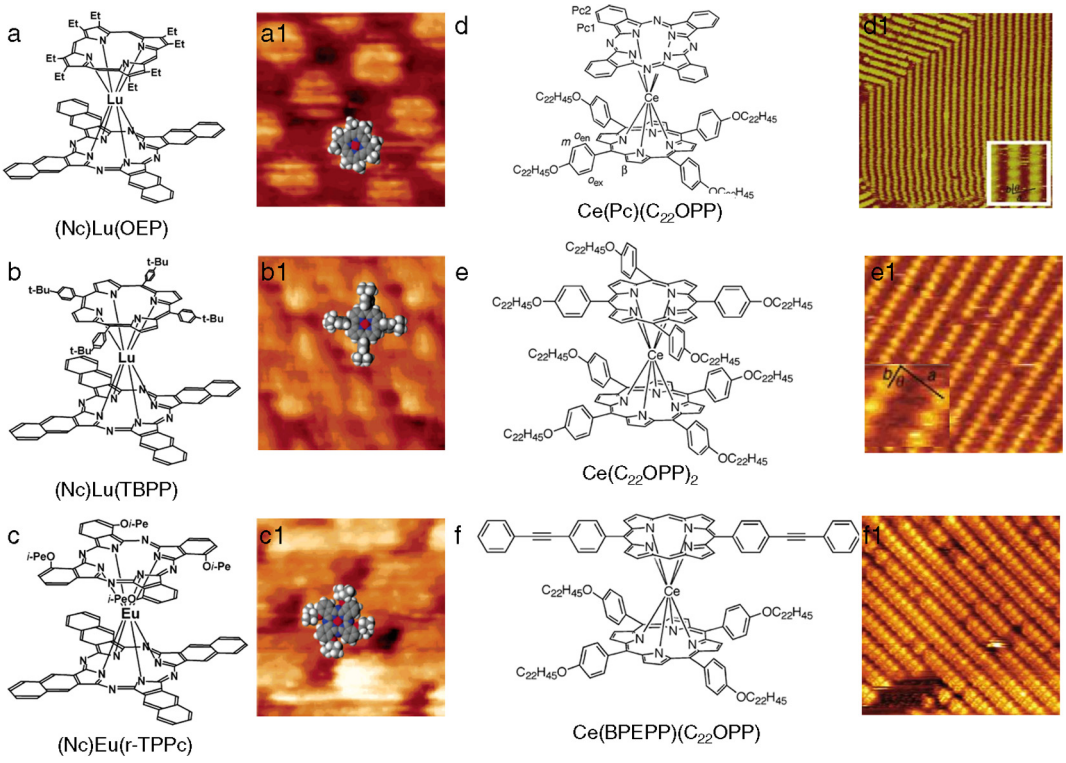

Fig. 22. The chemical structures, and the corresponding scanning tunneling microscope images of double-decker complexes of (Nc)Lu(OEP) (a, a1), (Nc)Lu(TBPP) (b, b1), (Nc)Eu(RTPPc) (c, c1), Ce(Pc)(C_{22}OPP) (d, d1), Ce(C_{22}OPP)$_2$ (e, e1) and Ce(BPEPP)(C_{22}OPP) (f, f1). (Reprinted with permission from Refs. [193,194]).

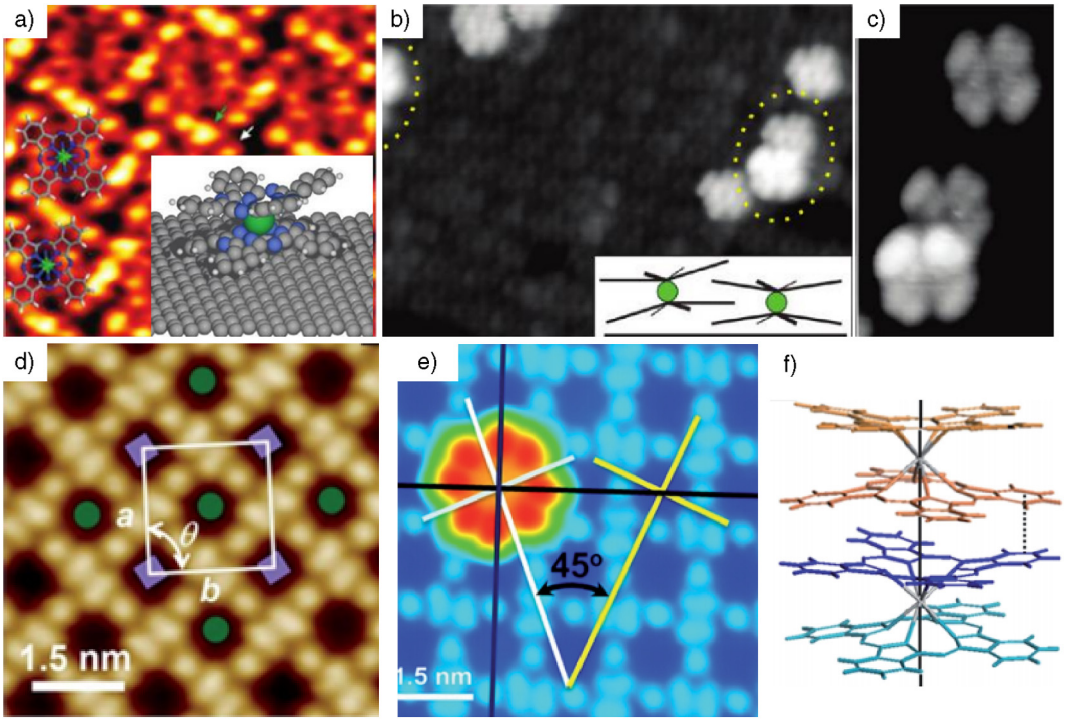

Fig. 23. (a) Highly resolved STM image of a monolayer of $LuPc_2$ showing intramolecular features of the molecular with the model of single complex $LuPc_2$ on HOPG. (b) STM image of a third ML of $LuPc_2$ on HOPG with adsorbed single $LuPc_2$ and three formations of two $LuPc_2$ molecules with overlapping Pc ligands with a sketch of the arrangement. (c) Magnification of an overlapping $LuPc_2$ pair. (d) STM image of the $DyPc_2$ SAM on Pb (111) showing the "chessboard" pattern. (e) STM image of an individual $DyPc_2$ molecule on top of the first $DyPc_2$ SAM. (f) Molecular model showing the co-axial alignment of two $DyPc_2$ molecules in different layers. (Reprinted with permission from Refs. [195,196]).

deposition of the solutions onto the HOPG surface, ordered monolayers of three complexes formed. The C_{22}OPP adsorbed onto the HOPG surface, owing to the affinity of the long alkyl chains toward the surface as well as the alkyl-alkyl interactions. Then, the other macrocycle ligands—Pc, C_{22}OPP, and BPEPP—became the upper units, which could be reflected by the STM images. Therefore, As for [Ce(Pc)(C_{22}OPP)], rows of bright circular spots separated by dark rows are recorded in the STM. In contrast, the homoleptic molecules of [Ce(C_{22}OPP)$_2$] are imaged as bright square protrusions, whereas the BPEPP ring in [Ce(BPEPP)(C_{22}OPP)] is oblong-shaped, which is reflected in the STM images.

A study on the growth, conformation, and electronic structure of the complex bis(phthalocyaninato)lutetium(III) ($LuPc_2$) adsorbed on HOPG were comprehensively performed by using STM [195]. $LuPc_2$ molecules adsorbed onto HOPG and form a highly ordered closely packed self-assembly molecular structure (Fig. 23). The molecules are parallel to the surface in the first layer, which increases the π-π interaction between the Pc ligand and the graphite surface. At the multilayer coverage surface, the upper Pc ligand from the upper-layer molecule rotated by 45° with respect to the upper Pc ligand of the underlying molecules. Therefore, the adjoining Pc ligands have the same orientation. Along one direction of underlying lattice vector, a small amount of complexes adsorbed on top can form pairs, in which the distance between the two molecules is slightly smaller than that in the ordered layer. The center of the upper $LuPc_2$ molecule is higher than that of the underlying $LuPc_2$, and the upper Pc ligand clearly overlaps the underlying molecule. Similar to the molecules in the closed layer, this tilt leads to low repulsion between the adjacent phenylene groups. For this system, the intermolecular interaction played a dominant role on the formation of the structure, whereas the graphite substrate hexagonal lattice defined the direction of the molecular layer and affected its length. The double-decker $DyPc_2$ can adsorbed on the Pb (111) surface, which was grown on silicon wafers [196]. First, the $DyPc_2$ molecules organized into a monolayer in which two adjacent molecules rotated an angle of 6° with respect to each other. On top of the first monolayer formed, the $DyPc_2$ molecules scattered as the second layer (Fig. 23). Note that the upper $DyPc_2$ molecule co-axially aligned with the underlying molecules in the first self-assembly monolayer. The π-π stacking interaction between the lower Pc ligand in the second layer and the upper Pc ligand from the first layer determined such co-axial alignment. In the monolayer of the decker molecules, only the upper ligand can be observed directly by STM; therefore, the molecular configurations are still a topic of considerable debate. This result offered us an approach to directly determine the molecular configurations of double-decker molecules, in particular, those assembled on the Pb substrate.

In the past decades, tremendous effort has focused on investigating single-molecule magnets (SMMs) [197,198]. After thermally evaporating three kinds of double-decker compounds MPc_2 (M = Tb^{3+}, Dy^{3+} and Y^{3+}) in ultrahigh vacuum, the adsorbed morphologies on Au (111) surface was investigated through STM experiments [199]. Among of them, $TbPc_2$ and $DyPc_2$ are single-molecule magnets, whereas YPc_2 is not. The STM images showed that MPc_2 exhibited eight-lobed features, whereas the MPc displayed four-lobed images because of the one lost Pc ligand. Both the shape and the nominal heights for these three molecules on the Au (111) surface were similar. As observed through STM investigations, the double-decker YPc_2 can adsorb onto the Au (111) substrate [200]. As an isolated complex, such double-decker molecules show four-lobed and eight-lobed types of STM contrasts depending on the substrate symmetry property. In the film, the shape of each molecule is similar to the isolated one, however the adjacent molecules rotated with each other by approximately 30°. The results indicate that the molecule–substrate interactions mainly determine the orientation of molecules, whereas the molecule–molecule interaction implies a large influence on the assembly on the surface. The ordered quadratic 2D self-assembly of Er($PcOC_{12}$)$_2$ is identical to an analogue $CoPcOC_{12}$ with one Pc ligand [201]. Also, the mixtures of these two molecules show phase separation on the surface, which would provide insight for the development of double-decker assemblies with Pc as a ligand.

4.2.2. Triple-decker assemblies

Observing triple-decker complexes by STM is a challenge because of their nonplanar characteristics. The assembly of triple-decker complexes at the liquid–HOPG interface is not ordered [202]. Without dissociation sandwich structures, a monolayer film of triple-decker Y_2Pc_3 molecules with a height of 0.55 nm such complexes adsorbed onto the Au (111) surface with a flat-lying configuration [203,204]. After pulse injection, a triple-decker complex was deposited onto the Au (111) surface. The attached moiety can control the adsorption configuration and the assembly of molecules on the surface [205]. In fact, the alkyl side chains attached to the bithiophene groups enable the porphyrin to be perpendicular to the substrate. This kind of molecular aggregate would open large spaces for molecular manipulation by STM, which will be discussed in the later section.

5. Dynamics of metal–organic coordination

As discussed previously, metal–ligand interactions have been considered an excellent means for fabricating various supramolecular structures as imaged by STM. Although the coordination energies are enough to allow the reaction at ambient temperatures, the demand persists to understand the evolution of coordination on the surface.

5.1. Molecular rotation

The exact alignment of molecules on the substrate is an important parameter for potential applications. Thus, visualization of the individual molecular rotation is important to understand the rotational dynamics and to further find paths for controlling. Double-decker complexes exhibit interesting dynamic behavior such as rotational liberation of the macrocyclic ligands with respect to each other. This rotation can be controlled by coordination to specific functional groups within the molecule or through the redox properties of the central rare-earth metal. To obtain insight into the orientation of sandwich double-decker complexes in contact with substrate, the surface rotation of double-decker complex was investigated after observing the structure of the [(C_{12}OPc)$_2$Er] [206]. The lack of fine structures on the top ligand might be attributed to the relative orientation of both ligands, the rotational mobility of the discal phthalocyanine, or the electronic effects induced by the lanthanide ion. However, the reason for the double-decker complex showing unstable structure still requires further research.

To clarify the parameters determining the motion of molecules aligned on solid surfaces, STM technique were used to study the ordered structures of the homoleptic double-decker complexes [(C_8OPc)$_2$Ce] and [(C_{12}OPc)$_2$Ce] and the heteroleptic double-decker complexes [(C_8OPc)Ce(Pc)] and [(C_8OPc)Ce(TPP)] on the HOPG surface as well as the relationship between these structures and their molecular motions [207]. The double-decker complexes [(C_8OPc)$_2$Ce], [(C_{12}OPc)$_2$Ce], and [(C_8OPc)Ce(Pc)] can independently form well-ordered self-organized structures with the fine intramolecular structure of the top Pc ligands. However, the (C_8OPc)Ce(TPP) complex, composed of C_8OPc and TPP ligands, did not form such a self-organized structure on its own. The

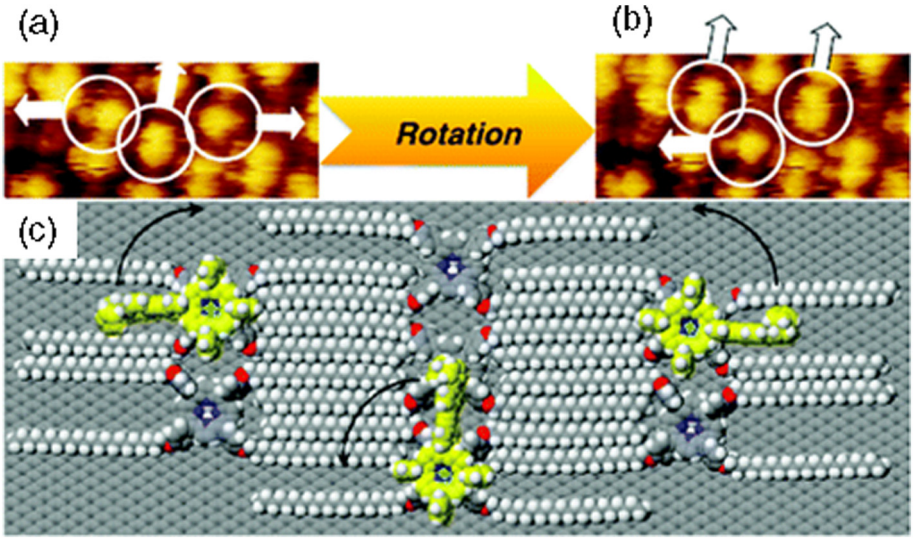

Fig. 24. (a) STM images of mixture of [Ce(FcTPP)(C_{22}OPP)] and H_2(C_{22}OPP); (b) STM image recorded immediately after the image (a). (c) The illustration of the orientated three-circled units in the upper regions of the images. (Reprinted with permission from Ref. [208])

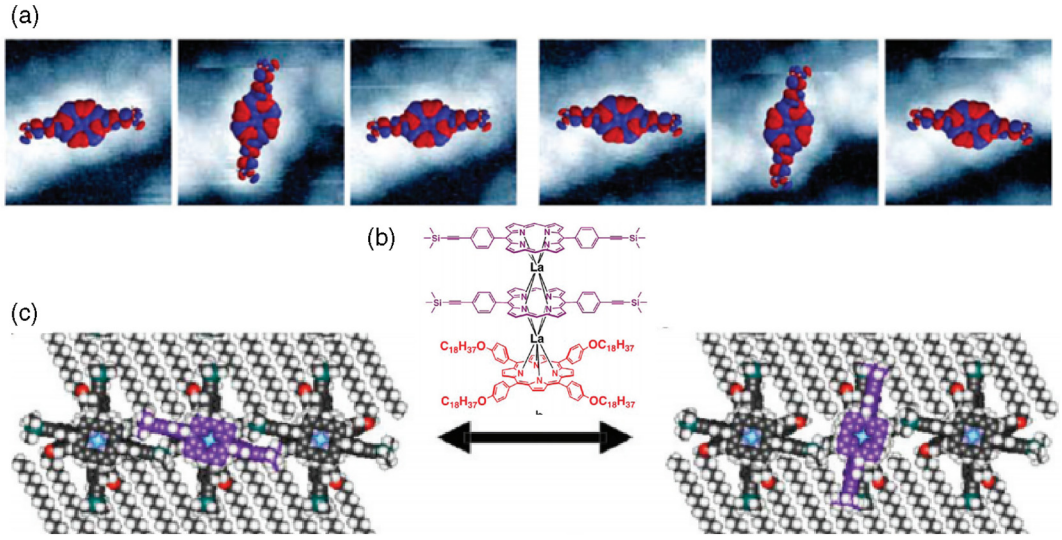

Fig. 25. (a) Consecutive STM images of the LaTDP molecule. (b) Molecular structure of multidecker porphyrin complex LaTDP. (c) Space-filling model of LaTDP molecule prior to and following reorientation. (Reprinted with permission from Ref. [209]).

intramolecular feature of the TPP ligands was completely lost and difficult to observe. Furthermore, after mixing [(C_8OPc)$_2$Ce], [(C_{12}OPc)$_2$Ce], or [(C_8OPc)Ce(Pc)] with C_8OPc or C_{12}OPc, square-shaped images can also be observed. One possible interpretation of these phenomena might be that the top Pc ligand does not undergo rotation or any other significant movement affected by the surrounding environment, whereas the top TPP ligand undergoes some degree of movement in the form of rotational libration or trampoline-like movement. These results strongly suggest that the free space presented around the top ligand of the double-decker complexes is an important factor in controlling the molecular motion of immobilized double-decker complexes on solid surfaces.

As inferred previously, the rotation of double-decker complexes depends on the structures of the complexes. To date, however no strong evidence has been presented. The shape of Ce(BPEPP)(C_{22}OPP) was elliptical when located within its own row, whereas the shape is isotropic when flanked by free-base porphyrin H_2(C_{22}-OPP) molecules [194]. Such isotropic shapes might have been caused by the rotation of the top ligand, as this complex undergoes interring rotational libration as revealed by temperature-variable ^{1}H NMR spectroscopy. However, the STM image of the mixture of Ce(FcTPP)(C_{22}OPP) and H_2(C_{22}OPP) differs significantly, in which the same molecular alignment, as in the case of [Ce(FcTPP)(C_{22}OPP)] and H_2(C_{22}OPP), was observed [208]. The STM record the orientation quantitative change of individual double-decker complexes in real space based on hundreds of double-decker molecules collected from dozens of scans of several different samples. Two successively recorded images (Fig. 24) show that most of the double-decker complexes remained in the same orientation, however some of them had reoriented during these two scans. From the illustration of the orientations and reorientations, it can be seen that the perpendicular-to-parallel flips were perturbed by adjacent molecules, whereas the reverse processes were less influenced.

A more complicated rotation system of a lanthanum triple-decker porphyrin (LaTDP) complex was studied under

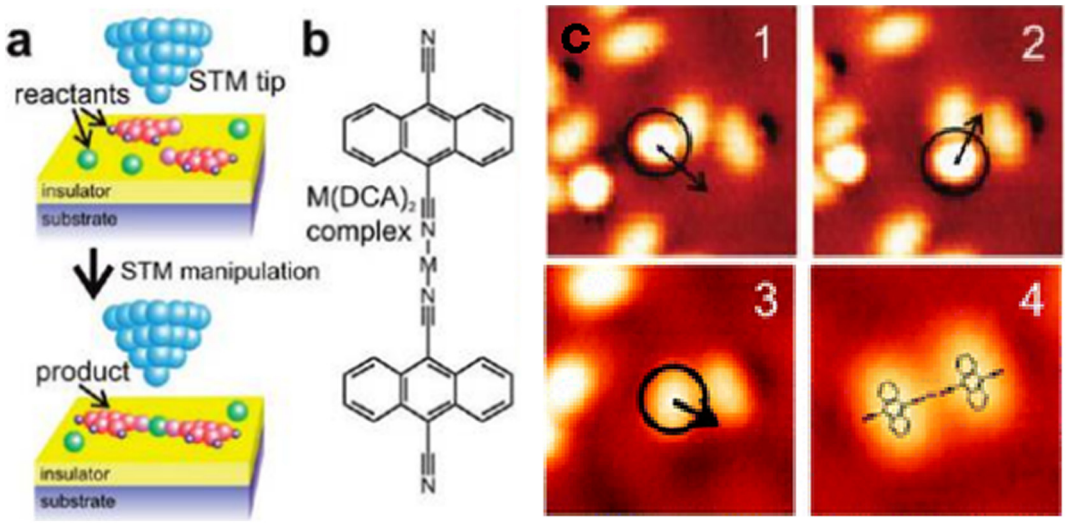

Fig. 26. (a) Schematic of the formation of a metal-ligand complex on an ultrathin insulating film by STM manipulation. (b) The target molecule, linear $M(DCA)_2$ complex. (c) Series of lateral manipulation steps resulting in the formation of a linear $Fe(DCA)_2$ complex. (Reprinted with permission from Ref. [210]).

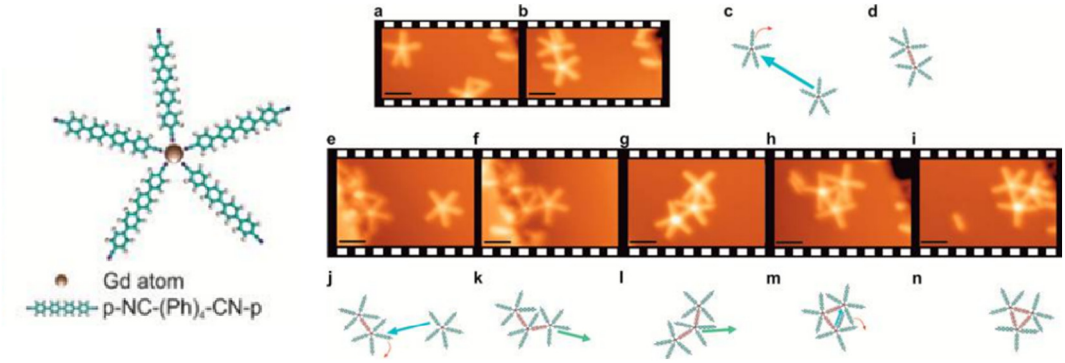

Fig. 27. Atomistic model of a pentameric unit and *in situ* fabrication of nonameric and dodecameric species by the lateral manipulation of self-assembled Gd-carbonitrile coordinated supramolecules on Ag (111). (Reprinted with permission from Ref. [188]).

low-temperature STM [209]. The topographic heights of this multidecker porphyrin complex and the internal structure were clearly visualized (Fig. 25). Although the alkyl chain-substituted double-decker (CeDDP) complex can also form a well-defined two-dimensional monolayer array on Au (111) substrate, the high-resolution STM images suggest that CeDDP was sufficiently adsorbed onto the substrate with the top porphyrin ligand rarely rotating. STM images show that the top porphyrin ligand of the three-thicker LaTDP was reversibly rotation-oscillated by a slight perturbation. These findings are unequivocal evidence of the rotation-oscillation of the multidecker porphyrin complex self-organized on a solid surface. These results would encourage further research on the applications of molecular-scale mechanical machines and single-molecule storage memory.

5.2. Coordination bond manipulation

STM manipulation has been considered as a direct way to perturb the coordination bond between the metal center and organic molecules. After co-evaporating iron or nickel atoms and DCA molecules onto an insulating NaCl layer on a Cu (111) surface, the DCA molecules adsorb with several orientations, indicating a weak interaction between the DCA and the underlying NaCl film [210]. Many $M(DCA)_2$ (M = Fe or Ni) complexes were synthesized directly through lateral STM manipulation of the metal atoms and the organic molecules (Fig. 26). The formed $M(DCA)_2$ complexes aligned with the [011] direction of the insulating NaCl film. Once the complex successfully forms, it is difficult to break these complexes by STM manipulation. This study demonstrates the formation of coordination bonds between molecular units with strong electronic coupling. Not only the formation but also the breaking of the coordination bond can be manipulated by STM [182]. As discussed previously, a small protrusion pot attributed to an Au adatom was left after a bright molecule was manipulated to the left. When the molecule is manipulated back to the initial position, the STM image shows an ambiguous molecular state, in which the Au adatom is located at the periphery of TPP molecule, not the molecular center, resulting in asymmetric geometry. In addition, this finding also indicates that the coordinated adatom was underneath rather than on top of the molecules.

For the rigid molecules, it is difficult to directly change the coordination bonding scheme of a single molecule. The lateral STM manipulations can change the coordination bonding scheme of a flexible G-quartet-Fe complex [211]. One of the G-quartets in the original G-quartet-Fe complex rotates counterclockwise 50°, and another G-quartet molecule undergoes the same rotation. A local perturbation of the coordination bond within the G-quartet-Fe complex occurred. With the decoupling of molecules, the central Fe atoms adsorb closer to the Au (111) substrate. These findings give us insight into the formation mechanism of coordination

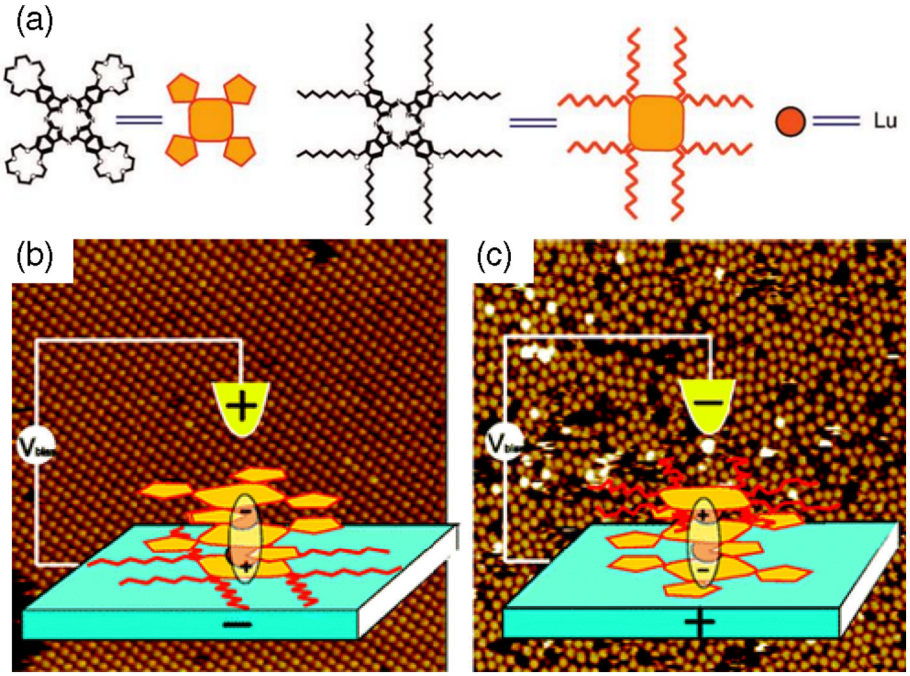

Fig. 28. (a) Molecular structures. (b) High resolution STM images obtained on ordered assembling monolayer of [[Pc(15C5)$_4$]Lu[Pc(15C5)$_4$]Lu[PcOC$_8$]] revealed under negative bias (V = -0.50 V; I = 362 pA) with schematic illustration of the possible mechanism of the bias induced flipping of the complex. (c) Amorphous monolayer structure of [[Pc(15C5)$_4$]Lu[Pc(15C5)$_4$]Lu[PcOC$_8$]] revealed under positive bias (V = 1.50 V; I = 362 pA) with schematic illustration of the possible mechanism of the bias induced flipping of the complex. (Reprinted with permission from Ref. [216]).

bonding. Based on the manipulation of individual pentamers on the surface, tetrameric, pentameric, nonameric, and dodecameric supramolecules were created [188]. A nonameric group formed after placing one pentamer close to another (Fig. 27). Subsequently, a dodecamer formed after one pentamer crashed closely to the formed nonamer. Across the surface, the conformation changed because of the amount of molecular space and a certain lability of coordination. These results reveal the *in situ* coordination chemical procedure as well as the robustness of the rare-earth Gd coordination property.

5.3. STM manipulation

Manipulation techniques, including direct tip–adsorbate forces (lateral or vertical direction), electric fields, and tunneling electrons, have been used to manipulate linker molecules or metal-based complex molecules [212,213]. In regards to the method of lateral manipulation, the interactions (attractive or repulsive) between the tip and the adsorbate allow the adsorbates to move across the surface without breaking coordination bonds.

5.3.1. Single-molecule manipulation

By using STM probe tip, heteroleptic double-decker molecules ([Lu(Nc)(OEP)], [Lu(Nc)(TBPP)], and [Sm(Nc)(OctOPc)]) were manipulated at the 1-phenyloctane/HOPG interface [214]. Through the use of nanografting, phthalocyanines (OctOPc) and double-decker molecules were displaced in single-layer matrices. At low-bias voltage, the STM tip scans resulted in the removal of the pre-adsorbed double-deckers and their substitution with OctOPc molecules from the phenyloctane solution. The substituted OctOPc domains formed bilayer stacks on the substrate. With voltage pulses, a single [Lu(Nc)(OEP)] complex was decomposed from the probe tip. The STM results indicated that the top OEP ligand was removed, whereas the bottom Nc ligand remained on the surface. These results demonstrated that it is feasible to control the composition distribution of the self-assembled monolayer consisting of more than two components through the scanning probe lithography. In addition, a triple-decker complex [Eu(TPP)(CRPc)(CRPc)] (EuTCC) coordinated by Eu^{III} can form a three-dimensional functional molecular architecture on an Au (111) support [215]. STM results reveal that EuTCC formed a unique molecular assembly, and new surface properties of were observed as a result of the adsorption orientation and electrochemical potential variation on Au (111). These observations indicate that controlling the molecular orientation and the rotation of the ligands has potential applications in the bottom-up fabrication of the surface.

An orientation-dependent adsorption ordering of an asymmetric triple-decker complex [[Pc(15C5)$_4$]Lu[Pc(15C5)$_4$]Lu[PcOC$_8$]] was tuned at the liquid–solid interface [216]. This transform of configuration was attributed to the interaction of the molecular intrinsic dipole upon the external electric field. It is an efficient strategy to attach functional groups to the top and bottom moieties of the triple-decker. Under negative substrate bias potential, this triple-decker complex formed a well-ordered square lattice on the graphite surface (Fig. 28). The lattice constant is 2.6 nm, which is similar to that of another double-decker complex, Eu[Pc(15C5)$_4$]$_2$ (2.3 nm). This triple-decker complex adsorbed onto the HOPG substrate with the PcOC$_8$ ligand towards the substrate and the hydrocarbon chains interdigitating with each other. In contrast, disordered assemblies with intermolecular distances 2.3–2.8 nm can be observed when the positive bias potentials are applied onto the substrate. It was proposed that, under a positive bias, the molecule can flip, resulting in the [Pc(15C15)$_4$] ligand pointing toward the substrate surface because of the interactions between the molecular dipole moment and the electric field. By controlling the applied bias potentials, order–disorder can be reversibly switched by the molecular flip. This approach provides a possible pathway to preparing organic films with switchable structure and electronic properties upon an external field.

Another study indicated that a new non-centrosymmetric triple-decker sandwich-type complex without any long chains also performed such bias-dependent adsorption configuration on a

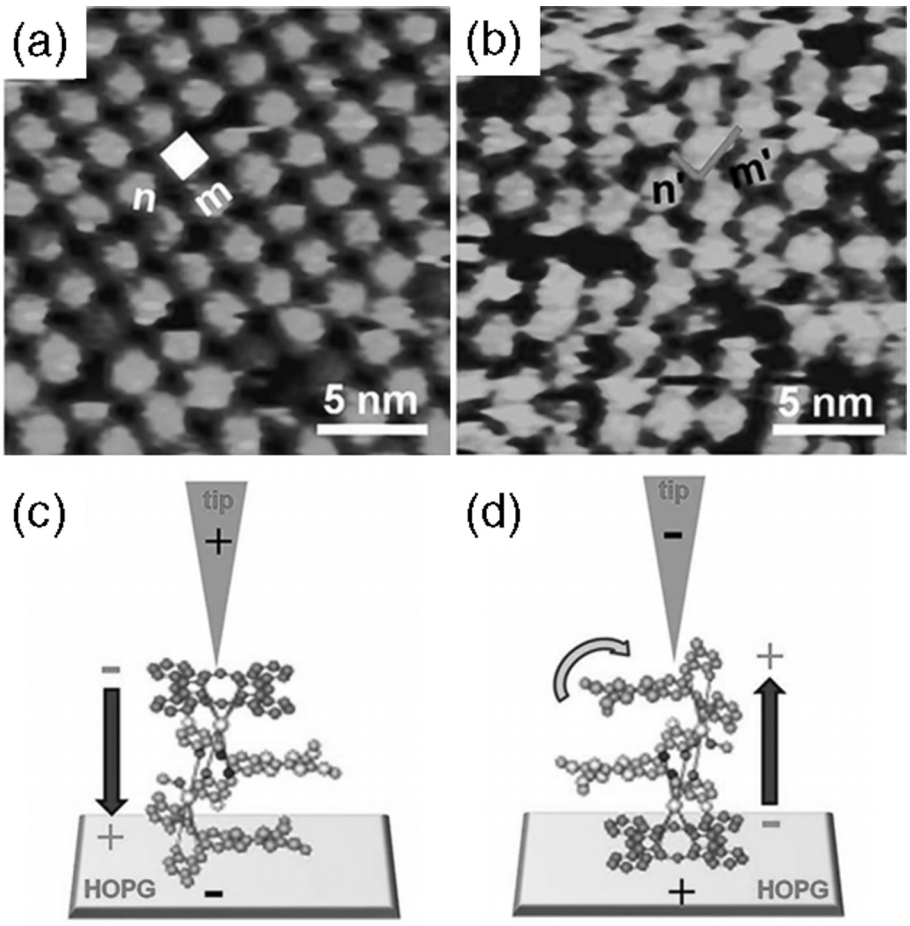

Fig. 29. High resolution STM images of TCDB/complex scanned at 700 mV (a) and -500 mV (b), respectively (I_{set} = 225.1 pA). Tentative scheme models for illustrating the conformation of the complex on HOPG surface at an applied positive bias (c) and negative bias (d). (Reprinted with permission from Ref. [217]).

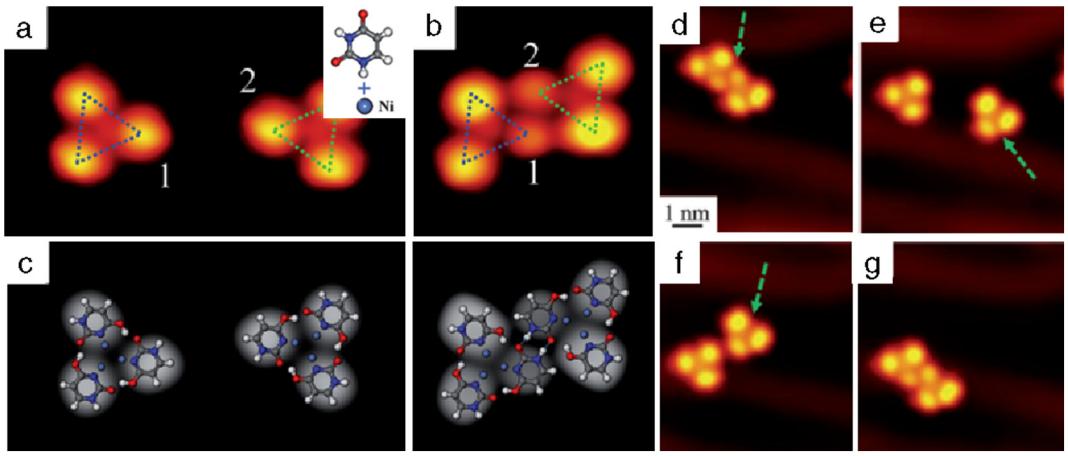

Fig. 30. (a, b) Close-up STM images showing two triangular clusters with distinct orientations (indicated in blue and green) and a parallelogrammic cluster, respectively. (c) Simulated STM images of triangular and parallelogrammic clusters superimposed with the DFT-optimized models on Au (111). (d–g) The whole reversible switching processes between a parallelogrammic cluster and two triangular clusters by STM manipulation. The arrows indicate the directions of the STM manipulations. (Reprinted with permission from Ref. [220]).

HOPG surface by means of a supramolecular template formed by the famous TCDB molecule [217]. The target complex consisted of phthalocyanine, dysprosium acetylacetonate, and a TTF-supported Schiff base ligand (H_2L) in a 1:2:2 M ratio. The STM results reveal that this triple-decker can selectively adsorb onto the HOPG surface depending on the applied electrical field (Fig. 29). The H_2L units adsorb on the HOPG surface, whereas the Pc units are located on the top, at a positive bias scanning condition. However, the H_2L is located at the top, and the Pc is located at the bottom, on a negative bias. Under the negative bias situation, the assembled structures show an obvious free rotation because of the non-symmetric structure of the top H_2L units. Furthermore,

DFT calculations indicate that the triple-decker showed intrinsic molecular dipole *P* (4.94 Debye). The interaction between the molecular dipole and the applied external electric field was calculated to be 0.06–0.15 eV. Therefore, we propose that such electrical-field-dependent selective adsorption might be induced and controlled by the interaction between the external electric field and the intrinsic molecular dipole.

However, temperature has yet to be confirmed as an important factor for molecular manipulation of the double-decker on the solid surface. A notable chirality manipulation of $TbPc_2$ on Ir (111) surface was conducted under low-temperature [218]. All the $TbPc_2$ double-deckers displayed achiral eight-lobed configurations at a substrate temperature (~100 K). After heating the sample to room temperature, all of the complexes displayed chiral configurations. Therefore, a thermally assisted process can induce molecular conformation reverse-switching from the achiral state to the chiral state with an azimuthal rotation of the upper Pc ligand. During the switching manipulations, the molecular chiral configuration can be mutually exchanged between left- and right-handedness. Thereby, the chiral switching could lead to promising nanotechnological applications. These results support the theory that the manipulation of coordination complexes on substrate is a key issue in the development of controlled architectures.

More recently, the donor–acceptor complex of double-decker Ce $(TPP)_2$ with stabilized C_{60} by noncovalent interactions were successfully manipulated [219]. The C_{60} cage exhibited three specific orientations in the $Ce(TPP)_2$ identified by STM experiments in combination of the simulations. The STM tip stimulation resulted in the ability of the individual C_{60} cages to reversibly switch among the previously mentioned three orientations. STS results reveal that a negative differential resistance (NDR) region emerges and that the band gap increases. Thus, electronic decoupling of the hovering C_{60} units from the metal substrate is evident, which is a prerequisite for charge separation in the donor–acceptor complex on optical excitation. These results revealed the C_{60} cage on $Ce(TPP)_2$ displays as a tristable system, which can be controlled by STM manipulation, and the induced rotations of the C_{60} affect the intradyad coupling.

5.3.2. Cluster manipulation

In addition to manipulating single molecules to trigger translation, rotation, and isomerization, STM can also be used to manipulate the coordination cluster [220]. A nucleobase, uracil was chosen as a potential ligand to coordinate with Ni atoms. Isolated clusters first formed on co-depositing ligand molecules and metal atoms on an Au (111) surface. Then, with the help of hydrogen bonds, these triangular clusters assembled into the complicated polygonal structures. After lateral STM manipulation on such self-assembled structures, the complicated structures were disrupted into free elementary motifs by splitting the hydrogen bonds (Fig. 30). Note that the coordination bonds organizing the cluster were not disturbed. Higher level formed again by the reformation of hydrogen bonds. Although the coordination bonds remained unperturbed, the electronic properties of the central metal Ni were adjusted and confirmed by DFT calculations. In any case, the presented results can be extended to other systems focusing on studying the precise fabrication of coordinating molecular nanostructure on substrates.

As mentioned previously, individual pentameric mononuclear molecules composed of Gd centers surrounded by five p-NC-pH_4-CN-p linkers on their surfaces can be manipulated [188]. Besides, highly flexible polymeric multi-porphyrin chains can also be manipulated on both Cu (111) and Ag (111) surfaces [161]. Not only can they move the terminating unit of the chain, but they can also displace entire segments without breaking the assemblies. It is remarkable that the chain segments could also be reversed back to the initial position on the Ag (111) surfaces.

6. Reaction activity of metal-based coordination complexes

6.1. Stability of coordination bond

Metal-coordinated complex can be easily attacked due to the weak coordination bond, in particular metal-N bond. When a complex is adsorbed onto a dissimilar metal surface, the metal-coordination bond in complex may be weakened by sufficiently large and effective surface-adspecies interaction. After Ag coordinated complex dissociated via charge transfer from both Au (111) and Au (100) substrate surfaces, surface-sensitive Ag adlayers formed [221]. Phthalocyanines and porphyrins are among the most promising precursors of coordinated molecules, not only because they can coordinate with numerous metal ions, but also because they form stable and planar coordination complexes as discussed previously. Such geometry is readily available through the formation of well-ordered structures. The adsorbed metalloporphyrins on the surfaces can be obtained directly by metalation of these derivatives with vapor-deposited metal atoms. This *in situ* coordination of porphyrin monolayers can be used to fabricate uniform monolayers of metalloporphyrins [222,223], and the coordination reaction rapidly proceeds at room temperature with a high yield. STM images showed that the Fe atoms exclusively coordinate with the central N atoms, not the peripheral *meso*-bridging N atoms. All the deposited Fe atoms can coordinate with H_2Pc, which indicates that the Fe atoms are sufficiently mobile on the surface of densely packed monolayers.

In addition to evaluating the $[Cu(TMA)_4]^{n-}$ complexes, the mechanism for the formation of the compounds through STM measurements has also been evaluated [167]. Note that the individual Cu adatoms and the TMA molecules are mobile on the surface. They monitored the thermal rotations of single TMA molecules because the diffusion is restricted. When the Cu atoms were held by carboxylate ligands, they could be resolved. Moreover, two adjacent $Cu(TMA)_4$ species are much more stable than the isolated ones because the movement of the neighboring molecules is hindered, owing to the higher energy barriers for rotation or movement. Therefore, the reaction proceeded under equilibrium. Such observations would provide a wide application of coordination complexes in the future search for multicomponent chemical reactions on templates. STM observations revealed that the Cu-TMA linear nanostructures can be transformed into Fe-TMA chains in the presence of iron on the surfaces at low temperatures.

In addition, transition metals such as Fe can be captured by the pyridyl groups attached on the porphyrin species, which are anchored onto a Cu (111) substrate at a low temperature [224]. At 8 K, the isolated TPyP molecules are immobile; in other words, the thermal diffusion of TPyP is frozen. After a slight increase in temperature to 15 K, the Fe adatoms can freely migrate, even though TPyP still cannot diffuse. Subsequently, the Fe is captured by the pyridyl groups after the surface cooled. As a result, Fe-TPyP complex formed on a Ag (111) surface (Fig. 31) [225]. By increasing the Fe adatoms, the H_2-TPyP precursors interact with the Fe, and the number of Fe-TPyP can be tuned up to full saturation. However, the molecular packing parameters of H_2-TPyP remain unaffected. The pyrrolic protons are reduced, whereas the Fe is oxidized and then incorporated into the porphyrinato core. This approach would be easily applicable to other porphyrin species on a large variety of substrates, which can be metalated by other metal centers.

6.2. Organic molecule adsorption

Because of planar conformation, metalloporphyrin and phthalocyanine complexes are suitable for anchoring onto various solid

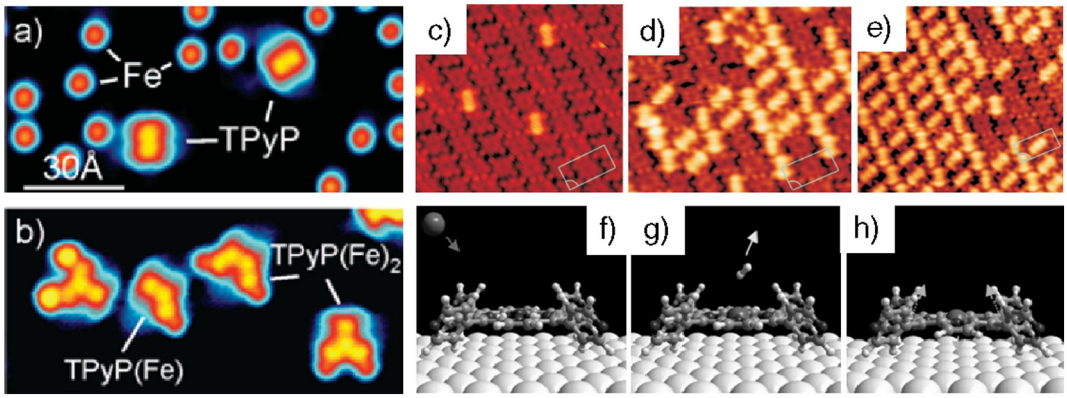

Fig. 31. (a and b) Selective attachment of Fe adatoms to the pyridyl groups of TPyP (a: V = 30 mV, I = 0.2 nA; b: V = 20 mV, I = 0.2 nA). (c–e) Reaction of H_2-TPyP precursor layer with increasing the Fe dose (b, c: V = 1.2 V, I = 0.7 nA, and d, e: V = 0.3 V, I = 0.85 nA). (f–h) Formation of metallo-porphyrin on surface. [Reprinted with permission from Ref. [225]

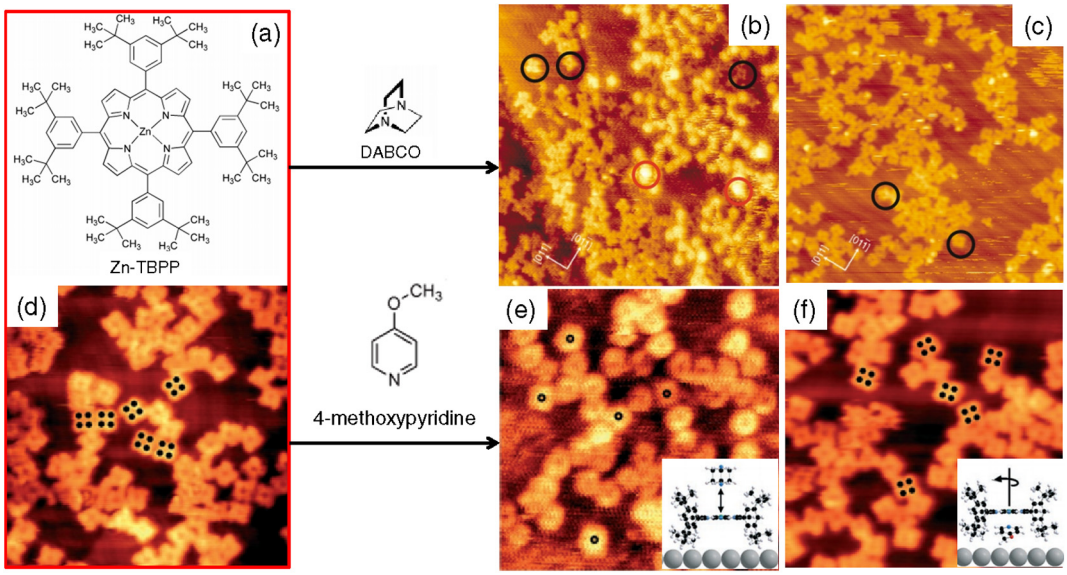

Fig. 32. (a) Structures of Zn-TBPP. Sequence of STM images of Zn-TBPP on Ag (100) taken at 123 K after: (b) dosing 50 L of DABCO, (c) after warming to room temperature (V = 1.5 V, I = 0.1 nA, 30 nm × 30 nm). (d) STM image of Zn-TBPP molecules adsorbed on Ag (100) at 298 K (V = 0.75 V, I = 0.1 nA, 20 nm × 20 nm). Sequence of STM images of Zn-TBPP on Ag (100) taken at 123 K after: (e) following a dosing of 100 Langmuirs of 4-methoxypyridine at 123 K, (f) after warming to 298 K (V = 1.0 V, I = 0.1 nA, 20 nm × 20 nm). (Reprinted with permission from Refs. [226,227]).

surfaces, resulting in ordered monolayers through the self-assembly process. It is important to note that these complexes possess two axial coordination sites available for reacting with other molecules or sensing gases. These unsaturated coordinated metal ions are keys to the specific reactivity. The discussion that follows focuses on the reaction activity of metalloporphyrin- and phthalocyanine-based coordinated complexes.

Zn-TBPP coordinated with the ligand DABCO leading to a supramolecular structure on the Ag (100) surface (Fig. 32) [226]. Each Zn-TBPP molecule exhibits adsorption geometry with an apparent height of approximately 0.08 nm, which indicates that the porphyrin rings are parallel to the Ag substrate surface. At the low temperature of 123 K, the DABCO molecule can adsorb onto the top of the porphyrin ring because of the favorable interaction between the Zn in the upper face of the adsorbed Zn-TBPP and one of the N atoms in the DABCO molecule. After warming the system to 298 K, the DABCO molecules can desorb from the Zn-TBPP surface. These results indicate that the reversible reaction of DABCO with the adsorbed porphyrin derivatives happening depended on the temperature. After that, they chose another bifunctional ligand, 4-methoxypyridine, which can interact with Zn^{2+} from Zn-TBPP through one of the N atoms in 4-methoxypyridine (Fig. 32) [227]. Notice that 4-methoxypyridine can adsorb onto the Ag (100) surface through the O → Ag interaction with the silver surface. This action differs from that of previous DABCO ligands, which cannot adsorb onto Ag (100) at 123 K. Despite the greater apparent height, the Zn-TBPP/4-methoxypyridine complexes display essentially the same diameter and height characteristics as those of the porphyrin molecule. Compared with the Zn-TBPP/DABCO complex, the ligand binds to the upper face of the porphyrin. In this case, the upper linked 4-methoxypyridine with porphyrin yields a distinct central depression. In the case of bright protrusions, the 4-methoxypyridine is located beneath the porphyrin and tethered to the porphyrin and the Ag surface through its N and O atoms, respectively. The weakened porphyrin-surface interaction permits the Zn-TBPP to rotate, and thus the four lobes of the initial porphyrin are reduced to a torus. This rotation can be switched on or off simultaneously by altering the degree of coupling. It should be noted that the phenomenon cannot be observed if methoxybenzene is used. Therefore, this novel ligand can be used to convert the array

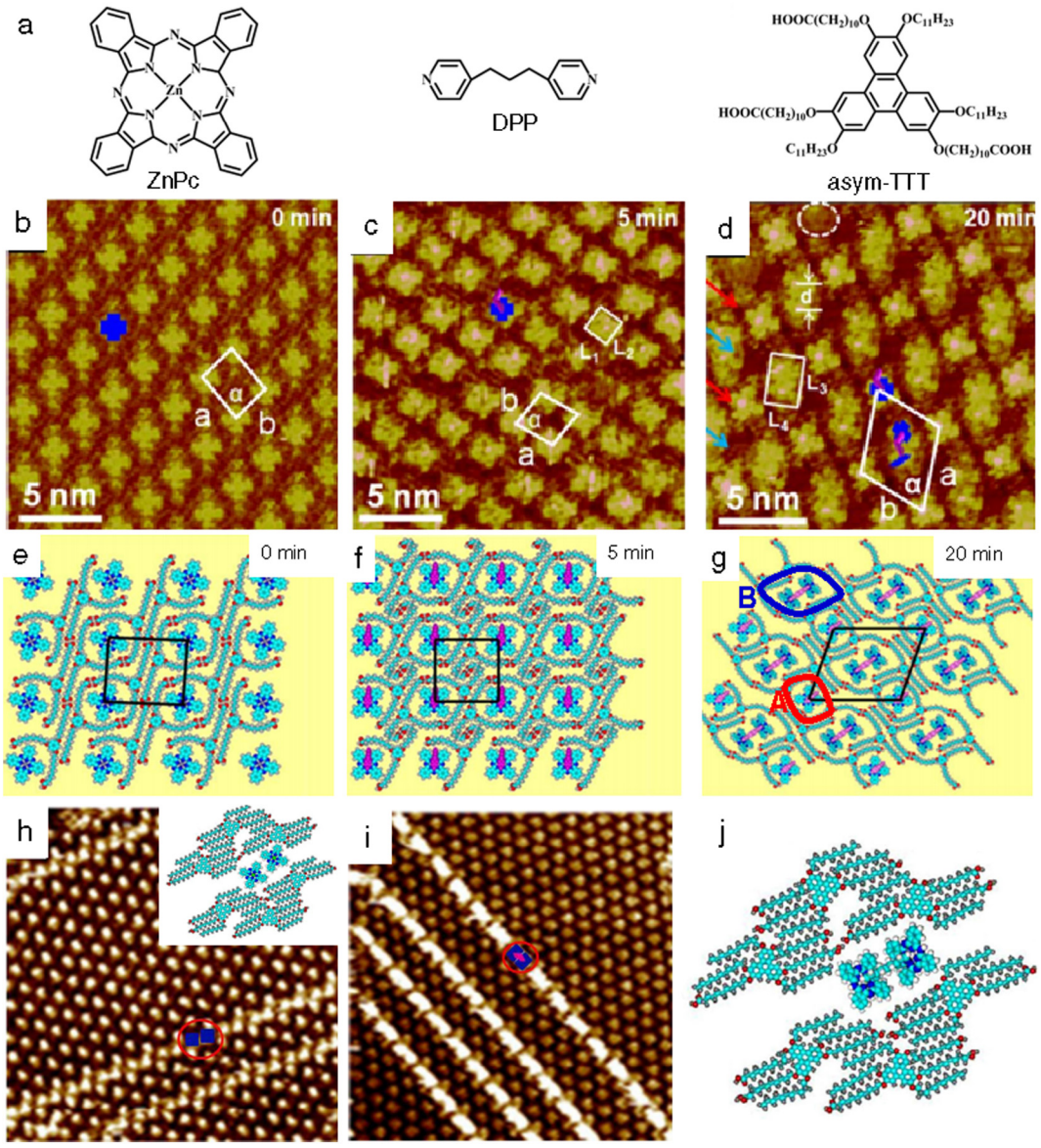

Fig. 33. (a) Chemical structures of ZnPc, DPP and *asym*-TTT. STM images of TCDB/Zn-Pc before (b) and after the DPP molecule was added for 5 min (c) and 20 min (d). (e–g) Suggested molecular models corresponding to (b-d), respectively. (h) STM image showing assembled structure of *asym*-TTT/Zn-Pc with molecular model. (i) STM image showing entirely assembled structure of *asym*-TTT/Zn-Pc/DPP system after the DPP molecule was added. (j) Molecular model for the observed area in (i). (Reprinted with permission from Refs. [108,109]).

of Zn-TBPP into an assembly of surface-mounted rotors. Zn-TDPs coordinated with 3-nitropyridine displayed a higher tendency to locate onto the HOPG surface [228]. The physisorbed Zn-TDPs are better binding sites for nitropyridines, leading to the formation of a supramolecular complex of Zn-TDP/pyridine.

Except for the ligands adsorbed onto the upper face of the complex with the macrocycle planes parallel to the surface, the coordinated organic ligands can also be on the side of the macrocycles, leading to the rotation of the macrocycle planes with respect to the surface. An amazing odd–even alternately arranged structure formed by the template-controlled supramolecular coordination of the Zn-Pc with a V-shaped DPP ligand [108]. In solution, one ZnPc can only coordinate with one DPP molecules through the zinc-pyridine interactions, forming a "⊥"-shaped complex (Zn-Pc/DPP) [229]. However, an interesting odd–even alternately aligned structure can be clearly viewed by STM when the coordination reaction occurred in the TCDB networks (Fig. 33). A sequence of STM images in the same region suggests that a two-step process might occur during the coordination of Zn-Pc with DPP in the TCDB network. First, the Zn-Pc molecule coordinates with one DPP molecule, generating the bright "⊥"-shaped complex Zn-Pc/DPP ("even" pattern). At the same time, the alkyl chains of the TCDB network stretch to adjust the cavity size to immobilize the formed complex suitably. Second, the other non-coordinated pyridine of the coordinated DPP molecule catches another Zn-Pc molecule from the solution to form the bright "⌒"-shaped complex Zn-Pc/DPP/Zn-Pc ("odd" pattern). Simultaneously, the alkyl chains of the TCDB molecules extend to form much larger cavities to accommodate the odd complex. As a result, two kinds of cavities, including larger A and smaller B, are formed (Fig. 33g). In the smaller B-typed cavity, the complex Zn-Pc/DPP can no longer coordinate sequentially with another Zn-Pc molecule from the solution. Notice that the non-coordinated complex Zn-Pc/DPP that stayed in the A-typed cavity easily escapes from the network and causes defects.

Therefore, the synergies of the ligands and the template play an important role in the whole coordination process. Afterwards, another *asym*-TTT template was selected to accommodate the coordination complex formed ZnPc and DPP (Fig. 33) [109]. The results indicate that, in one nano-reactor, every two ZnPc molecules connect with each other via one DPP molecules through the metal–organic coordination interaction. When two kinds of linkers, DPP and DPE were used and heterocaryotic and homonuclear complexes of ZnPc-DPP-ZnTPP and ZnPc-DPE-ZnPc can be observed on the TCDB template [230]. This study helps in understanding the coordination stereo aggregation structure. The study describes the stepwise preparation of molecular wires from ZnOEP complexes bridged by BP via coordination interaction between zinc and nitrogen atom on HOPG [231]. Therefore, it is possible to obtain well-defined organization by careful control.

Other small molecules, such as water and carbon monoxide, can also coordinate with porphyrin derivatives and form 1D polymers. The self-assembly of Zn-TMP through axial coordination with oxygen-containing ligands, such as water and carbon monoxide, formed long-range ordered nanorods on both the Cu (100) and the Au (111) surfaces [232]. High-resolution STM images revealed 1D rod-looking structures, hundreds of nanometers long, on both noble-metal surfaces. Each porphyrin molecule was rotated by 45° around its C4 axis with respect to its neighbors, and the Zn-TMP molecules were linked to each other with bridging water molecules to form a Zn-TMP/water/Zn-TMP complex. The formed polymers laid parallel to the surface with the porphyrin planes perpendicular to the substrate.

6.3. Gas molecule adsorption

The binding of small molecules, in particular gas to metalloporphyrins or phthalocyanines, has fundamental scientific and technological significance. In general, STM/STS measurements can be performed to probe the geometric and electronical structures of the gas-adsorbed metalporphyrins and phthalocyanines. The information provided by molecule-level investigations might be useful for a better understanding of the transport of respiratory gases, the electronic sensory behavior of organic semiconductors, and the catalytic processes in biological systems. Moreover, such special adsorption provides opportunities to explore 2D coordination systems with flexible species in a highly controlled environment. This section summarizes findings on gas molecules adsorbed onto macrocycles.

Under ambient atmosphere, the influence of ambient oxygen on the electronic structure of TiOPc was identified by using STM/STS in combination with CV methods [62]. The STS results showed a positive shift in the energy gap center compared with the Fermi energy of the substrate. In this system, the charge transfer between the bonded O_2 and the central metal Ti greatly affects the ionization and affinity levels of the Pc ring. This study is of much importance prior to fabricating the TiOPc-based nanoelectronic devices.

There is another STM/STS investigation on the interaction of two kinds of small gas molecules (CO, NO) with Co-TPP and Fe-TPP anchored onto the Ag (111) surface [233]. For the Co-TPP/NO system, the STM data indicated that some of the Co-TPP molecules in the array show an evidently modified appearance after dosing small amounts of NO at 150 K. Also, the previous 2-fold symmetry of the Co-TPP core was gradually transformed into one round central protrusion corresponding to the new NO/Co-TPP species. The changed appearance can be attributed to the weakening of the Co-Ag bond induced by the anchored NO ligand. Therefore, the molecule–substrate interactions were reduced as a consequence of the adsorption of NO axial ligand. In addition, the NO ligand coordinated to the Co ion can suppress the interaction between the Co and the substrate Ag [234]. The Co-TPP array can interact with NO on Ag (111) surface [235]. The initially ordered Co-TPP layer reorganizes because of lateral dipole–dipole interactions. The results suggest a novel method, not only to tune the arrangement of porphyrins on surface, but also to fabricate functional layers from large organic molecules after exposure to small molecules. However, in the CO/Co-TPP system, the CO molecules can attach weakly to the surface-adsorbed Co-TPP molecule. Upon attachment of CO, two related cross-like structures can be identified. In contrast to NO, the attachment of one or two CO ligands onto the Co-TPP does not induce the change of the electronic structure [233]. For Fe-TPP anchored onto Ag (111), results similar to the Co-TPP/NO or Co-TPP/Co system were obtained. These findings open up new ways to tune the reactivity of the on-surface molecular arrays and thus could be used in sensing or catalysis applications [233].

NO molecules affect the surface chemical bonds between the adsorbed tetraphenylporphyrins-M(II) (MTTPs, M = Fe, Co, Zn) and a Ag (111) surface [236]. With axial coordination of NO to either the Co or the Fe center of the adsorbed MTPPs, the state induced by the interaction of the MTPPs and the substrate was completely quenched (Fig. 34). The combination of experimental and computational results indicates that the Ag(5s) orbitals become nonbonding with Co-TPP and weakly bonding with Fe-TPP. Besides, the additional NO coordination can change the magnetic properties of the metal ions. After removing the NO ligands by thermal desorption, the MTPPs restore their original properties. Therefore, the process of formation and the fracture of the substrate-metal coordination bond are fully reversible. Notice that ZnTPP did not interact with the Ag surface, indicating that the coordination bond strength depends on the property of the central metal.

Except for the metalporphyrins and phthalocyanines mentioned previously, the open 2D-MOCN can also provide metal sites to bind small gas molecules. The oxygen dissociation is controlled by the catalytic action of mono-iron or di-iron sites on a Cu (100) surface [237]. *In situ* STM investigations were performed to characterize the local structure before and after O_2 exposure. From the sequence, through high-resolution STM images (Fig. 35), the long-range order of the pristine phase of TPA was gradually destroyed by increasing the molecular oxygen dosage, which revealed the structural modifications of MOCNs with O_2 exposure. At the initial steps, a characteristic structure containing the unaffected pristine phase was observed as a function of the oxygen adsorption. At last, a sufficient high-oxygen exposure induced disordered structures driven by the thermal-induced diffusion at room temperature.

7. Conclusions and perspectives

Supramolecular coordination chemistry, including the structures, dynamics, and activities recorded by the STM technique, has been described. Through this effective technique, STM details the supramolecular coordination phenomena on solid supports under vacuum conditions as well as in ambient environments. Because of its ability to probe locally, STM provides more detailed information at submolecular-scale levels on the organization, dynamics, and reactivity at the interfaces. This information helps provide a deeper understanding of the surface-confined coordination process and mechanism. These findings give insight into the principles underlying the coordination of organic ligands and metal centers on surfaces and illustrate their potential for rational metallosupramolecular engineering. Through careful discussion of the chosen examples from the reported studies, it can be concluded that the coordination chemistry of metals and organic ligands can bring uniquely assembled coordination architectures on confined

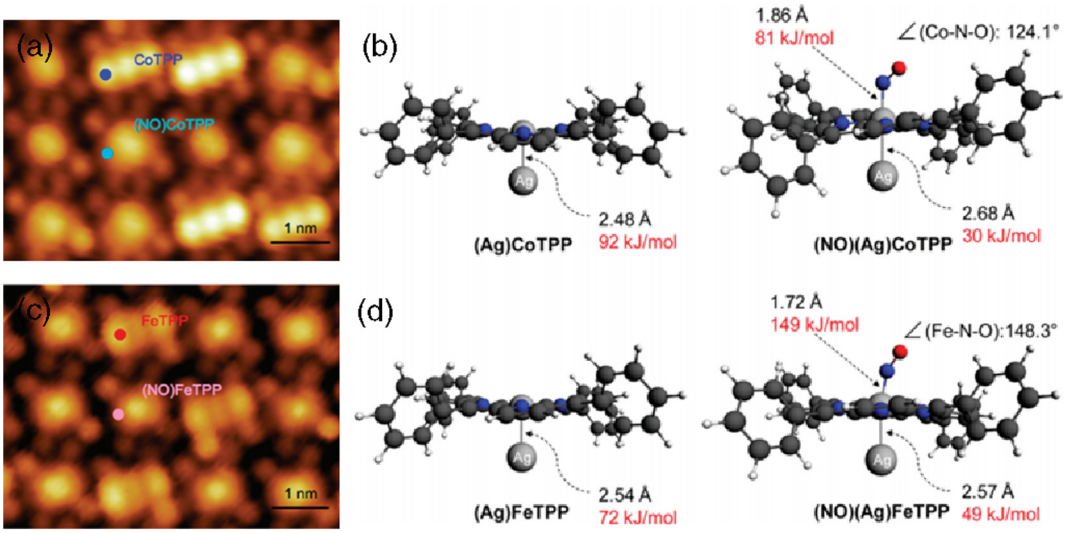

Fig. 34. (a) STM image of a mixed Co-TPP and (NO)Co-TPP array (I = 55 pA, V = 0.7 V). (b) Optimized geometries and ligand binding energies of (Ag)Co-TPP and (NO)(Ag)Co-TPP. (c) Mixed Fe-TPP and (NO)Fe-TPP array (I = 0.1 nA, V = 0.7 V). (d) Optimized geometries and ligand binding energies of (Ag)Fe-TPP and (NO)(Ag)Fe-TPP. (Reprinted with permission from Ref. [236]).

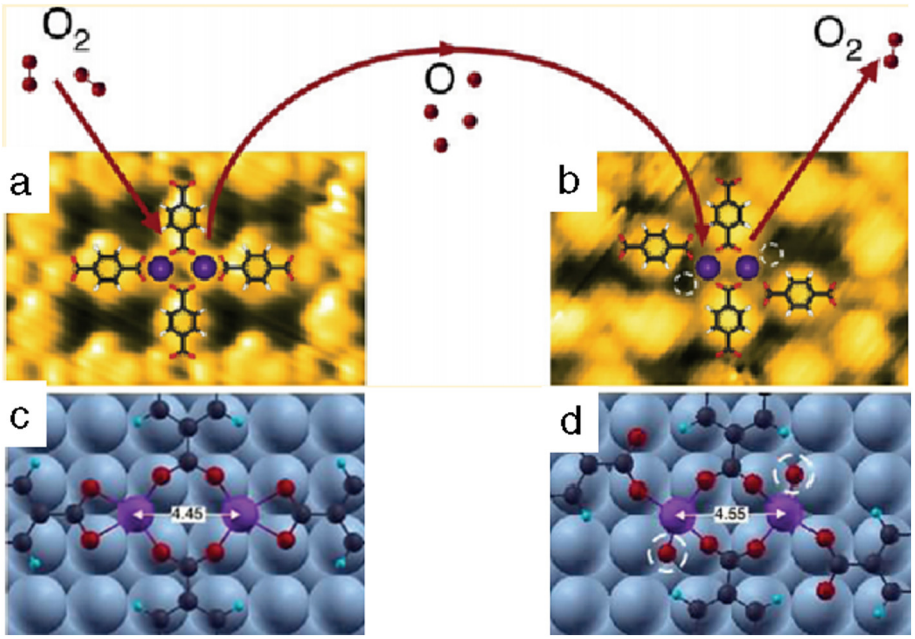

Fig. 35. Oxygen dissociation by concerted action of di-Iron centers in MOCN at surfaces. High-resolution STM topograph of the di-iron MOCN before oxygen exposure (a) and after O_2 exposure (b), corresponding equilibrium geometries (c and d). (Reprinted with permission from Ref. [237]).

solid surfaces, such as 1D nano chains, 2D metal-organic networks, and 3D sandwich structures. Various strategies for constructing metallosupramolecular organizations on surfaces are described. Furthermore, the surface-confined supramolecular coordination assembly often undergoes in an unusual manner, which differs from what occurred in the solution. Notably, some coordination reactions that were inhibited in the solution phase can occur on the metal substrate; thus, the substrate effect should not be ignored. The coordination of pre-assembled molecules has been established as a convenient tool for modifying surface-confined functional molecules. The coordination requires moderate annealing to overcome the barriers for the ligands or for metal atom diffusion. More important, the coordination-assembled nanostructures can be used as particular molecular templates for trapping small functional organic molecules and gas molecules, showing a potential application in gas or energy storage.

In the future, theoretical and experimental study on the coordination-assembled structures and the electron properties will help facilitate molecular engineering, and predictable specific properties are keys to further development. The metallosupramolecules exhibit ample functionality with a high degree of symmetry and unique morphologies, which makes them ideally suited for the realization of large-area molecular devices on flexible substrates. The conformation, orientation, and packing structure of these molecules in the first layer on the solid substrate can determine the performance of such devices, thus gaining the properties of single molecules, and the molecular arrangement at the interfaces is important prior to fabricating metallosupramolecule-based hybrid

devices. In addition, the self-organization of multiple biological subunits into well-defined highly ordered structures promotes the development of supramolecular assemblies to resemble the natural systems. The functional groups substituted on the subunits affect the self-organization by the interactions. Future investigations of coordination chemistry will continue to build upon these results.

Acknowledgements

We thank all of the co-workers who have contributed to this review, whose names can be found in the literatures cited herein. Financial supports from the National Basic Research Program of China (2016YFA0200700) and National Natural Science Foundation of China (Nos. 21472029, 71273152, 71573148) are also gratefully acknowledged.

References

[1] M. Shimomura, T. Sawadaishi, Curr. Opin. Colloid Interface Sci. 6 (2001) 11.
[2] M. Geissler, Y.N. Xia, Adv. Mater. 16 (2004) 1249.
[3] D. Philp, J.F. Stoddart, Angew. Chem. Int. Ed. 35 (1996) 1155.
[4] J.V. Barth, G. Costantini, K. Kern, Nature 437 (2005) 671.
[5] A.J. Blake, N.R. Champness, P. Hubberstey, W.S. Li, M.A. Withersby, M. Schroder, Coord. Chem. Rev. 183 (1999) 117.
[6] S. Leininger, B. Olenyuk, P.J. Stang, Chem. Rev. 100 (2000) 853.
[7] J.M. Lehn, Angew. Chem. Int. Ed. 29 (1990) 1304.
[8] G. Decher, Science 277 (1997) 1232.
[9] S.G. Zhang, Nat. Biotech. 21 (2003) 1171.
[10] A. Rosler, G.W.M. Vandermeulen, H.A. Klok, Adv. Drug Delivery Rev. 53 (2001) 95.
[11] J.H. Fendler, Chem. Mater. 8 (1996) 1616.
[12] R.K. Smith, P.A. Lewis, P.S. Weiss, Prog. Surf. Sci. 75 (2004) 1.
[13] K.J.M. Bishop, C.E. Wilmer, S. Soh, B.A. Grzybowski, Small 5 (2009) 1600.
[14] L.J. Prins, D.N. Reinhoudt, P. Timmerman, Angew. Chem. Int. Ed. 40 (2001) 2382.
[15] F. Wurthner, C.C. You, C.R. Saha-Moller, Chem. Soc. Rev. 33 (2004) 133.
[16] D.W. Zhang, X. Zhao, J.L. Hou, Z.T. Li, Chem. Rev. 112 (2012) 5271.
[17] C.G. Claessens, J.F. Stoddart, J. Phys. Org. Chem. 10 (1997) 254.
[18] P.A. Gale, Coord. Chem. Rev. 240 (2003) 191.
[19] P.A. Gale, Coord. Chem. Rev. 213 (2001) 79.
[20] P.A. Gale, Coord. Chem. Rev. 199 (2000) 181.
[21] P.A. Gale, R. Quesada, Coord. Chem. Rev. 250 (2006) 3219.
[22] C.F.J. Faul, M. Antonietti, Adv. Mater. 15 (2003) 673.
[23] A. Werner, Z. Anorg, Allg. Chem. 3 (1893) 267.
[24] M. Fujita, M. Tominaga, A. Hori, B. Therrien, Acc. Chem. Res. 38 (2005) 369.
[25] M. Ruben, J. Rojo, F.J. Romero-Salguero, L.H. Uppadine, J.M. Lehn, Angew. Chem. Int. Ed. 43 (2004) 3644.
[26] S.H. Sun, Adv. Mater. 18 (2006) 393.
[27] K.T. Holman, A.M. Pivovar, J.A. Swift, M.D. Ward, Acc. Chem. Res. 34 (2001) 107.
[28] X.M. Chen, M.L. Tong, Acc. Chem. Res. 40 (2007) 162.
[29] P.J. Steel, Acc. Chem. Res. 38 (2005) 243.
[30] C.J. Jones, Chem. Soc. Rev. 27 (1998) 289.
[31] G.X. Jin, Coord. Chem. Rev. 248 (2004) 587.
[32] J. Zhang, X. Wang, G.X. Jin, Coord. Chem. Rev. 250 (2006) 95.
[33] K. Matyjaszewski, N.V. Tsarevsky, Nat. Chem. 1 (2009) 276.
[34] S.S. Li, B.H. Northrop, Q.H. Yuan, L.J. Wan, P.J. Stang, Acc. Chem. Res. 42 (2009) 249.
[35] R. Chakrabarty, P.S. Mukherjee, P.J. Stang, Chem. Rev. 111 (2011) 6810.
[36] N. Lin, S. Stepanow, M. Ruben, J.V. Barth, Top. Curr. Chem. 287 (2009) 1.
[37] M. Baalousha, M. Motelica-Heino, S. Galaup, P. Le Coustumer, Microsc. Res. Techniq. 66 (2005) 299.
[38] J.B. Hightower, D.R. Olmos, J.A. Walmsley, J. Phys. Chem. B 113 (2009) 12214.
[39] W.J. Chung, J.W. Oh, K. Kwak, B.Y. Lee, J. Meyer, E. Wang, A. Hexemer, S.W. Lee, Nature 478 (2011) 364.
[40] M. Ye, Y. Zhang, H. Li, M.Y. Xie, J. Hu, J. Phys. Chem. B 114 (2010) 15759.
[41] L. Liu, L. Zhang, L. Niu, M. Xu, X.B. Mao, Y.L. Yang, C. Wang, ACS Nano 5 (2011) 6001.
[42] X.B. Mao, C.X. Wang, X.K. Wu, X.J. Ma, L. Liu, L. Zhang, L. Niu, Y.Y. Guo, D.H. Li, Y.L. Yang, C. Wang, P. Natl, Acad. Sci. USA 108 (2011) 19605.
[43] D. Zhan, L. Liu, Y.N. Xu, Z.H. Ni, J.X. Yan, C. Zhao, Z.X. Shen, Sci. Rep. 1 (2011) 00012.
[44] G. Binning, H. Rohrer, C. Gerber, E. Weibel, Phys. Rev. Lett. 49 (1982) 57.
[45] G. Binnig, H. Rohrer, Rev. Mod. Phys. 59 (1987) 615.
[46] S. De Feyter, F.C. De Schryver, Chem. Soc. Rev. 32 (2003) 139.
[47] S. De Feyter, F.C. De Schryver, J. Phys. Chem. B 109 (2005) 4290.
[48] K.S. Mali, J. Adisoejoso, E. Ghijsens, I. De Cat, S. De Feyter, Acc. Chem. Res. 45 (2012) 1309.
[49] L.R. Xu, L. Yang, S.B. Lei, Nanoscale 4 (2012) 4399.
[50] S.B. Lei, K. Tahara, X.L. Feng, S.H. Furukawa, F.C. De Schryver, K. Mullen, Y. Tobe, S. De Feyter, J. Am. Chem. Soc. 130 (2008) 7119.
[51] S. Furukawa, S. De Feyter, Top. Curr. Chem. 287 (2009) 87.
[52] H. Liang, Y. He, Y.C. Ye, X.G. Xu, F. Cheng, W. Sun, X. Shao, Y.F. Wang, J.L. Li, K. Wu, Coord. Chem. Rev. 253 (2009) 2959.
[53] M. Li, K. Deng, S.B. Lei, Y.L. Yang, T.S. Wang, Y.T. Shen, C.R. Wang, Q.D. Zeng, C. Wang, Angew. Chem. Int. Ed. 47 (2008) 6717.
[54] S. De Feyter, A. Gesquiere, M.M. Abdel-Mottaleb, P.C.M. Grim, F.C. De Schryver, C. Meiners, M. Sieffert, S. Valiyaveettil, K. Mullen, Acc. Chem. Res. 33 (2000) 520.
[55] F. Besenbacher, J.V. Lauritsen, T.R. Linderoth, E. Laegsgaard, R.T. Vang, S. Wendt, Surf. Sci. 603 (2009) 1315.
[56] F. Rossel, M. Pivetta, W.D. Schneider, Surf. Sci. Rep. 65 (2010) 129.
[57] R.T. Vang, J.V. Lauritsen, E. Laegsgaard, F. Besenbacher, Chem. Soc. Rev. 37 (2008) 2191.
[58] Y.L. Yang, C. Wang, Chem. Soc. Rev. 38 (2009) 2576.
[59] X.M. Zhang, H.F. Wang, S. Wang, Y.T. Shen, Y.L. Yang, K. Deng, K.Q. Zhao, Q.D. Zeng, C. Wang, J. Phys. Chem. C 117 (2013) 307.
[60] X.H. Qiu, G.V. Nazin, W. Ho, Science 299 (2003) 542.
[61] S.B. Lei, K. Deng, D.L. Yang, Q.D. Zeng, C. Wang, J. Phys. Chem. B 110 (2006) 1256.
[62] X.H. Kong, M. Wang, S.B. Lei, Y.L. Yang, C. Wang, J. Mater. Chem. 16 (2006) 4265.
[63] Y.B. Li, J.H. Wan, G.C. Qi, K. Deng, Y.L. Yang, Q.D. Zeng, W. Huang, C. Wang, Chem. Phys. Lett. 474 (2009) 132.
[64] O. Fischer, M. Kugler, I. Maggio-Aprile, C. Berthod, C. Renner, Rev. Mod. Phys. 79 (2007) 353.
[65] J. Adisoejoso, K. Tahara, S. Okuhata, S. Lei, Y. Tobe, S. De Feyter, Angew. Chem. Int. Ed. 48 (2009) 7353.
[66] R.S. Xie, Y.H. Song, L.L. Wan, H.Z. Yuan, P.C. Li, X.P. Xiao, L. Liu, S.H. Ye, S.B. Lei, L. Wang, Anal. Sci. 27 (2011) 129.
[67] Y. Okawa, S.K. Mandal, C.P. Hu, Y. Tateyama, S. Goedecker, S. Tsukamoto, T. Hasegawa, J.K. Gimzewski, M. Aono, J. Am. Chem. Soc. 133 (2011) 8227.
[68] J. Mielke, F. Leyssner, M. Koch, S. Meyer, Y. Luo, S. Selvanathan, R. Haag, P. Tegeder, L. Grill, ACS Nano 5 (2011) 2090.
[69] D. Bleger, A. Ciesielski, P. Samori, S. Hecht, Chem. -Eur. J. 16 (2010) 14256.
[70] L. Grill, M. Dyer, L. Lafferentz, M. Persson, M.V. Peters, S. Hecht, Nat. Nanotech. 2 (2007) 687.
[71] X.M. Zhang, S.D. Xu, M. Li, Y.T. Shen, Z.Q. Wei, S. Wang, Q.D. Zeng, C. Wang, J. Phys. Chem. C 116 (2012) 8950.
[72] D.Y. Zhong, J.H. Franke, S.K. Podiyanachari, T. Blomker, H.M. Zhang, G. Kehr, G. Erker, H. Fuchs, L.F. Chi, Science 334 (2011) 213.
[73] K. Tahara, H. Yamaga, E. Ghijsens, K. Inukai, J. Adisoejoso, M.O. Blunt, S. De Feyter, Y. Tobe, Nat. Chem. 3 (2011) 714.
[74] J. Liu, T. Chen, X. Deng, D. Wang, J. Pei, L.J. Wan, J. Am. Chem. Soc. 133 (2011) 21010.
[75] I. De Cat, Z.X. Guo, S.J. George, E.W. Meijer, A.P.H.J. Schenning, S. De Feyter, J. Am. Chem. Soc. 134 (2012) 3171.
[76] Q. Chen, T. Chen, D. Wang, H.B. Liu, Y.L. Li, L.J. Wan, P. Natl, Acad. Sci. USA 107 (2010) 2769.
[77] Y.T. Shen, K. Deng, Q.D. Zeng, C. Wang, Small 6 (2010) 76.
[78] J.M. Cai, P. Ruffieux, R. Jaafar, M. Bieri, T. Braun, S. Blankenburg, M. Muoth, A.P. Seitsonen, M. Saleh, X.L. Feng, K. Mullen, R. Fasel, Nature 466 (2010) 470.
[79] X.M. Zhang, S. Wang, Y.T. Shen, Y.Y. Guo, Q.D. Zeng, C. Wang, Nanoscale 4 (2012) 5039.
[80] F.Y. Hu, X.M. Zhang, X.C. Wang, S. Wang, H.Q. Wang, W.B. Duan, Q.D. Zeng, C. Wang, A.C.S. Appl, Mater. Inter. 5 (2013) 1583.
[81] Y.Q. Zhang, N. Kepcija, M. Kleinschrodt, K. Diller, S. Fischer, A.C. Papageorgiou, F. Allegretti, J. Bjork, S. Klyatskaya, F. Klappenberger, M. Ruben, J.V. Barth, Nat. Commun. 3 (2012).
[82] F. Bebensee, C. Bombis, S.R. Vadapoo, J.R. Cramer, F. Besenbacher, K.V. Gothelf, T.R. Linderoth, J. Am. Chem. Soc. 135 (2013) 2136.
[83] X.M. Zhang, Q.D. Zeng, C. Wang, RSC. Adv. 3 (2013) 11351.
[84] Y.T. Shen, L. Guan, X.Y. Zhu, Q.D. Zeng, C. Wang, J. Am. Chem. Soc. 131 (2009) 6174.
[85] Y.T. Shen, K. Deng, X.M. Zhang, W. Feng, Q.D. Zeng, C. Wang, J.R. Gong, Nano Lett. 11 (2011) 3245.
[86] R. Gutzler, T. Sirtl, J.F. Dienstmaier, K. Mahata, W.M. Heckl, M. Schmittel, M. Lackinger, J. Am. Chem. Soc. 132 (2010) 5084.
[87] X.M. Zhang, Q.D. Zeng, C. Wang, Nanoscale 5 (2013) 8269.
[88] Y.F. Geng, J. Xu, J.D. Xue, X.M. Shen, M. Li, J.D. Huang, X.K. Li, Q.D. Zeng, Langmuir 31 (2015) 13394.
[89] J.T. Davis, G.P. Spada, Chem. Soc. Rev. 36 (2007) 296.
[90] A. Ciesielski, S. Lena, S. Masiero, G.P. Spada, P. Samori, Angew. Chem. Int. Ed. 49 (2010) 1963.
[91] W. Xu, J.G. Wang, M. Yu, E. Laesgaard, I. Stensgaard, T.R. Linderoth, B. Hammer, C. Wang, F. Besenbacher, J. Am. Chem. Soc. 132 (2010) 15927.
[92] D.P. Luo, X.M. Zhang, Y.T. Shen, J. Xu, L.J. Shu, Q.D. Zeng, C. Wang, Chem. Commun. 50 (2014) 9369.
[93] Y.M. Lin, C. Dimitrakopoulos, K.A. Jenkins, D.B. Farmer, H.Y. Chiu, A. Grill, P. Avouris, Science 327 (2010) 662.
[94] R.F. Zou, Q. Wang, J.C. Wu, J.X. Wu, C. Schmuck, H. Tian, Chem. Soc. Rev. 44 (2015) 5200.
[95] Y.B. Li, C.H. Liu, Y.Z. Xie, X. Li, X.L. Fan, L.H. Yuan, Q.D. Zeng, Chem. Commun. 49 (2013) 9021.

[96] Y.B. Wang, L. Niu, Y.B. Li, X.B. Mao, Y.L. Yang, C. Wang, Langmuir 26 (2010) 16305.
[97] J.R. Gong, L.J. Wan, Q.H. Yuan, C.L. Bai, H. Jude, P.J. Stang, P. Natl, Acad. Sci. USA 102 (2005) 971.
[98] Q.H. Yuan, L.J. Wan, H. Jude, P.J. Stang, J. Am. Chem. Soc. 127 (2005) 16279.
[99] L.J. Wan, Acc. Chem. Res. 39 (2006) 334.
[100] T. Chen, G.B. Pan, H. Wettach, M. Fritzsche, S. Hoger, L.J. Wan, H.B. Yang, B.H. Northrop, P.J. Stang, J. Am. Chem. Soc. 132 (2010) 1328.
[101] J. Otsuki, Coord. Chem. Rev. 254 (2010) 2311.
[102] J. Lu, S.B. Lei, Q.D. Zeng, S.Z. Kang, C. Wang, L.J. Wan, C.L. Bai, J. Phys. Chem. B 108 (2004) 5161.
[103] Y. Li, C. Liu, Y. Xie, X. Li, X. Li, X. Fan, K. Deng, Q. Zeng, C. Wang, Phys. Chem. Chem. Phys. 15 (2013) 125.
[104] J. Liu, T. Lin, Z.L. Shi, F. Xia, L. Dong, P.N. Liu, N. Lin, J. Am. Chem. Soc. 133 (2011) 18760.
[105] Y. Li, K. Deng, X. Wu, S. Lei, K. Zhao, Y. Yang, Q. Zeng, C. Wang, J. Mater. Chem. 20 (2010) 9100.
[106] Y. Shen, L. Zeng, D. Lei, X. Zhang, K. Deng, Y. Feng, W. Feng, S. Lei, S. Li, L. Gan, Q. Zeng, C. Wang, J. Mater. Chem. 21 (2011) 8787.
[107] Y. Shen, K. Deng, M. Li, X. Zhang, G. Zhou, K. Mullen, Q. Zeng, C. Wang, CrystEngComm 15 (2013) 5526.
[108] X.M. Zhang, Y.T. Shen, S. Wang, Y.Y. Guo, K. Deng, C. Wang, Q.D. Zeng, Sci. Rep. 2 (2012) 00742.
[109] Y.B. Li, L.X. Cheng, C.H. Liu, W. Liu, Y.L. Fan, X.L. Fan, Q.D. Zeng, Sci. Rep. 5 (2015) 10972.
[110] J.H. Mao, H.G. Zhang, Y.H. Jiang, Y. Pan, M. Gao, W.D. Xiao, H.J. Gao, J. Am. Chem. Soc. 131 (2009) 14136.
[111] R. Gutzler, S. Stepanow, D. Grumelli, M. Lingenfelder, K. Kern, Acc. Chem. Res. 48 (2015) 2132.
[112] W. Auwarter, D. Ecija, F. Klappenberger, J.V. Barth, Nat. Chem. 7 (2015) 105.
[113] S. Mohnani, D. Bonifazi, Coord. Chem. Rev. 254 (2010) 2342.
[114] D.M. Guldi, Chem. Soc. Rev. 31 (2002) 22.
[115] H. Imahori, S. Fukuzumi, Adv. Funct. Mater. 14 (2004) 525.
[116] O. Shoji, S. Okada, A. Satake, Y. Kobuke, J. Am. Chem. Soc. 127 (2005) 2201.
[117] O. Shoji, H. Tanaka, T. Kawai, Y. Kobuke, J. Am. Chem. Soc. 127 (2005) 8598.
[118] D. Ecija, K. Seufert, D. Heim, W. Auwarter, C. Aurisicchio, C. Fabbro, D. Bonifazi, J.V. Barth, ACS Nano 4 (2010) 4936.
[119] L. Cui, Y.F. Geng, C.F. Leong, Q. Ma, D.M. D'Alessandro, K. Deng, Q.D. Zeng, J.L. Zuo, Sci. Rep. 6 (2016) 25544.
[120] J.Y. Zhang, S.Q. Chang, B.H.R. Suryanto, C.H. Gong, X.H. Zeng, C. Zhao, Q.D. Zeng, J.L. Xie, Inorg. Chem. 55 (2016) 5585.
[121] C.J. Kuehl, Y.K. Kryschenko, U. Radhakrishnan, S.R. Seidel, S.D. Huang, P.J. Stang, P. Natl, Acad. Sci. USA 99 (2002) 4932.
[122] Q.H. Yuan, C.J. Yan, H.J. Yan, L.J. Wan, B.H. Northrop, H. Jude, P.J. Stang, J. Am. Chem. Soc. 130 (2008) 8878.
[123] J.B. Beck, S.J. Rowan, J. Am. Chem. Soc. 125 (2003) 13922.
[124] G.R. Whittell, I. Manners, Adv. Mater. 19 (2007) 3439.
[125] S.K. Yang, A.V. Ambade, M. Weck, Chem. Soc. Rev. 40 (2011) 129.
[126] F. Buchner, K. Flechtner, Y. Bai, E. Zillner, I. Kellner, H.P. Steinrueck, H. Marbach, J.M. Gottfried, J. Phys. Chem. C 112 (2008) 15458.
[127] Y.B. Li, K.Q. Zhao, Y.L. Yang, K. Deng, Q.D. Zeng, C. Wang, Nanoscale 4 (2012) 148.
[128] Y.F. Geng, M.Q. Liu, J.D. Xue, P. Xu, Y.F. Wang, L.J. Shu, Q.D. Zeng, C. Wang, Chem. Commun. 51 (2015) 6820.
[129] A.P. Seitsonen, M. Lingenfelder, H. Spillmann, A. Dmitriev, S. Stepanow, N. Lin, K. Kern, J.V. Barth, J. Am. Chem. Soc. 128 (2006) 5634.
[130] S. Stepanow, N. Lin, J.V. Barth, K. Kern, J. Phys. Chem. B 110 (2006) 23472.
[131] S. Stepanow, N. Lin, D. Payer, U. Schlickum, F. Klappenberger, G. Zoppellaro, M. Ruben, H. Brune, J.V. Barth, K. Kern, Angew. Chem. Int. Ed. 46 (2007) 710.
[132] A.G. Trant, T.E. Jones, C.J. Baddeley, J. Phys. Chem. C 111 (2007) 10534.
[133] A.G. Trant, C.J. Baddeley, Langmuir 27 (2011) 1788.
[134] H.M. Zhang, W. Zhao, Z.X. Xie, L.S. Long, B.W. Mao, X. Xu, L.S. Zheng, J. Phys. Chem. C 111 (2007) 7570.
[135] S. De Feyter, M.M.S. Abdel-Mottaleb, N. Schuurmans, B.J.V. Verkuijl, J.H. van Esch, B.L. Feringa, F.C. De Schryver, Chem. -Eur. J. 10 (2004) 1124.
[136] Y. Kikkawa, E. Koyama, S. Tsuzuki, K. Fujiwara, K. Miyake, H. Tokuhisa, M. Kanesato, Chem. Commun. (2007) 1343.
[137] Y.X. Gong, S.Q. Zhang, Y.F. Geng, C.M. Niu, S.C. Yin, Q.D. Zeng, M. Li, Langmuir 31 (2015) 11525.
[138] J. Adisoejoso, Y. Li, J. Liu, P.N. Liu, N. Lin, J. Am. Chem. Soc. 134 (2012) 18526.
[139] Z.L. Shi, N. Lin, ChemPhysChem. 11 (2010) 97.
[140] Y. Li, J. Xiao, T.E. Shubina, M. Chen, Z.L. Shi, M. Schmid, H.P. Steinruck, J.M. Gottfried, N. Lin, J. Am. Chem. Soc. 134 (2012) 6401.
[141] F. Studener, K. Muller, N. Marets, V. Bulach, M.W. Hosseini, M. Stohr, J. Chem. Phys. 142 (2015).
[142] P. Przychodzen, T. Korzeniak, R. Podgajny, B. Sieklucka, Coord. Chem. Rev. 250 (2006) 2234.
[143] U. Schlickum, R. Decker, F. Klappenberger, G. Zoppellaro, S. Klyatskaya, W. Auwarter, S. Neppl, K. Kern, H. Brune, M. Ruben, J.V. Barth, J. Am. Chem. Soc. 130 (2008) 11778.
[144] U. Schlickum, R. Decker, F. Klappenberger, G. Zoppellaro, S. Klyatskaya, M. Ruben, I. Silanes, A. Arnau, K. Kern, H. Brune, J.V. Barth, Nano Lett. 7 (2007) 3813.
[145] D. Kuhne, F. Klappenberger, R. Decker, U. Schlickum, H. Brune, S. Klyatskaya, M. Ruben, J.V. Barth, J. Am. Chem. Soc. 131 (2009) 3881.
[146] U. Schlickum, F. Klappenberger, R. Decker, G. Zoppellaro, S. Klyatskaya, M. Ruben, K. Kern, H. Brune, J.V. Barth, J. Phys. Chem. C 114 (2010) 15602.
[147] N. Henningsen, R. Rurali, C. Limbach, R. Drost, J.I. Pascual, K.J. Franke, J. Phys. Chem. Lett. 2 (2011) 55.
[148] T.C. Tseng, C.S. Lin, X.Q. Shi, S.L. Tait, X. Liu, U. Starke, N. Lin, R.Q. Zhang, C. Minot, M.A. Van Hove, J.I. Cerda, K. Kern, Phys. Rev. B 80 (2009).
[149] Q. Sun, L.L. Cai, H.H. Ma, C.X. Yuan, W. Xu, Chem. Commun. 51 (2015) 14164.
[150] F. Bischoff, Y.Q. He, K. Seufert, D. Stassen, D. Bonifazi, J.V. Barth, W. Auwarter, Chem. -Eur. J. 22 (2016) 15298.
[151] P. Messina, A. Dmitriev, N. Lin, H. Spillmann, M. Abel, J.V. Barth, K. Kern, J. Am. Chem. Soc. 124 (2002) 14000.
[152] H. Spillmann, A. Dmitriev, N. Lin, P. Messina, J.V. Barth, K. Kern, J. Am. Chem. Soc. 125 (2003) 10725.
[153] Y. Wang, S. Fabris, G. Costantini, K. Kern, J. Phys. Chem. C 114 (2010) 13020.
[154] Y.F. Zhang, N. Zhu, T. Komeda, J. Phys. Chem. C 111 (2007) 16946.
[155] C.S. Kley, J. Cechal, T. Kumagai, F. Schramm, M. Ruben, S. Stepanow, K. Kern, J. Am. Chem. Soc. 134 (2012) 6072.
[156] W. Li, J. Jin, X.L. Leng, Y. Lu, X.Q. Liu, L. Wang, J. Phys. Chem. C 120 (2016) 12605.
[157] C. Joachim, J.K. Gimzewski, A. Aviram, Nature 408 (2000) 541.
[158] R. Gonzalez-Moreno, C. Sanchez-Sanchez, M. Trelka, R. Otero, A. Cossaro, A. Verdini, L. Floreano, M. Ruiz-Bermejo, A. Garcia-Lekue, J.A. Martin-Gago, C. Rogero, J. Phys. Chem. C 115 (2011) 6849.
[159] S.L. Tait, A. Langner, N. Lin, S. Stepanow, C. Rajadurai, M. Ruben, K. Kern, J. Phys. Chem. C 111 (2007) 10982.
[160] F. Klappenberger, A. Weber-Bargioni, W. Auwarter, M. Marschall, A. Schiffrin, J.V. Barth, J. Chem. Phys. 129 (2008).
[161] D. Heim, D. Ecija, K. Seutert, W. Auwarter, C. Aurisicchio, C. Fabbro, D. Bonifazi, J.V. Barth, J. Am. Chem. Soc. 132 (2010) 6783.
[162] D. Ecija, M. Marschall, J. Reichert, A. Kasperski, D. Nieckarz, P. Szabelski, W. Auwarter, J.V. Barth, Surf. Sci. 643 (2016) 91.
[163] W.H. Wang, S.Y. Wang, Y.N. Hong, B.Z. Tang, N. Lin, Chem. Commun. 47 (2011) 10073.
[164] L.A. Fendt, M. Stohr, N. Wintjes, M. Enache, T.A. Jung, F. Diederich, Chem. -Eur. J. 15 (2009) 11139.
[165] G.E. Pacchioni, M. Pivetta, H. Brune, J. Phys. Chem. C 119 (2015) 25442.
[166] A. Dmitriev, N. Lin, J. Weckesser, J.V. Barth, K. Kern, J. Phys. Chem. B 106 (2002) 6907.
[167] N. Lin, A. Dmitriev, J. Weckesser, J.V. Barth, K. Kern, Angew. Chem. Int. Ed. 41 (2002) 4779.
[168] J.V. Barth, J. Weckesser, N. Lin, A. Dmitriev, K. Kern, Appl. Phys. A 76 (2003) 645.
[169] T. Classen, M. Lingenfelder, Y. Wang, R. Chopra, C. Virojanadara, U. Starke, G. Costantini, G. Fratesi, S. Fabris, S. de Gironcoli, S. Baroni, S. Haq, R. Raval, K. Kern, J. Phys. Chem. A 111 (2007) 12589.
[170] B. Hammer, J.K. Norskov, Nature 376 (1995) 238.
[171] S.Y. Quek, M.M. Biener, J. Biener, J. Bhattacharjee, C.M. Friend, U.V. Waghmare, E. Kaxiras, J. Phys. Chem. B 110 (2006) 15663.
[172] Z.H. Li, T. Wandlowski, J. Phys. Chem. C 113 (2009) 7821.
[173] J.A. Boscoboinik, F.C. Calaza, Z. Habeeb, D.W. Bennett, D.J. Stacchiola, M.A. Purino, W.T. Tysoe, Phys. Chem. Chem. Phys. 12 (2010) 11624.
[174] H. Huang, Z.Y. Tan, Y.W. He, J. Liu, J.T. Sung, K. Zhao, Z.H. Zhou, G. Tian, S.L. Wong, A.T.S. Wee, ACS Nano 10 (2016) 3198.
[175] M.N. Faraggi, N. Jiang, N. Gonzalez-Lakunza, A. Langner, S. Stepanow, K. Kern, A. Arnau, J. Phys. Chem. C 116 (2012) 24558.
[176] Z.C. Yang, M. Corso, R. Robles, C. Lotze, R. Fitzner, E. Mena-Osteritz, P. Bauerle, K.J. Franke, J.I. Pascual, ACS Nano 8 (2014) 10715.
[177] T. Dretschkow, A.S. Dakkouri, T. Wandlowski, Langmuir 13 (1997) 2843.
[178] T. Dretschkow, T. Wandlowski, J. Electroan. Chem. 467 (1999) 207.
[179] Y. Li, N. Lin, Phys. Rev. B 84 (2011).
[180] Z.L. Shi, N. Lin, J. Am. Chem. Soc. 131 (2009) 5376.
[181] T.A. Pham, F. Song, M.N. Alberti, M.T. Nguyen, N. Trapp, C. Thilgen, F. Diederich, M. Stohr, Chem. Commun. 51 (2015) 14473.
[182] J. Mielke, F. Hanke, M.V. Peters, S. Hecht, M. Persson, L. Grill, J. Am. Chem. Soc. 137 (2015) 1844.
[183] L. Smykalla, P. Shukrynau, D.R.T. Zahn, M. Hietschold, J. Phys. Chem. C 119 (2015) 17228.
[184] J. Rodriguez-Fernandez, K. Lauwaet, M. Angeles Herranz, N. Martin, J. Maria Gallego, R. Miranda, R. Otero, J. Chem. Phys. 142 (2015).
[185] G. Antczak, W. Kaminski, K. Morgenstern, J. Phys. Chem. C 119 (2015) 1442.
[186] D. Ecija, J.I. Urgel, A.C. Papageorgiou, S. Joshi, W. Auwarter, A.P. Seitsonen, S. Klyatskaya, M. Ruben, S. Fischer, S. Vijayaraghavan, J. Reichert, J.V. Barth, P. Natl, Acad. Sci. USA 110 (2013) 6678.
[187] J.I. Urgel, D. Ecija, W. Auwarter, A.C. Papageorgiou, A.P. Seitsonen, S. Vijayaraghavan, S. Joshi, S. Fischer, J. Reichert, J.V. Barth, J. Phys. Chem. C 118 (2014) 12908.
[188] J.I. Urgel, D. Ecija, W. Auwarter, J.V. Barth, Nano Lett. 14 (2014) 1369.
[189] J.I. Urgel, B. Cirera, Y. Wang, W. Auwarter, R. Otero, J.M. Gallego, M. Alcami, S. Klyatskaya, M. Ruben, F. Martin, R. Miranda, D. Ecija, J.V. Barth, Small 11 (2015) 6358.
[190] J.I. Urgel, D. Ecija, W. Auwarter, D. Stassen, D. Bonifazi, J.V. Barth, Angew. Chem. Int. Ed. 54 (2015) 6163.
[191] J. Otsuki, Supramol. Chem 23 (2011) 169.
[192] Y.Q. Liu, D.B. Zhu, L.K. Ruan, C.L. Bai, A. Yamada, K. Shigehara, Chin. J. Chem. 9 (1991) 126.

[193] T. Takami, T. Ye, D.P. Arnold, K. Sugiura, R.M. Wang, J.Z. Jiang, P.S. Weiss, J. Phys. Chem. C 111 (2007) 2077.
[194] J. Otsuki, S. Kawaguchi, T. Yamakawa, M. Asakawa, K. Miyake, Langmuir 22 (2006) 5708.
[195] L. Smykalla, P. Shukrynau, M. Hietschold, J. Phys. Chem. C 116 (2012) 8008.
[196] Y. He, Y.J. Zhang, I.P. Hong, F. Cheng, X. Zhou, Q. Shen, J.L. Li, Y.F. Wang, J.Z. Jiang, K. Wu, Nanoscale 6 (2014) 10779.
[197] L. Krusin-Elbaum, T. Shibauchi, B. Argyle, L. Gignac, D. Weller, Nature 410 (2001) 444.
[198] L. Bogani, W. Wernsdorfer, Nat. Mater. 7 (2008) 179.
[199] K. Katoh, Y. Yoshida, M. Yamashita, H. Miyasaka, B.K. Breedlove, T. Kajiwara, S. Takaishi, N. Ishikawa, H. Isshiki, Y.F. Zhang, T. Komeda, M. Yamagishi, J. Takeya, J. Am. Chem. Soc. 131 (2009) 9967.
[200] Y.F. Zhang, H. Isshiki, K. Katoh, Y. Yoshida, M. Yamashita, H. Miyasaka, B.K. Breedlove, T. Kajiwara, S. Takaishi, T. Komeda, J. Phys. Chem. C 113 (2009) 9826.
[201] A.S. Klymchenko, J. Sleven, K. Binnemans, S. De Feyter, Langmuir 22 (2006) 723.
[202] T. Takami, D.P. Arnold, A.V. Fuchs, G.D. Will, R. Goh, E.R. Waclawik, J.M. Bell, P. S. Weiss, K.-I. Sugiura, W. Liu, J. Jiang, J. Phys. Chem. B 110 (2006) 1661.
[203] H. Isshiki, J. Liu, K. Katoh, M. Yamashita, H. Miyasaka, B.K. Breedlove, S. Takaishi, T. Komeda, J. Phys. Chem. C 114 (2010) 12202.
[204] H. Isshiki, J. Liu, K. Katoh, M. Yamashita, H. Miyasaka, B.K. Breedlove, S. Takaishi, T. Komeda, Japan, J. Appl. Phys. 49 (2010).
[205] H. Tanaka, T. Ikeda, K. Yamashita, M. Takeuchi, S. Shinkai, T. Kawai, Langmuir 26 (2010) 210.
[206] K. Binnemans, J. Sleven, S. De Feyter, F.C. De Schryver, B. Donnio, D. Guillon, Chem. Mater. 15 (2003) 3930.
[207] K. Miyake, M. Fukuta, M. Asakawa, Y. Hori, T. Ikeda, T. Shimizu, J. Am. Chem. Soc. 131 (2009) 17808.
[208] J. Otsuki, Y. Komatsu, D. Kobayashi, M. Asakawa, K. Miyake, J. Am. Chem. Soc. 132 (2010) 6870.
[209] H. Tanaka, T. Ikeda, M. Takeuchi, K. Sada, S. Shinkai, T. Kawai, ACS Nano 5 (2011) 9575.
[210] P. Liljeroth, I. Swart, S. Paavilainen, J. Repp, G. Meyer, Nano Lett. 10 (2010) 2475.
[211] L.K. Wang, H.H. Kong, C. Zhang, Q. Sun, L.L. Cai, Q.G. Tan, F. Besenbacher, W. Xu, ACS Nano 8 (2014) 11799.
[212] S.W. Hla, K.F. Braun, B. Wassermann, K.H. Rieder, Phys. Rev. Lett. 93 (2004).
[213] H. Marbach, Acc. Chem. Res. 48 (2015) 2649.
[214] T. Takami, T. Ye, B.K. Pathem, D.P. Arnold, K. Sugiura, Y.Z. Bian, J.Z. Jiang, P.S. Weiss, J. Am. Chem. Soc. 132 (2010) 16460.
[215] S. Yoshimoto, T. Sawaguchi, W. Su, J.Z. Jiang, N. Kobayashi, Angew. Chem. Int. Ed. 46 (2007) 1071.
[216] S.B. Lei, K. Deng, Y.L. Yang, Q.D. Zeng, C. Wang, J.Z. Jiang, Nano Lett. 8 (2008) 1836.
[217] F. Gao, X.M. Zhang, L. Cui, K. Deng, Q.D. Zeng, J.L. Zuo, Sci. Rep. 4 (2014) 05928.
[218] Y.S. Fu, J. Schwobel, S.W. Hla, A. Dilullo, G. Hoffmann, S. Klyatskaya, M. Ruben, R. Wiesendanger, Nano Lett. 12 (2012) 3931.
[219] S. Vijayaraghavan, D. Ecija, W. Auwarter, S. Joshi, K. Seufert, A.P. Seitsonen, K. Tashiro, J.V. Barth, Nano Lett. 12 (2012) 4077.
[220] H.H. Kong, L.K. Wang, Q. Sun, C. Zhang, Q.G. Tan, W. Xu, Angew. Chem. Int. Ed. 54 (2015) 6526.
[221] X.M. Xu, H.P. Zhong, H.M. Zhang, Y.R. Mo, Z.X. Xie, L.S. Long, L.S. Zheng, B.W. Mao, Chem. Phys. Lett. 386 (2004) 254.
[222] Y. Bai, F. Buchner, M.T. Wendahl, I. Kellner, A. Bayer, H.P. Steinruck, H. Marbach, J.M. Gottfried, J. Phys. Chem. C 112 (2008) 6087.
[223] F. Buchner, K. Flechtner, Y. Bai, E. Zillner, I. Kellner, H.P. Steinruck, H. Marbach, J.M. Gottfried, J. Phys. Chem. C 112 (2008) 15458.
[224] S. Stepanow, N. Lin, J.V. Barth, J. Phys. Condens. Mater. 20 (2008).
[225] W. Auwärter, A. Weber-Bargioni, S. Brink, A. Riemann, A. Schiffrin, M. Ruben, J.V. Barth, ChemPhysChem 8 (2007) 250.
[226] F.J. Williams, O.P.H. Vaughan, K.J. Knox, N. Bampos, R.M. Lambert, Chem. Commun. (2004) 1688.
[227] O.P.H. Vaughan, F.J. Williams, N. Bampos, R.M. Lambert, Angew. Chem. Int. Ed. 45 (2006) 3779.
[228] J. Visser, N. Katsonis, J. Vicario, B.L. Feringa, Langmuir 25 (2009) 5980.
[229] Q.D. Zeng, M. Li, D.X. Wu, C.M. Liu, S.B. Lei, S.Y. An, C. Wang, Cryst. Growth. Des. 7 (2007) 1497.
[230] Y.F. Geng, S.L. Wu, J. Xu, H.L. Dai, X.K. Li, K. Deng, Q.D. Zeng, Chin. Chem. Lett. 27 (2016) 602.
[231] Q. Ferreira, L. Alcacer, J. Morgado, Nanotechnology 22 (2011).
[232] M. Trelka, C. Urban, C. Rogero, P. de Mendoza, E. Mateo-Marti, Y. Wang, I. Silanes, D. Ecija, M. Alcami, F. Yndurain, A. Arnau, F. Martin, A.M. Echavarren, J.A. Martin-Gago, J.M. Gallego, R. Otero, R. Miranda, CrystEngComm 13 (2011) 5591.
[233] K. Seufert, W. Auwarter, J.V. Barth, J. Am. Chem. Soc. 132 (2010) 18141.
[234] K. Flechtner, A. Kretschmann, H.P. Steinruck, J.M. Gottfried, J. Am. Chem. Soc. 129 (2007) 12110.
[235] F. Buchner, K. Seufert, W. Auwärter, D. Heim, J.V. Barth, K. Flechtner, J.M. Gottfried, H.-P. Steinrück, H. Marbach, ACS Nano 3 (2009) 1789.
[236] W. Hieringer, K. Flechtner, A. Kretschmann, K. Seufert, W. Auwärter, J.V. Barth, A. Görling, H.-P. Steinrück, J.M. Gottfried, J. Am. Chem. Soc. 133 (2011) 6206.
[237] S. Fabris, S. Stepanow, N. Lin, P. Gambardella, A. Dmitriev, J. Honolka, S. Baroni, K. Kern, Nano Lett. 11 (2011) 5414.